nature portfolio

Peer Review File

Directed heterogeneous hydride transfer enables selective CO2 reduction using a Janus palladium membrane electrode

Corresponding Author: Professor Yujie Sun

This file contains all reviewer reports in order by version, followed by all author rebuttals in order by version.

Version 0:

Reviewer comments:

Reviewer #1

(Comments for the Author)
Hu et al. report a Janus palladium membrane (J-Pdm) system for CO2 electroreduction in which hydrogen generated on one side of a Pd membrane permeates through the metal and forms Pd-H species on the CO2-facing side. The authors propose that these Pd-H species react with CO2 through a heterogeneous hydride transfer pathway to produce formate, thereby bypassing the conventional proton-coupled electron transfer (PCET) mechanism. The Janus Pd membrane concept itself was previously introduced by the authors (J. Am. Chem. Soc. 2025, 147, 28015–28023), where the design and hydrogen permeation chemistry were clearly demonstrated. In the present work, the authors extend this concept to CO2RR and aim to provide mechanistic insights into how hydride-mediated pathways may operate in this system. The level of novelty is thus reduced from this perspective.
Overall, the study offers an interesting perspective on alternative reaction pathways for CO2 reduction and could provide useful insights into the role of metal hydride species in heterogeneous electrocatalysis. However, several aspects of the manuscript would benefit from further clarification, particularly regarding the analysis of electrochemical data, the interpretation of the proposed mechanism, and the broader implications of the system for CO2RR research. Addressing the points below would help strengthen the presentation and improve the clarity of the conclusions.
From the standpoint of practical CO2RR applications, even setting aside the cost of Pd, the architecture of the J-Pdm electrode appears to restrict the system to an H-cell configuration. In such a setup, CO2 must first dissolve in the electrolyte before reaching the electrode interface. Given that CO2RR is widely investigated in the context of carbon neutrality and scalable carbon utilization, reactor configuration and mass transport considerations are often important aspects of system evaluation. Current CO2RR studies employ gas-diffusion electrodes and flow-cell (or MEA) architectures to achieve higher current densities and improved mass transport (e.g., ref. 1 cited by the authors). In comparison, the J-Pdm configuration may be more challenging to integrate into such reactor designs because the reaction relies on hydrogen permeation through the Pd membrane and the separation of two electrochemical chambers. While this design may be particularly valuable for mechanistic investigations, it would be helpful if the authors could discuss more explicitly how the J-Pdm concept relates to practical reactor configurations and whether coupling this approach with flow-cell systems could be feasible or inherently challenging.
In the Supporting Information, the authors state that FE is calculated using Qt, defined as the charges passed through the reaction. However, it is unclear which reaction this refers to: the HER chamber, the CO2RR chamber, or the overall system. Regardless of which chamber is used in the calculation, the reported formate FE exceeding 100% indicates that the electron accounting is incomplete. According to the mechanism proposed by the authors, non-PCET formate formation occurs through hydride transfer via the reaction $H^- + CO_2 \rightarrow HCOO^-$, where the hydride originates from hydrogen produced in the HER chamber. In contrast, formate generated through PCET would be associated with electrons supplied to the CO2RR chamber. Therefore, if both electrochemical chambers are considered together, the electrons supplied to the overall system must be distributed among several possible pathways: formate formation, H2 evolution, possible CO formation, and potentially hydrogen storage within the Pd lattice. Under this framework, the reviewer finds it difficult to understand how the electron balance of the full system closes. If the currents from both chambers are considered simultaneously, what are the resulting FE values for HCOOH, H2, and CO (if present)? Providing a complete charge balance across both chambers would significantly improve the transparency of the data analysis and clarify the true energy efficiency of the system.
The isotope labeling experiments show that the hydrogen incorporated into formate largely originates from the HER chamber rather than from water in the CO2RR electrolyte. While this observation supports the idea that permeated hydrogen participates in the reaction, it does not necessarily prove that the elementary step involves true hydride transfer rather than hydrogen atom transfer or surface hydrogenation following electron transfer. In heterogeneous catalytic systems,

distinguishing between hydride transfer, hydrogen atom transfer, and coupled electron-proton transfer can be challenging. The authors attribute the observed behavior to tunable hydricity of Pd-H species under cathodic polarization, yet the relationship between applied potential and hydricity is not quantitatively discussed. A more detailed thermodynamic or kinetic analysis of the hydride donor strength of Pd-H under electrochemical bias would strengthen the mechanistic interpretation and help clarify whether the process indeed corresponds to a true hydride transfer step.
The authors show that the mixture of KHCO3 and NaClO4 provides the highest formate activity. However, the manuscript does not clearly explain why bicarbonate plays such a strong role in promoting the reaction. It remains unclear whether KHCO3 mainly acts as a CO2 reservoir, a buffering species controlling local pH, or whether it participates more directly in the reaction pathway. Considering that bicarbonate concentration significantly affects the observed activity, a more detailed discussion of its mechanistic role would be beneficial.
In addition to the above major concerns, several technical issues should also be clarified:
1. In Supplementary Figure S1, the cyclic voltammetry curves in panel b show only a very small difference between the scan rates of 100 mV s-1 and 200 mV s-1, whereas in panel c the calculated capacitance values differ significantly. The reviewer suggests that the authors provide the raw current values corresponding to each scan rate or label the current values directly in panel b. Furthermore, the data in panel c appear not strictly linear. It should also be noted that the double-layer capacitance of smooth metal foils is typically around ~30 uF cm-2, whereas the value reported here is approximately 120 uF cm-2. The authors should explain the origin of this discrepancy.
2. In Supplementary Figure S2, the open circuit potential varies significantly under different conditions. The authors should provide a more detailed explanation of the factors responsible for these OCP shifts.
3. In lines 162–163, the authors attribute the decrease in formate FE at jHER = –50 mA cm-2 to hydrogen bubble accumulation affecting CO2 transport. However, CO2RR in H-cells is typically mass transport limited at much lower currents. The reviewer would like to know whether the cell design used in this study has any special features that enable such current densities. If so, the authors should provide either a photograph or a schematic illustration of the experimental setup.
4. In lines 192–196 (Figure S17), when no potential is applied on the CO2RR side but jHER = –10 mA cm-2 is applied in the HER chamber, almost no formate is produced. The authors should clarify whether Pd-H species exist on the CO2RR side under this condition. If Pd-H is present, it would be useful to explain why hydride transfer to CO2 does not occur or what competing processes dominate.
5. In several figures (for example Figure 2b, 2d, 2e, 2f and Figure 3b), only FE values are reported, while the corresponding current densities are not shown. Providing the actual current values would help readers better evaluate the catalytic performance.
6. In Figure 3b, the formate FE at –0.15 V appears higher than that reported in Figure 2b, while the value at –0.25 V appears lower. The origin of this discrepancy should be clarified. In addition, because the isotope labeling experiment involves hydrogen and deuterium sources, it would be helpful if the authors could also report the FE of H2, HD, and D2.
7. In Figure 5e, the experiments are conducted in acetonitrile. The reviewer would like to know whether any water is present in the electrolyte. If CO is produced through CO2 reduction, the hydrogen required for the reaction must originate from some source. The authors should clarify the origin of hydrogen in this system. In addition, if hydrogen evolution occurs, the reviewer wonders whether a signal near a retention time of approximately 1 min appears in the GC analysis. In Figure 5f, CO is detected by GC, yet Pd surfaces are known to strongly adsorb CO. The authors should therefore explain why no *CO signal is observed in the IR spectra.
8. The stability of acetonitrile within the applied potential window should also be discussed. Specifically, the authors should clarify whether acetonitrile remains electrochemically stable in the tested potential range and whether it could react with Pd-H species.
9. In Supplementary Figure S8, the numbering appears to contain a typographical error and the label “8” is missing.
10. The manuscript would benefit from a more detailed description of the proposed mechanism for formate formation via Pd-H. In particular, the authors should clarify whether the key elementary step is $H^- + CO_2 \rightarrow HCOO^-$, whether CO2 adsorption on Pd precedes hydride transfer, and how this pathway differs mechanistically from conventional surface hydrogenation reactions.
11. The supplementary materials provide SEM images of the electrode surface. To better illustrate the structural characteristics of the Janus design, the authors are encouraged to include cross-sectional SEM images of the electrode. Such images would help reveal the thickness of the deposited Pd layer and the structural relationship between the deposited Pd nanoparticles and the underlying Pd membrane.

Reviewer #2

(Comments for the Author)
This manuscript by Sun and co-workers reports on a Janus palladium membrane electrode (J-Pdm) that spatially separates hydrogen generation from CO2 reduction and enables selective CO2-to-formate conversion via heterogeneous hydride transfer. The authors claim that electrochemically tunable Pd–H hydricity allows the reaction to bypass the conventional proton-coupled electron transfer (PCET) paradigm. This concept is potentially innovative and interesting. However, several mechanistic claims do not have rigorous substantiation, and certain interpretations may be overstated relative to the evidence provided. Hence, this manuscript does not meet the requirement for publication in Nature Chemistry.

Specific questions and concerns are listed below.

1. Authors claim upon cathodic polarization on this CO2-facing side of J-Pdm, those permeated hydrogen atoms are reduced to hydride species that can undergo direct transfer to CO2, leading to the production of formate.

A key mechanistic ambiguity arises from the fact that the observed reactivity does not necessarily require a true hydride transfer mechanism. Specifically, the authors propose that CO2 reduction proceeds via direct hydride transfer from $Pd–H^-$ to

CO2: Pd–H– + CO2 → HCOO–. However, the experimental observations presented in the manuscript cannot rule out an alternative pathway in which hydrogenation occurs through a coupled electron–proton process involving neutral surface hydrogen: Pd–H + CO2 + e– → HCOO–. In this scenario, the hydrogen atom originates from surface Pd–H, while the additional electron required for formate formation is directly from the electrode to electrochemically activated CO2. As a result, the process would correspond to a surface hydrogenation coupled with electron transfer, rather than a genuine hydride transfer.

Because both pathways could produce identical isotopic labeling results and similar electrochemical signatures, the current evidence does not unambiguously distinguish between: hydride transfer: $Pd–H^- + CO2 \rightarrow HCOO^-$ and electron-assisted hydrogenation: $Pd–H + CO2 + e^- \rightarrow HCOO^-$. That is, an alternative mechanism involving neutral Pd–H reacting with an electrochemically activated CO2 intermediate cannot be ruled out. Therefore, additional mechanistic evidence would be required to conclusively establish the proposed heterogeneous hydride transfer mechanism.

2. Regardless of the specific mechanism, once Pd–H species generated on the HER side are involved, the conversion of CO2 to formate on the CO2-facing side effectively corresponds to a one-electron electrochemical step, rather than the conventional two-electron CO2 reduction process assumed in the Faradaic efficiency analysis.

3. The observed cation effect on the CO2-facing side also raises questions about the proposed mechanism. Alkali metal cations are well known to influence the structure of the electrical double layer and the local electrochemical environment. The fact that the catalytic performance varies with the identity of the cation could suggest that the reaction likely involves electrochemical steps occurring within the double layer. Consequently, a mechanism involving neutral Pd–H reacting with CO2 coupled with a single electron transfer ($Pd–H + CO2 + e^- \rightarrow HCOO^-$) cannot be excluded.

4. The role of KHCO3 in the CO2-facing electrolyte also requires clarification. The authors show that formate production is negligible in pure NaClO4 but increases substantially when KHCO3 is present, indicating that bicarbonate plays a critical role in the reaction. It is therefore unclear whether the improved performance arises from enhanced CO2 buffering, or changes in local pH. The possible influence of electrolyte pH and interfacial electrochemical processes on the CO2 reduction pathway should be more carefully examined.

5. The article lacks a lot of critical information, such as the H2 production rate and potentials on the HER side; the currents, as well as the FE and production rate of H2 on the CO2 side.

6. In an aprotic organic electrolyte, the performance data for ePMR is absent. Moreover, how do ePMR and J-Pdm behave when the current on the HER side is varied in the organic system?

7. The caption for Figure S7 is wrong.

8. There are two data for -1.85V in Figure S25. At the same time, I'm curious why the formate signals in the NMR are very different at -1.85 V and -1.95 V, while the production rates in Fig. 5c are similar?

9. For Fig. 2d and Figure S4, the formate FE approaching 160% at jHER = –10 mA cm–2. Nevertheless, further increasing jHER to –50 mA cm–2 resulted in a lower formate FE of 130%. However, the relative peak areas for formate in NMR are 0.21 and 0.11, respectively. The results indicate that the current density on CO2ER side at jHER = –50 mA cm–2 is much smaller than the current density on CO2ER side at jHER = –10 mA cm–2. This trend is opposite to that in Fig. 2c.

10. Why must the CO2 reduction side require electrodeposition of high surface area Pd? Are the results substantially different with a smooth flat Pd surface?

Reviewer #3

(Comments for the Author)
In this manuscript, Hu et. al. reported a Janus palladium membrane electrode, affording CO2-to-formate conversion via hydride transfer mechanism, rather than conventional PCET mechanism. This was achieved by tuning the hydricity of Pd–H species via external polarization. The key point of the study is very clear, and I believe the tunable hydricity in the Pd-membrane provides great insights for more reaction systems for value-added chemicals synthesis. Therefore, I support its publication, and have the following concerns for the authors.

1. The calculation of FE in this work is significant but not clarified, especially in regard to the FE higher than 100%. According to the Figure 2e and 2f, it is speculated that the total charge used in the FE calculation formula only contains that of the CO2ER chamber. Considering that the applied polarization circuits at the HER and CO2ER chamber are independent, it is theoretically impossible for total FE more than 100%. Hence, the detailed calculation process on FE should be provided and re-checked.

2. According to the previous study (Joule 2024, 8, 728-745), the OCP value at the *H/H+ polarization interface is significantly influenced by the solution pH. Hence, the more positive OCP values after introducing CO2 should be discussed thoroughly regarding the change of solution pH.

3. Hunt et al. (J. Am. Chem. Soc. 2023, 145, 14316–14323) proposed that the hydrogenation thermodynamics of CO2 in Pd

membrane reactor is significantly affected by HER chamber current density and almost no product at low current density. Therefore, I think that it is more reasonable to compare the CO2 hydrogenation efficiency of different reaction modes (ePMR, conventional CO2ER and Janus CO2ER) under higher HER chamber's current density.

4. As a more comprehensive evaluation, the FE corresponding to the H2 evolution in the HER chamber and CO2ER chamber should also be provided to demonstrate the respective distributions of electrons in the two circuits.

5. The Janus hydrogenation system features two independent circuits and their respective polarization effects on hydrogen species. However, whether a synergistic interaction exists between these two circuits remains unexplored. This study (Chem Catal. 2026, https://doi.org/10.1016/j.checat.2025.101602) aims to address this gap.

6. In the Figure 1b, it is proposed that HCOOH production in aprotic solvents is forbidden in ePMR. The CO2 hydrogenation experimental results without the CO2ER polarization in aprotic solvents should be provided as a response.

7. I noticed that when applying a more negative potential at the chemical compartment, FE of formate reduced under different conditions (Fig. 2b, Fig. 3b, Fig. 5c). The reason for this observation under specific conditions requires further explanation, more than simply attribute it to the competition of HER. I assumed that delta G of Pd-H species should be larger at more negative potential, making it easier for CO2RR. In addition, since the current density at electrochemical chamber is fixed, leading to a similar migrated H species amount and thus H species coverage at Pd surface in the chemical chamber, the recombination of H species to give H2 may not be more competitive.

Reviewer #4

(Comments for the Author)
This manuscript by Sun and Hu presents an original and potentially impactful concept for CO2 reduction using a Janus palladium membrane electrode that spatially separates hydrogen generation from the CO2-reduction interface supported by an additional electrochemical bias. The study is scientifically interesting, and the combination of isotopic labelling, SEIRAS and experiments in aprotic media make the work promising. However, in its current form, the manuscript still feels somewhat premature to me. Several central claims are intriguing but not yet supported with sufficient rigor or require clearer discussion. I therefore recommend reconsideration after major revisions. The following points deserve attention:

- The reported formate Faradaic efficiencies above 100%, especially at the beginning, are central to the paper but are not yet resolved rigorously enough. Beyond very initial measurements there should not be any FE beyond 100% here. Since the authors are clearly aware of this issue, the manuscript should provide a more transparent charge balance and clearly distinguish between compartment-specific values and overall device-level efficiencies.

- The long-term data are still rather superficial. A 20 h stability test is encouraging, but still limited for such a central claim. In addition, Fig. S28 appears to show noticeable structural changes of the Pd electrode, which are not discussed in sufficient detail. Longer measurements and more thorough structural post-analysis would be needed to support the durability claims.

- The experimental setup and its scalability should be discussed more clearly.
The cell design/configuration is important for the mechanistic argument, but the setup is not described in enough detail. A clearer schematic and more information on chamber dimensions and cell geometry would be helpful. Moreover, the active area appears very small, and the use of a 25 μm Pd foil raises obvious questions regarding scalability and capital cost. A brief discussion of larger-area operation or the possible use of alternatives would improve the practical relevance of the study.

- The claim of "tunable hydricity" is currently very strong. Although it is one of the most interesting ideas in the manuscript, at present it is not yet quantitatively established. The authors should either weaken this claim or explain more clearly what range of tuning is actually implied, how it is supported experimentally, and what broader reactivity consequences may realistically follow from it.

Minor points:

- - There appear to be inconsistencies in how the isotope experiments are described. In the main text and Fig. 3 caption, the experiment is presented as a potential-dependent study and the HER chamber is specified as 1.0 M KOH in D2O. In the SI methods, the HER chamber is described as 1.0 M NaClO4 in D2O, and the electrolysis is described at –0.35 V vs. RHE, which reads as a single-point experiment rather than the broader potential series.

- The aprotic electrolyte should be characterized more rigorously, for example by Karl Fischer titration, to assess residual water.

- I am not fully convinced by the use of DMSO as an internal standard for NMR quantification, especially given its hygroscopic nature and the use of solvent suppression. The authors should clarify whether specific precautions were taken to ensure quantitative accuracy.

Version 1:

Reviewer comments:

Reviewer #1

(Comments for the Author)
Authors have satisfactorily addressed my comments raised in the last round.

Reviewer #2

(Comments for the Author)
Authors have addressed the Reviewer comments quite comprehensively and I am happy to support publication.

Reviewer #3

(Comments for the Author)
The authors provide a detailed response to my questions, but I think the authors do not fully understand and response my questions. Therefore, I think further substantial revision is still required, with the following concerns shown below:

1. When reading the response letter, I felt deeply confused because the authors almost did not directly provide any revision figures corresponding to their descriptions in the response to my questions. Although I know that the authors have made revisions in the manuscript and SI and even displayed them in the responses to the other reviewers, this has not improved my reading experience. I am not obliged to manually match the descriptions with the corresponding figures in SI that are embedded in a long and cumbersome text during the review process. This should be the authors' work. I hope that the responses to each reviewer can receive equal attention.
2. Regarding Q2 in my previous comment, the authors explained the influence of pH variation before and after the CO2 saturation in the interfacial potential of CO2 chamber. The authors attributed the major reasons of potential variation to the change of Pd phase during electrolysis. However, the applied current density can not only increase the bulk hydrogen concentration to vary PdHx phase, but also increase the interfacial hydrogen coverage at the CO2ER chamber side. In fact, the pH effect influences the EOCP values via the chemical polarization of interfacial *H /H+ equilibrium. Hence, the role of interfacial H coverage should also be taken into consideration.
3. Regarding Q3 in my previous comment, the authors did not provide additional performance data on the conventional CO2ER system just like the work J. Am. Chem. Soc. 2019, 141, 7815–7821. And please explain why the authors did not response to it.
4. Regarding the response to Q3, I have an additional question that the performance data in the Supplementary Figs. 45 and 46 do not match well. In Supplementary Fig. 45, it is demonstrated that FE values of reaction systems with jHER of –10 mA/cm2 and –100 mA/cm2 are almost equal (~100% vs. ~90%). However, according to the raw data in Supplementary Fig. 46, the relative peak area of reaction systems with jHER of –10 mA/cm2 and –100 mA/cm2 are also almost equal (0.16 vs. 0.13), which is confusing. Considering a difference of 10 times between their total charges, the FE with jHER of –10 mA/cm2 and –100 mA/cm2 should also differ by ~10 times. Or there is another possibility that the author did not change their FE calculation method as they promised in the response to Q1? But this issue also substantially reduces confidence in the care with which the manuscript was prepared.

Reviewer #4

(Comments for the Author)
The authors have addressed my major concerns in a satisfactory manner. In particular, the revised Faradaic-efficiency analysis, the additional flow-cell stability data, and the added controls substantially strengthen the manuscript.

I still consider the term “tunable hydricity” somewhat strong. However, thihs point should not prevent publication.

I therefore support the acceptance of the manuscript.

Version 2:

Reviewer comments:

Reviewer #3

(Comments for the Author)
The authors have well addressed my concerns, and I support the publication of the revised manuscript.

Open Access This Peer Review File is licensed under a Creative Commons Attribution 4.0 International License, which permits use, sharing, adaptation, distribution and reproduction in any medium or format, as long as you give appropriate credit to the original author(s) and the source, provide a link to the Creative Commons license, and indicate if changes were made.
In cases where reviewers are anonymous, credit should be given to 'Anonymous Referee' and the source.
The images or other third party material in this Peer Review File are included in the article's Creative Commons license, unless indicated otherwise in a credit line to the material. If material is not included in the article's Creative Commons license and your intended use is not permitted by statutory regulation or exceeds the permitted use, you will need to obtain permission directly from the copyright holder.
To view a copy of this license, visit https://creativecommons.org/licenses/by/4.0/

Point-by-Point Response to Reviewer Comments

Reviewer #1

Hu et al. report a Janus palladium membrane (J-Pd_m) system for CO_2 electroreduction in which hydrogen generated on one side of a Pd membrane permeates through the metal and forms Pd-H species on the CO_2-facing side. The authors propose that these Pd-H species react with CO_2 through a heterogeneous hydride transfer pathway to produce formate, thereby bypassing the conventional proton-coupled electron transfer (PCET) mechanism. The Janus Pd membrane concept itself was previously introduced by the authors (J. Am. Chem. Soc. 2025, 147, 28015–28023), where the design and hydrogen permeation chemistry were clearly demonstrated. In the present work, the authors extend this concept to CO_2RR and aim to provide mechanistic insights into how hydride-mediated pathways may operate in this system. The level of novelty is thus reduced from this perspective.

Response: We thank the reviewer for this thoughtful comment. We agree that the Janus palladium membrane (J-Pd_m) architecture builds upon our previous work reported in J. Am. Chem. Soc. 2025, 147, 28015–28023, in which the membrane design and hydrogen permeation behaviour were established for hydrodehalogenation chemistry. However, we respectfully emphasize that the central novelty of the present study lies not in the membrane architecture itself, but in the discovery and mechanistic investigation of electrochemically controlled heterogeneous hydride transfer for CO_2 reduction. This work demonstrates that spatial separation of hydrogen generation from CO_2 reduction, together with independent polarization of the CO_2-facing interface, enables permeated hydrogen species to function as hydride donors with tunable hydricity. This reconfigures the interfacial reaction environment and redirects the dominant pathway from conventional proton-coupled electron transfer (PCET) to heterogeneous hydride transfer, enabling selective CO_2-to-formate conversion.

Importantly, this work establishes several advances beyond the previously reported J-Pd_m platform, including: (i) electrochemically controlled hydricity at a heterogeneous interface, (ii) directional hydride flux from water to CO_2, (iii) suppression of PCET-mediated pathways and competing HER, and (iv) efficient CO_2-to-formate conversion in fully aprotic electrolytes where traditional proton-mediated CO_2 reduction pathways are inaccessible. Together, these features define a spatially and mechanistically decoupled catalytic platform in which CO_2 activation proceeds via a hydride-transfer pathway independent of direct proton availability. In this context, hydride-mediated CO_2-to-formate conversion is thermodynamically demanding in both media, as reflected by the solvent-dependent hydricity of formate (approximately 24.1 kcal mol^{-1} in water and 44 kcal mol^{-1} in acetonitrile) (Acc. Chem. Res. 2024, 57, 3488–3499), highlighting the non-trivial nature of achieving controllable heterogeneous hydride transfer across different solvent environments. In response to the reviewer's comments, we now provide extensive mechanistic data, including isotope labelling experiments, Faradaic efficiency analysis, gas analysis, and multiple control experiments, to further support the proposed heterogeneous hydride transfer pathway.

Overall, the study offers an interesting perspective on alternative reaction pathways for CO_2 reduction and could provide useful insights into the role of metal hydride species in heterogeneous electrocatalysis. However, several aspects of the manuscript would benefit from further clarification, particularly regarding the analysis of electrochemical data, the interpretation of the

proposed mechanism, and the broader implications of the system for CO_2RR research. Addressing the points below would help strengthen the presentation and improve the clarity of the conclusions.
Response: We thank the reviewer for this positive and constructive summary of our work. We are encouraged that the reviewer finds the study to provide an interesting perspective on alternative CO_2 reduction pathways and valuable insights into the role of metal hydride species in heterogeneous electrocatalysis. In response to the reviewer's suggestions, we have carefully revised the manuscript to further clarify the analysis of the electrochemical data, strengthen the justification of the proposed mechanistic interpretation, and better articulate the broader implications of the system for CO_2 reduction. We believe these revisions have significantly improved the rigor, clarity, and overall balance of the manuscript, and have strengthened the connection between the electrochemical data and the proposed heterogeneous hydride transfer mechanism.

From the standpoint of practical CO_2RR applications, even setting aside the cost of Pd, the architecture of the J-Pd_m electrode appears to restrict the system to an H-cell configuration. In such a setup, CO_2 must first dissolve in the electrolyte before reaching the electrode interface. Given that CO_2RR is widely investigated in the context of carbon neutrality and scalable carbon utilization, reactor configuration and mass transport considerations are often important aspects of system evaluation. Current CO_2RR studies employ gas-diffusion electrodes and flow-cell (or MEA) architectures to achieve higher current densities and improved mass transport (e.g., ref. 1 cited by the authors). In comparison, the J-Pd_m configuration may be more challenging to integrate into such reactor designs because the reaction relies on hydrogen permeation through the Pd membrane and the separation of two electrochemical chambers. While this design may be particularly valuable for mechanistic investigations, it would be helpful if the authors could discuss more explicitly how the J-Pd_m concept relates to practical reactor configurations and whether coupling this approach with flow-cell systems could be feasible or inherently challenging.
Response: We thank the reviewer for this thoughtful comment and agree that the present J-Pd_m design is particularly valuable for mechanistic investigation. Our primary objective in this work is to establish a new conceptual framework for CO_2 reduction through a heterogeneous hydride-transfer pathway, rather than to present a fully optimized industrial reactor configuration. In the current J-Pd_m system, continuous hydrogen permeation through the Pd membrane is required to maintain a hydride-rich Pd–H state under cathodic polarization, which is essential for enabling heterogeneous hydride transfer to CO_2. Consequently, because CO_2 must first dissolve into the electrolyte before reaching the polarized Pd–H interface, dissolved CO_2 transport inevitably becomes a limiting factor for achieving higher current density in the present H-cell configuration.

To further evaluate the scalability and tunability of the membrane platform, we additionally tested PdAg alloy membranes with the same thickness as the pure Pd membrane (Pd:Ag = 75:25 wt%). The PdAg membrane exhibited essentially unchanged hydrogen permeation behavior together with comparable hydride-transfer-mediated formate generation capability (**Supplementary Figs. 48** and **50**). These results further support the versatility of the heterogeneous hydride-transfer platform and suggest that multicomponent thin-film membrane architectures may be readily accessible using scalable deposition techniques.

In addition, to provide an initial assessment under flow-cell-related operating conditions, we performed preliminary continuous-flow experiments using the setup illustrated in **Supplementary**

Fig. 35. The present J-Pd_m system exhibited good operational stability, maintaining formate Faradaic efficiencies above 75% over 105 h continuous operation while the formate concentration continuously increased (**Fig. 4e** and **Supplementary Fig. 36**). Although engineering optimization is needed for practical large-scale implementation, these preliminary results suggest that the J-Pd_m concept is applicable beyond the H-cell configurations. We have added the corresponding discussion, preliminary flow-cell experiments, and related considerations regarding the potential of the J-Pd_m concept in the revised manuscript and Supplementary Information.

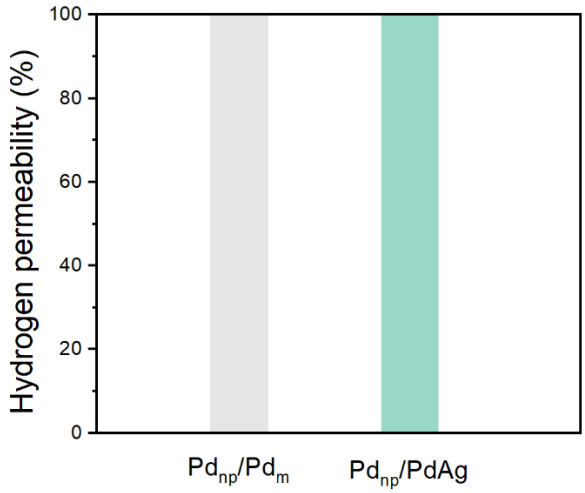

Supplementary Fig. 48. Comparison of hydrogen permeation between Pd_{np}/Pd_m (25 μm-thick Pd foil) and $Pd_{np}/PdAg$ (25 μm-thick PdAg foil, Pd:Ag = 75:25 wt%), both using maleic acid as the driving force to capture H atoms permeating through the membranes.

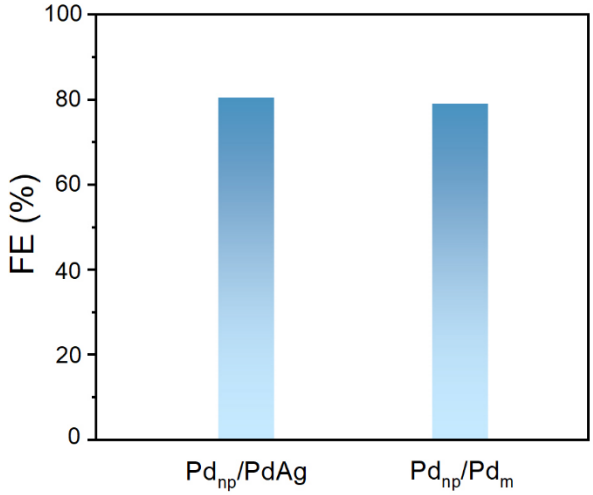

Supplementary Fig. 50. Faradaic efficiency of formate formation for Pd_{np}/Pd_m (25 μm-thick Pd foil) and $Pd_{np}/PdAg$ (25 μm-thick PdAg foil, Pd:Ag = 75:25 wt%) in a J-Pd_m system operated with a constant HER chamber current density of $j_{HER} = -10$ mA cm^{-2}. CO_2 reduction was performed at −0.25 V vs. RHE in the CO_2ER chamber after 3 h electrolysis in 50 mM $KHCO_3$ and 0.5 M $NaClO_4$.

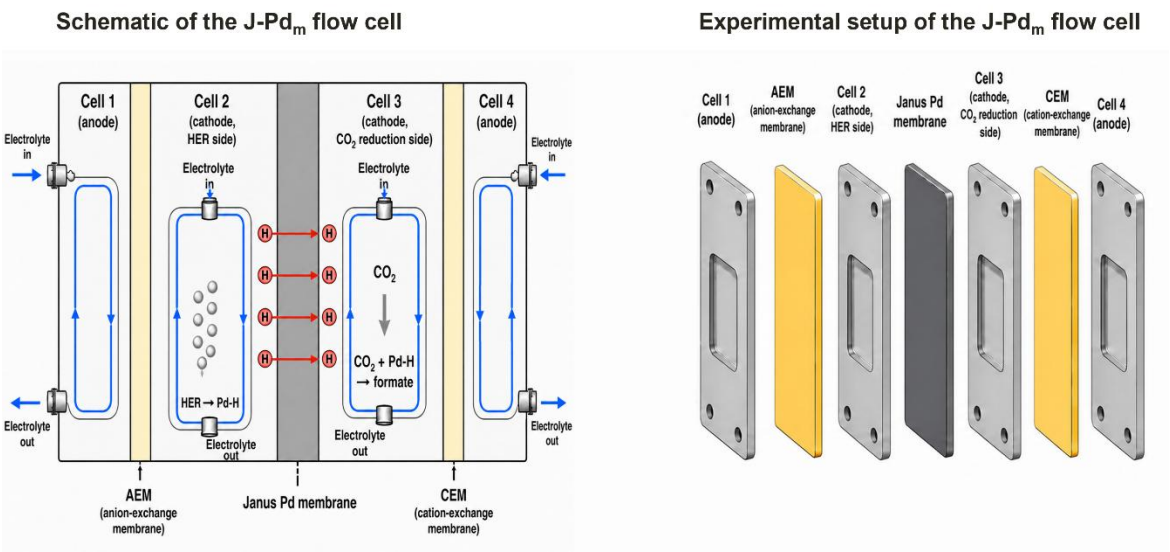

Supplementary Fig. 35. Schematic diagram of the J-Pd$_m$ flow cell setup.

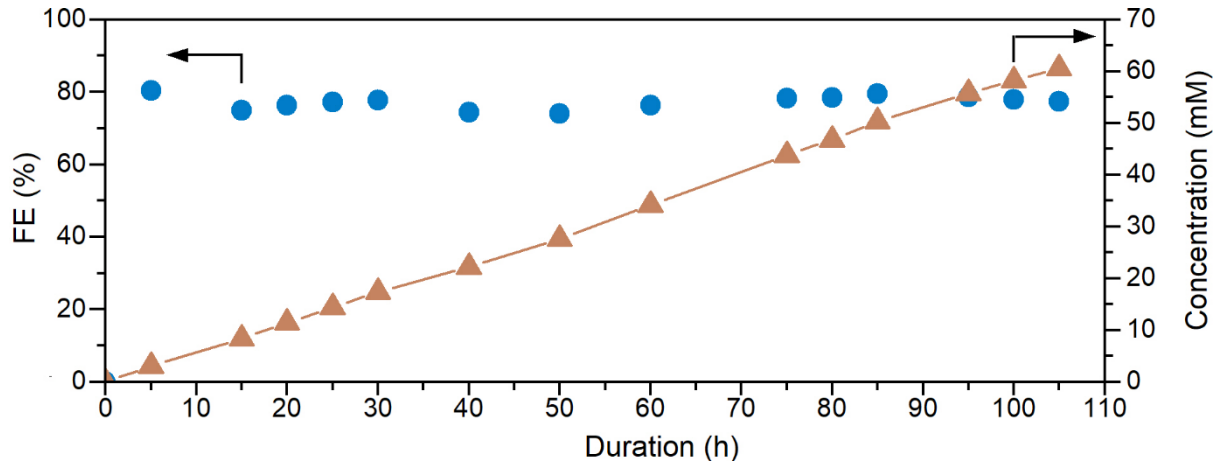

Fig. 4e. Stability test of J-Pd$_m$ in an aqueous flow cell system for CO_2 reduction to formate (j_{HER} = −2 mA cm^{-2}; j_{CO_2ER} = −1 mA cm^{-2}).

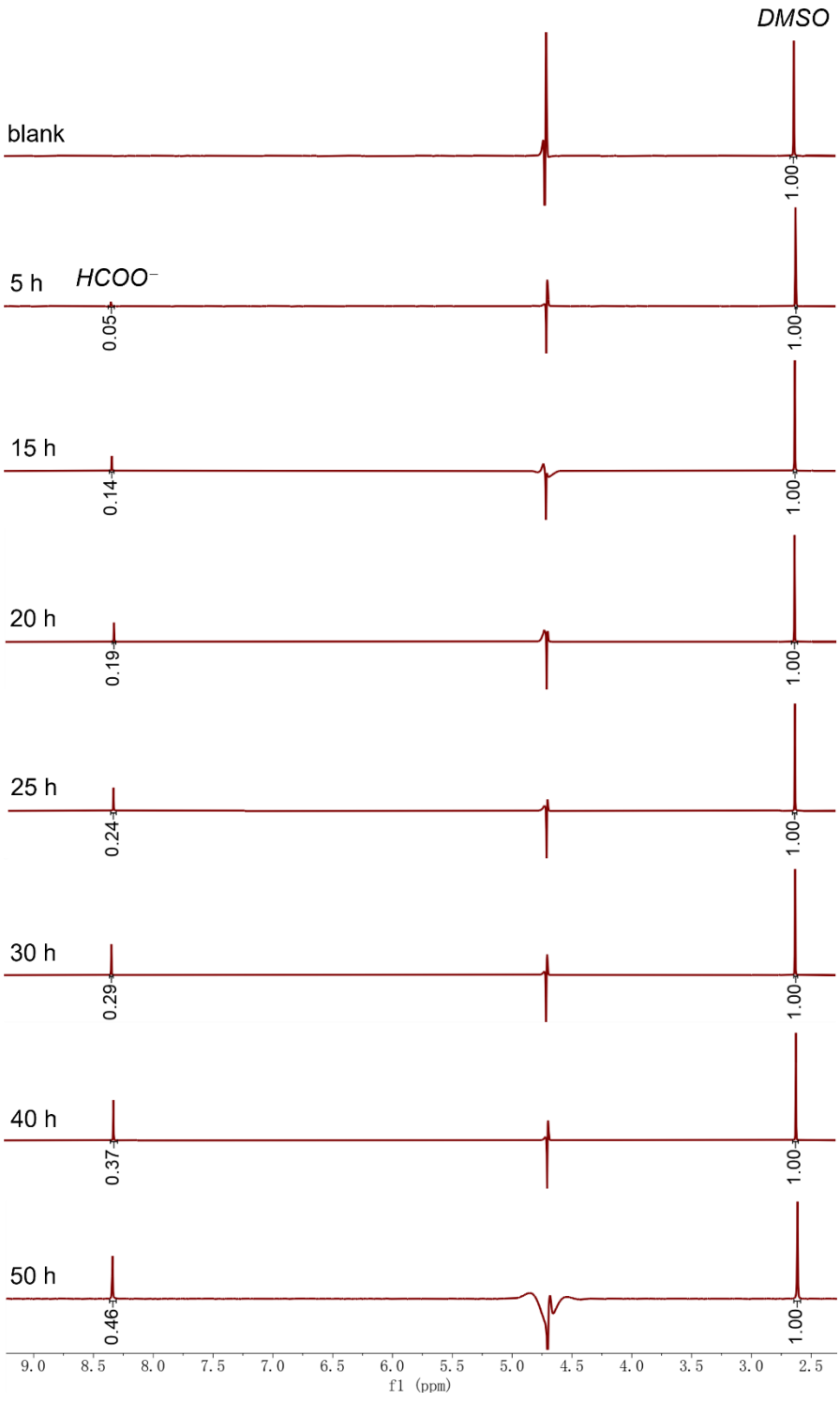
DMSO
blank
1.00
5 h
HCOO⁻
0.05
1.00
15 h
0.14
1.00
20 h
0.19
1.00
25 h
0.24
1.00
30 h
0.29
1.00
40 h
0.37
1.00
50 h
0.46
1.00
9.0 8.5 8.0 7.5 7.0 6.5 6.0 5.5 5.0 4.5 4.0 3.5 3.0 2.5
f1 (ppm)

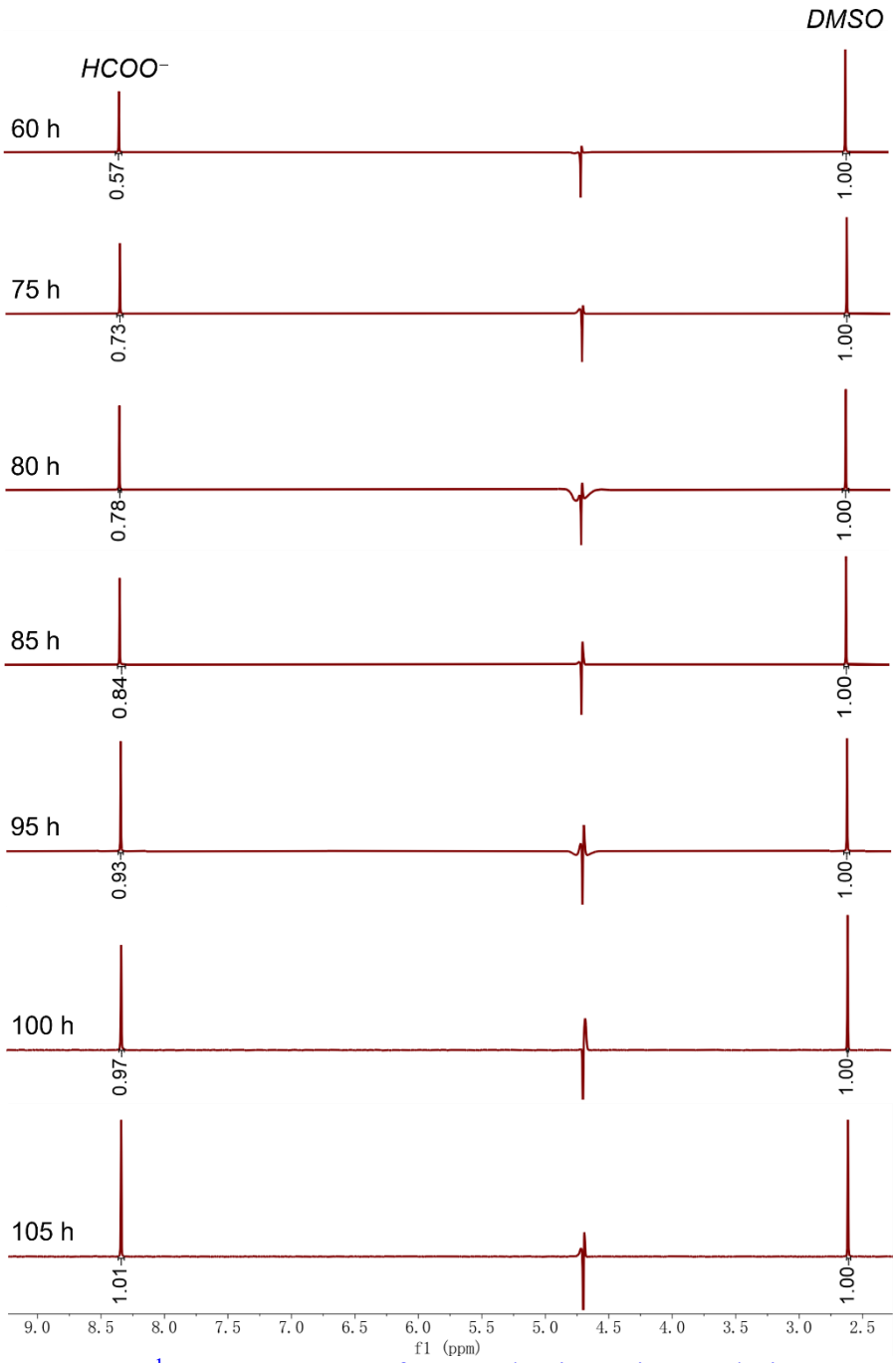

Supplementary Fig. 36. ^{1}H NMR spectra of CO_2 reduction using J-Pd_m in an aqueous flow cell configuration (j_{HER} = −2 mA cm^{-2}; j_{CO_2ER} = −1 mA cm^{-2}).

In the Supporting Information, the authors state that FE is calculated using Qt, defined as the charges passed through the reaction. However, it is unclear which reaction this refers to: the HER chamber, the CO_2RR chamber, or the overall system. Regardless of which chamber is used in the calculation, the reported formate FE exceeding 100% indicates that the electron accounting is incomplete. According to the mechanism proposed by the authors, non-PCET formate formation occurs through hydride transfer via the reaction $H^- + CO_2 \rightarrow HCOO^-$, where the hydride originates

from hydrogen produced in the HER chamber. In contrast, formate generated through PCET would be associated with electrons supplied to the CO_2RR chamber. Therefore, if both electrochemical chambers are considered together, the electrons supplied to the overall system must be distributed among several possible pathways: formate formation, H_2 evolution, possible CO formation, and potentially hydrogen storage within the Pd lattice. Under this framework, the reviewer finds it difficult to understand how the electron balance of the full system closes. If the currents from both chambers are considered simultaneously, what are the resulting FE values for HCOOH, H_2, and CO (if present)? Providing a complete charge balance across both chambers would significantly improve the transparency of the data analysis and clarify the true energy efficiency of the system.
Response: We appreciate the reviewer's careful comments regarding the ambiguity in the electron-counting basis, Faradaic efficiency definition, and overall charge balance in the dual-compartment J-Pd_m system. As pointed out by the reviewer, the polarization circuits used in the HER and CO_2ER compartments are electrically independent, and the current from the HER compartment is not included in the Faradaic efficiency calculation for the CO_2ER compartment. Importantly, the HER chamber serves only to provide sufficient permeated hydrogen for the formation of Pd–H species within the Pd membrane on the CO_2ER side (**Supplementary Fig. 38**), and therefore does not directly participate in the CO_2 reduction process occurring at the CO_2-facing interface.

In the original manuscript (**Fig. 2**), FE values were calculated using the conventional two-electron stoichiometry for CO_2-to-formate conversion based on a proton-coupled electron transfer (PCET) framework, and therefore represent apparent Faradaic efficiencies. Under this conventional PCET-based electron-counting framework, the calculated FE values can exceed 100%, which initially prompted us to further examine the underlying reaction mechanism. This apparent inconsistency motivated the mechanistic investigation presented in **Fig. 3**. Through the deuterium-labeling experiments, ^{2}H NMR spectroscopy confirmed that the liquid product is predominantly deuterated formate ($DCOO^-$), while isotope ratio mass spectrometry identified HD as the dominant gaseous side-product with no detectable H_2 formation (**Figs. 3e and 4b**). These observations demonstrate that the dominant reaction pathway in the CO_2ER chamber is hydride transfer from Pd–H species to CO_2 to generate $HCOO^-$, while the competing side reaction is proton–hydride coupling to produce H_2. Notably, no CO formation was observed under these hydride-transfer conditions. Consistently, GC analysis in **Fig. 4c** shows that, under hydride-transfer mode (i.e., continuous hydrogen permeation from the HER chamber to maintain a Pd–H-rich state within the Pd membrane), no CO byproduct is detected in the CO_2ER chamber. In contrast, when hydrogen permeation from the HER chamber is absent and the Pd membrane operates simply as metallic Pd for conventional CO_2 reduction, CO formation becomes detectable. These results clearly indicate that, in the J-Pd_m system, electrons are delivered through Pd–H species as hydride equivalents to CO_2 and protons in the CO_2ER chamber. Accordingly, given the hydride-transfer-dominated reaction mechanism established in this work, FE values should not be interpreted using the conventional two-electron PCET stoichiometry and should not exceed 100% under a physically consistent definition. We have therefore revised all FE values in **Fig. 2** and the corresponding discussions using a hydride-transfer-based electron-counting framework

This revision ensures consistency with the mechanistic picture established in **Fig. 3** and does not affect the observed experimental trends. The detailed FE calculation procedure has now been explicitly clarified in the revised Supplementary Information. All updated calculations, figures,

and corresponding discussions have been revised in the manuscript and Supplementary Information.

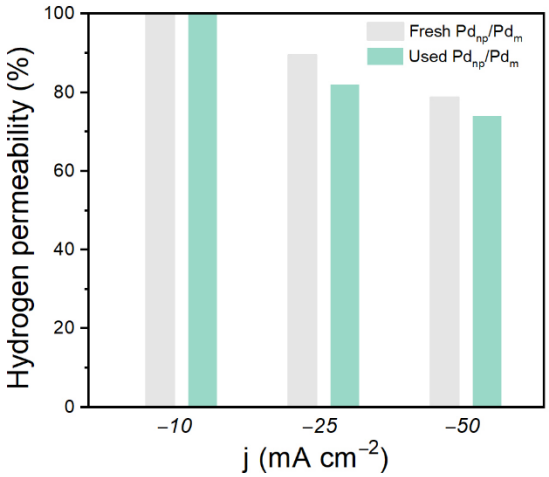

Supplementary Fig. 38. Comparison of hydrogen permeation between fresh Pd_{np}/Pd_m and Pd_{np}/Pd_m after stability testing, both using maleic acid as the substrate to capture H atoms permeating through the palladium membrane.

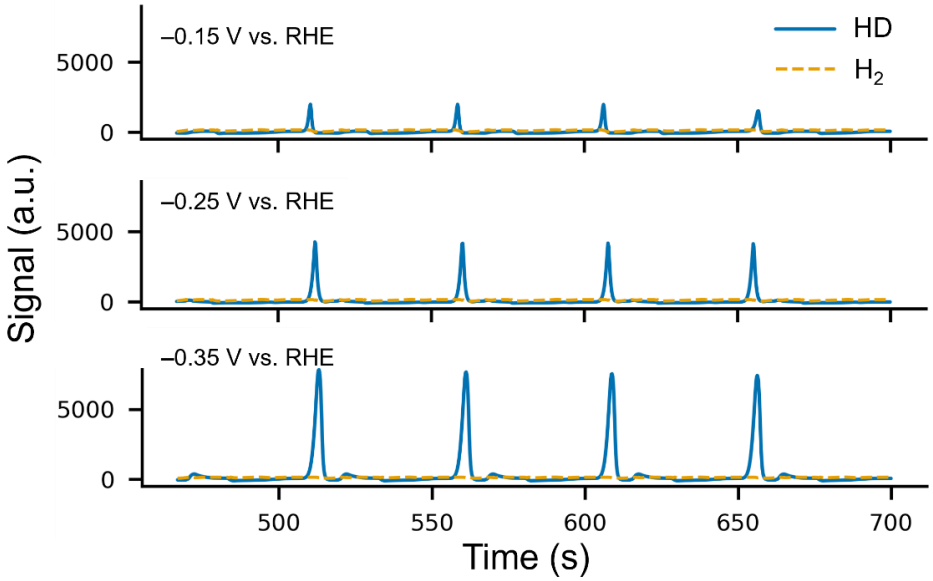

Fig. 4b. Isotope ratio mass spectrometry results recorded in the steady-state region of electrolysis at −0.15 V, −0.25 V and −0.35 V vs. RHE, illustrating highly reproducible HD signals (blue) and negligible H_2 response (orange) in the gas phase.

The isotope labeling experiments show that the hydrogen incorporated into formate largely originates from the HER chamber rather than from water in the CO_2RR electrolyte. While this observation supports the idea that permeated hydrogen participates in the reaction, it does not necessarily prove that the elementary step involves true hydride transfer rather than hydrogen atom transfer or surface hydrogenation following electron transfer. In heterogeneous catalytic systems, distinguishing between hydride transfer, hydrogen atom transfer, and coupled electron-proton transfer can be challenging. The authors attribute the observed behavior to tunable hydricity of Pd-H species under cathodic polarization, yet the relationship between applied potential and hydricity

is not quantitatively discussed. A more detailed thermodynamic or kinetic analysis of the hydride donor strength of Pd-H under electrochemical bias would strengthen the mechanistic interpretation and help clarify whether the process indeed corresponds to a true hydride transfer step.

Response: We appreciate the reviewer's comment regarding the mechanistic interpretation of the isotope labeling results and the distinction between hydride transfer, hydrogen atom transfer, and alternative electron-assisted hydrogenation pathways. As correctly pointed out, the isotope labeling experiments demonstrate that the hydrogen incorporated into formate originates predominantly from the HER chamber via permeation through the Pd membrane, confirming that interfacial Pd–H species are directly involved in CO_2-to-formate conversion. However, this observation alone does not distinguish between a true hydride transfer process and alternative pathways such as hydrogen atom transfer or sequential electron-transfer–hydrogenation mechanisms.

To address this mechanistic ambiguity, we evaluated whether CO_2 reduction could proceed via temporally separated electron-transfer and hydrogen-transfer steps. In aprotic acetonitrile, where proton-coupled processes are excluded, we performed control experiments. We employed two stepwise protocols: (i) CO_2-facing polarization at −1.75 V vs. $Fc^{+}/^{0}$ for a defined period to enable electron transfer, followed by termination of this step, after which hydrogen permeation from the HER chamber (ePMR, −10 mA cm^{-2}) was carried out for an equivalent time period (**Supplementary Fig. 65**); (ii) hydrogen permeation from the HER chamber (ePMR, −10 mA cm^{-2}) for a defined period, followed by termination of hydrogen permeation, after which the system was reconfigured using a fresh Pd membrane and electrochemical polarization at −1.75 V vs. $Fc^{+}/^{0}$ was applied for an equivalent time period (**Supplementary Fig. 66**). In both cases, no detectable formate formation was observed, indicating that CO_2 reduction does not occur via any stepwise pathway involving sequential electron and hydrogen transfer in either order.

In this context, we describe the CO_2-to-formate conversion as proceeding via a Pd–H-mediated heterogeneous hydride-transfer process at the J-Pd_m interface. In this heterogeneous regime, "hydride transfer" does not imply the release of a free solvated H^- species, but rather a surface-mediated interfacial hydride-transfer process in which hydrogen is transferred from Pd–H as a hydride equivalent, consistent with established descriptions of metal–hydride chemistry at electrified interfaces (Nat. Catal. 2023, 6, 351–362). Formally, this process can be expressed as $Pd–H + CO_2 + e^- \rightarrow HCOO^- + Pd$, which should be interpreted as an interfacial hydride-equivalent transfer rather than a stepwise sequence. To further substantiate the hydride-transfer capability of the J-Pd_m interface, we investigated the hydrogenation of BIM^+ (1,3-dimethyl-2-phenyl-1H-benzo[d]imidazol-3-ium), a well-established molecular hydride acceptor, using J-Pd_m (**Supplementary Figs. 67** and **68**). Upon hydride transfer, BIM^+ is converted to the corresponding hydride donor BIMH (1,3-dimethyl-2-phenyl-2,3-dihydro-1H-benzo[d]imidazole), which possesses a reported hydricity of approximately 50 kcal mol^{-1} in acetonitrile (*Nat. Catal.*, 2023, 6, 351–362). As shown in the linear sweep voltammograms (**Supplementary Fig. 67**), when no HER current was applied on the HER side of J-Pd_m (j_{HER} = 0 mA cm^{-2}), BIM^+ reduction only commenced at approximately −1.9 V vs. $Fc^{+}/^{0}$, corresponding to its direct electron-transfer reduction. In contrast, when a HER current density of −10 mA cm^{-2} was applied on the HER side of J-Pd_m, the onset potential for BIM^+ conversion shifted anodically from approximately −1.9 V to −1.25 V vs. $Fc^{+}/^{0}$. This substantial anodic shift indicates that polarized Pd–H species participate directly in BIM^+ hydrogenation, thereby facilitating BIM^+ conversion at substantially less negative

potentials. Further scanning toward more negative potentials resulted in a current plateau, consistent with mass-transport limitation of BIM^+ in solution.

To further verify hydride transfer, controlled-potential electrolysis was performed using 10 mM BIM^+ at −1.4 V vs. $Fc^{+/0}$ while maintaining a HER current density of −10 mA cm^{-2} on the HER side of J-Pd_m (**Supplementary Fig. 68**). After passing the theoretical charge required for complete conversion of BIM^+ through a one-electron hydride-transfer process in the HRR chamber, BIM^+ was quantitatively converted into BIMH, confirming that polarized Pd–H species are capable of mediating efficient heterogeneous hydride transfer. Importantly, the hydricity of formate in acetonitrile (~44 kcal mol^{-1}, *Acc. Chem. Res.*, 2024, 57, 3488–3499) is comparable to that of BIMH. The ability of J-Pd_m to generate BIMH through hydride transfer therefore supports the feasibility of Pd–H-mediated hydride-equivalent transfer to CO_2 under the conditions employed in this work. Together, these results support a Pd–H-mediated interfacial hydride-transfer mechanism in the J-Pd_m system.

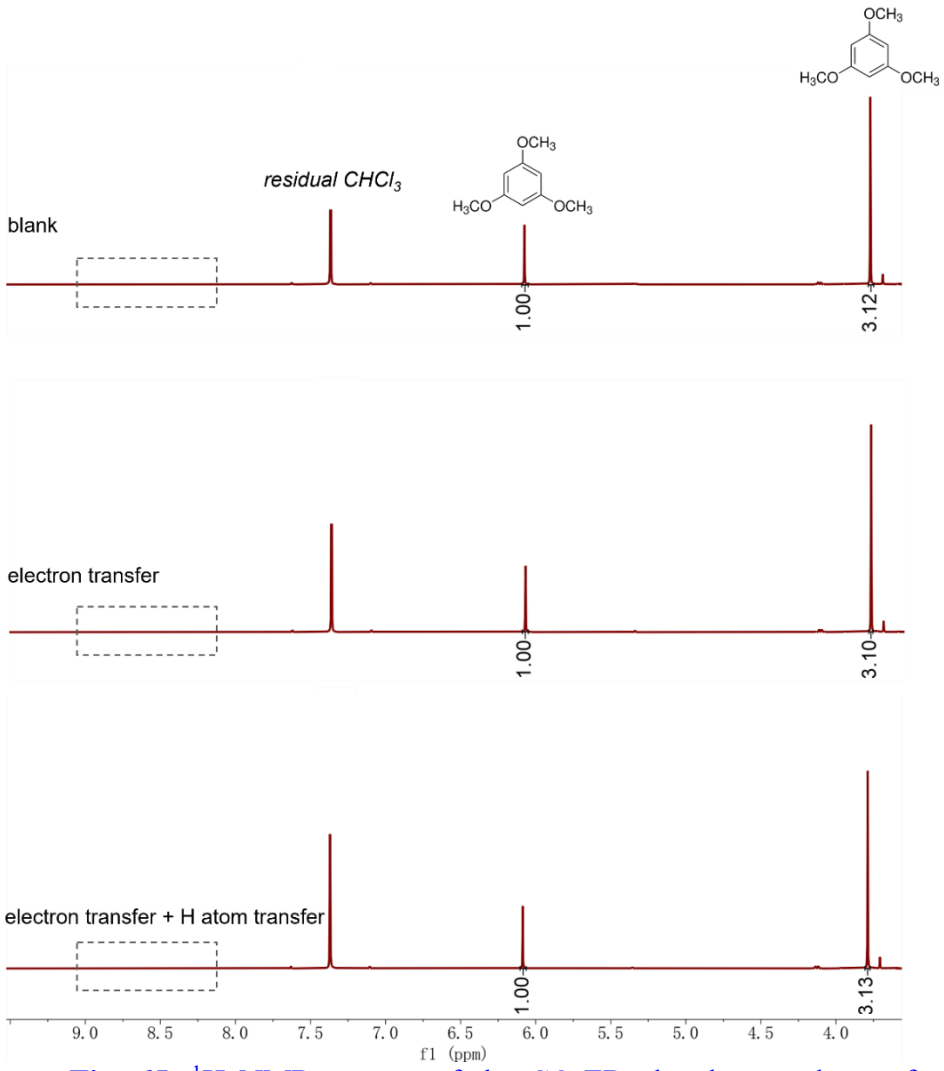

Supplementary Fig. 65. ^1H NMR spectra of the CO_2ER chamber products after sequential electron transfer (3 h) and H atom transfer (3 h).

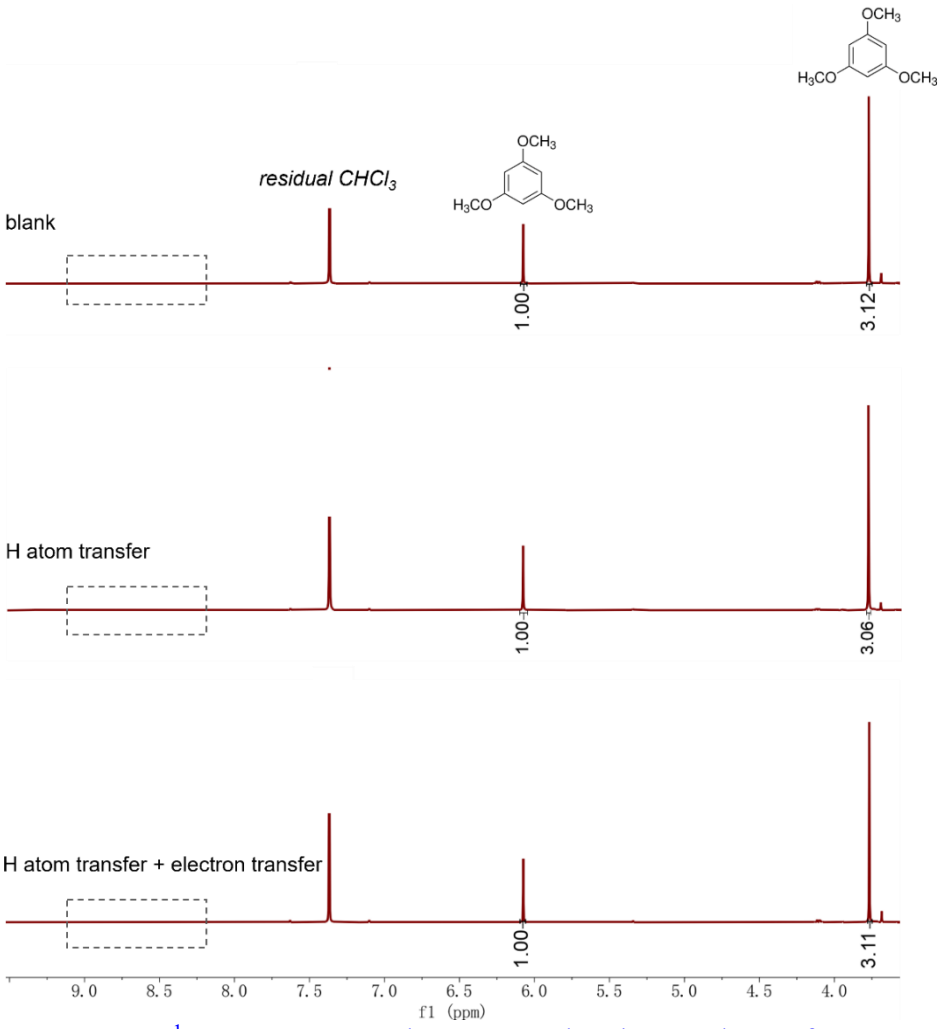

Supplementary Fig. 66. ^{1}H NMR spectra the CO_2ER chamber products after sequential H atom transfer (3 h) and electron transfer (3 h).

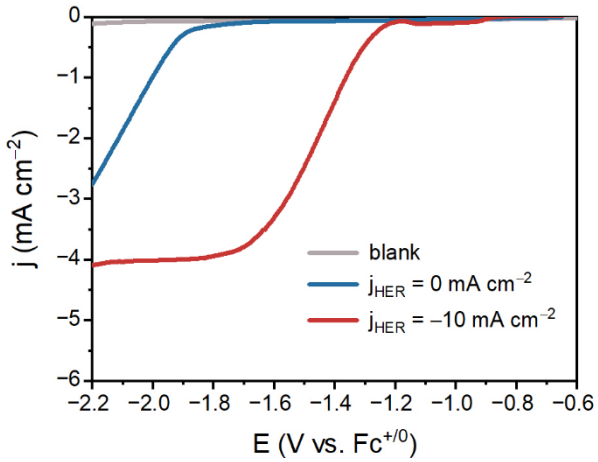

Supplementary Fig. 67. LSV curves of the hydride acceptor (BIM^+) measured with (j_{HER} = −10 mA cm^{-2}) and without (j_{HER} = 0 mA cm^{-2}) HER chamber current density at a scan rate of 2 mV s^{-1} in 0.1 M $TBABF_4/CH_3CN$.

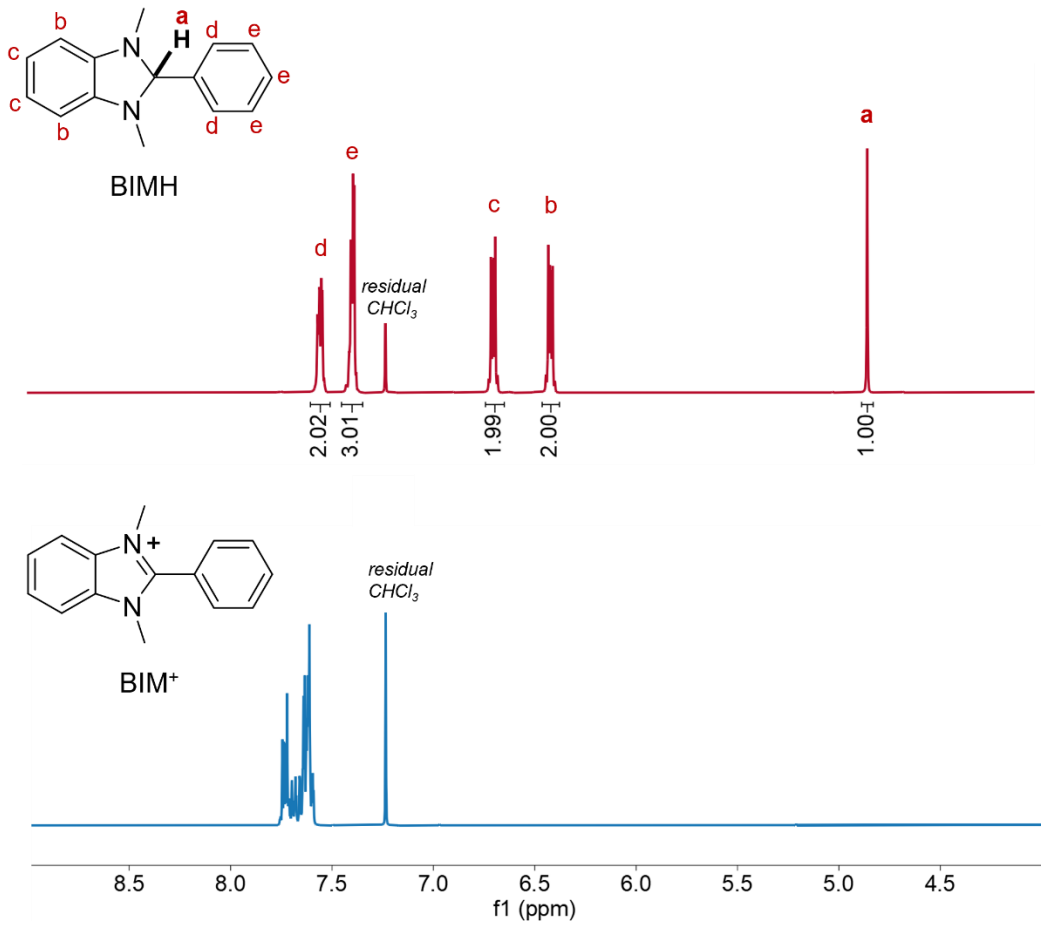

Supplementary Fig. 68. ^{1}H NMR spectra of BIM^{+} before and after the heterogeneous hydride transfer reaction mediated by J-Pd_m at −1.4 V vs. $Fc^{+}/^{0}$, showing the formation of BIMH.

The authors show that the mixture of $KHCO_3$ and $NaClO_4$ provides the highest formate activity. However, the manuscript does not clearly explain why bicarbonate plays such a strong role in promoting the reaction. It remains unclear whether $KHCO_3$ mainly acts as a CO_2 reservoir, a buffering species controlling local pH, or whether it participates more directly in the reaction pathway. Considering that bicarbonate concentration significantly affects the observed activity, a more detailed discussion of its mechanistic role would be beneficial.

Response: We thank the reviewer for raising this important question regarding the role of electrolyte composition in regulating the interfacial CO_2 reduction environment. $NaClO_4$ serves solely as an inert supporting electrolyte, providing ionic conductivity and enabling stable electrochemical polarization without participating in CO_2 conversion chemistry or acid–base equilibria. To establish the interfacial electrolyte environment, we first measured the pH values before and after CO_2 saturation (**Supplementary Tables 5** and **6**). Distinct pH variations were observed across 0.5 M $NaClO_4$, $KHCO_3$ + $NaClO_4$, and 0.5 M $KHCO_3$, confirming fundamentally different CO_2/HCO_3^- equilibrium conditions in each electrolyte. Electrochemical measurements show a clear performance trend of 0.5 M $NaClO_4$ < 0.5 M $KHCO_3$ < $KHCO_3$ + $NaClO_4$, indicating that neither pure buffering nor purely inert electrolyte conditions are optimal for formate formation (**Supplementary Fig. 22**). In $KHCO_3$-containing electrolytes, the CO_2/HCO_3^- equilibrium enhances local CO_2 availability at the Pd–H interface, whereas $NaClO_4$ provides high ionic

conductivity but lacks such CO_2 buffering capability. However, excessively high $KHCO_3$ concentration leads to reduced effective CO_2 availability and increased interfacial ion crowding. In contrast, the mixed electrolyte provides a more favorable interfacial environment that simultaneously enhances CO_2 availability and maintains sufficient ionic conductivity, thereby maximizing formate production. These observations are consistent with previous reports on electrolyte-mediated CO_2 hydrogenation, where the CO_2/HCO_3^- equilibrium and interfacial buffering capacity were shown to strongly influence catalytic performance and polarization-driven reaction pathways (J. Am. Chem. Soc. 2020, 142, 13384–13390.).

Under $j_{HER} = -10$ mA cm^{-2}, potentiostatic electrolysis experiments without CO_2 saturation produced no detectable formate in 0.5 M $KHCO_3$ or 50 mM $KHCO_3$ + 0.5 M $NaClO_4$ electrolytes (**Supplementary Figs. 23** and **24**), confirming that dissolved CO_2 is the essential carbon source, while bicarbonate species primarily function to regulate the interfacial CO_2 equilibrium environment rather than directly participating as reactants.

Overall, the reaction outcome is governed by competitive consumption of Pd–H species at the CO_2-facing interface, where CO_2 and protons act as competing acceptors. The mixed electrolyte optimizes this interfacial competition by simultaneously enhancing CO_2 accessibility while maintaining favorable polarization conditions, leading to preferential hydride transfer to CO_2 over hydride consumption by protons to form H_2.

Supplementary Table 5. Summary of electrolyte pH values.

Electrolyte	H_2O	0.5 M $NaClO_4$	5 mM $KHCO_3$, 0.5 M $NaClO_4$	10 mM $KHCO_3$, 0.5 M $NaClO_4$	20 mM $KHCO_3$, 0.5 M $NaClO_4$	50 mM $KHCO_3$, 0.5 M $NaClO_4$	75 mM $KHCO_3$, 0.5 M $NaClO_4$	0.5 M $KHCO_3$
pH	6.91±0.06	6.47±0.04	8.36±0.01	8.48±0.01	8.52±0.01	8.65±0.01	8.68±0.01	8.87±0.02

Supplementary Table 6. Summary of electrolyte pH values after CO_2 saturation

Electrolyte	H_2O	0.5 M $NaClO_4$	5 mM $KHCO_3$, 0.5 M $NaClO_4$	10 mM $KHCO_3$, 0.5 M $NaClO_4$	20 mM $KHCO_3$, 0.5 M $NaClO_4$	50 mM $KHCO_3$, 0.5 M $NaClO_4$	75 mM $KHCO_3$, 0.5 M $NaClO_4$	0.5 M $KHCO_3$
pH	4.03±0.02	3.97±0.02	5.46±0.02	5.75±0.01	6.01±0.01	6.44±0.02	6.58±0.02	7.45±0.01

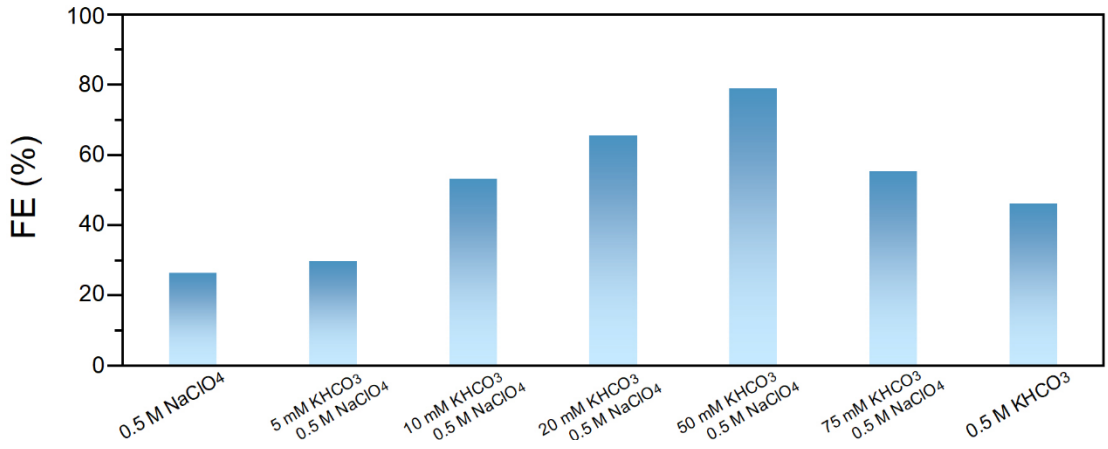

Supplementary Fig. 22. CO_2ER performance after 3-h electrolysis in various electrolytes at −0.25 V vs. RHE with $j_{HER} = -10$ mA cm^{-2}.

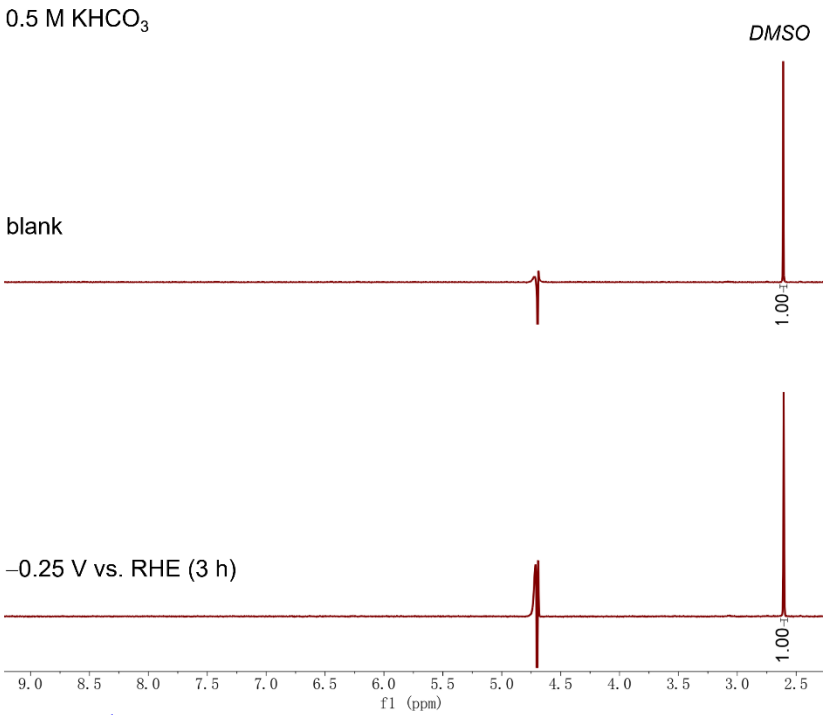

Supplementary Fig. 23. ^{1}H NMR spectra of the electrolyte after 3-h electrolysis in 0.5 M $KHCO_3$ at −0.25 V vs. RHE (Ar, j_{HER} = −10 mA cm^{-2}).

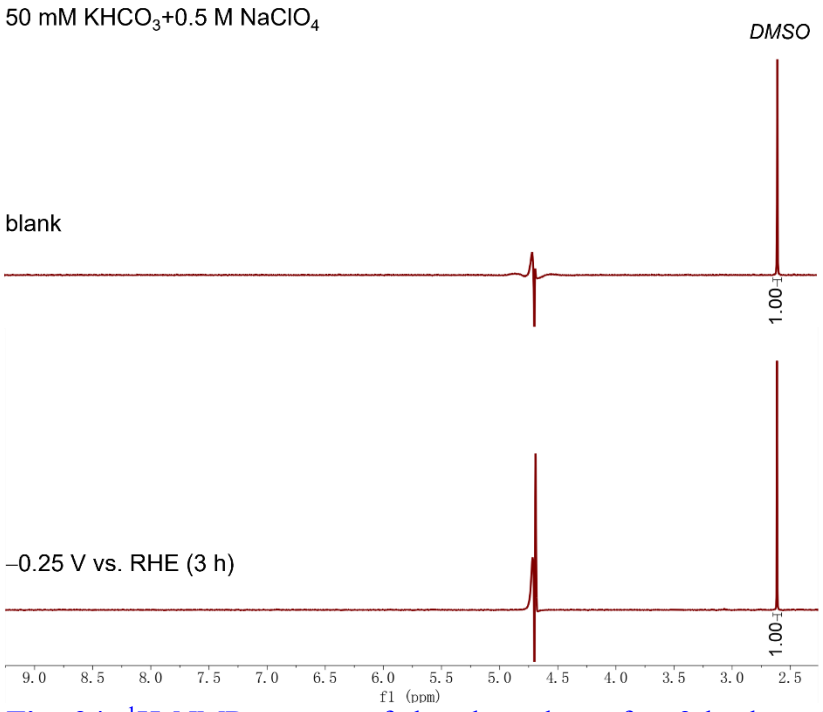

Supplementary Fig. 24. ^{1}H NMR spectra of the electrolyte after 3-h electrolysis in 50 mM $KHCO_3$ + 0.5 M $NaClO_4$ at −0.25 V vs. RHE (Ar, j_{HER} = −10 mA cm^{-2}).

In addition to the above major concerns, several technical issues should also be clarified:
1. In Supplementary Figure S1, the cyclic voltammetry curves in panel b show only a very small difference between the scan rates of 100 mV s^{-1} and 200 mV s^{-1}, whereas in panel c the calculated capacitance values differ significantly. The reviewer suggests that the authors provide the raw current values corresponding to each scan rate or label the current values directly in panel b. Furthermore, the data in panel c appear not strictly linear. It should also be noted that the double-layer capacitance of smooth metal foils is typically around ~30 uF cm^{-2}, whereas the value reported here is approximately 120 uF cm^{-2}. The authors should explain the origin of this discrepancy.
Response: We thank the reviewer for this careful comment regarding the capacitance analysis in **Supplementary Fig. 1**. In response, we have re-measured the double-layer capacitance and revised **Supplementary Fig. 1** accordingly. The corresponding capacitive current values at each scan rate are now provided in **Supplementary Tables 1 and 2**. The updated linear fitting now shows excellent linearity with an R^2 value of 0.99, indicating reliable capacitance estimation within the investigated scan-rate range. Regarding the capacitance magnitude, we note that the commonly referenced ~30 μF cm^{-2} value typically corresponds to ideally smooth metallic surfaces. In contrast, the commercial Pd foil used in this study is not atomically flat. As shown in the SEM image in **Supplementary Fig. 42**, the Pd foil surface contains noticeable microscopic surface roughness rather than an ideally planar morphology. Such surface roughness can increase the apparent electrochemically active surface area and consequently lead to higher measured capacitance values relative to ideal smooth-metal benchmarks. A corresponding explanation has now been added following the ECSA measurement section in the revised Supplementary Information. We have added the revised fitting results, raw current values, and corresponding discussion to the revised Supplementary Information (**Supplementary Fig. 1** and **Supplementary Tables 1** and **2**).

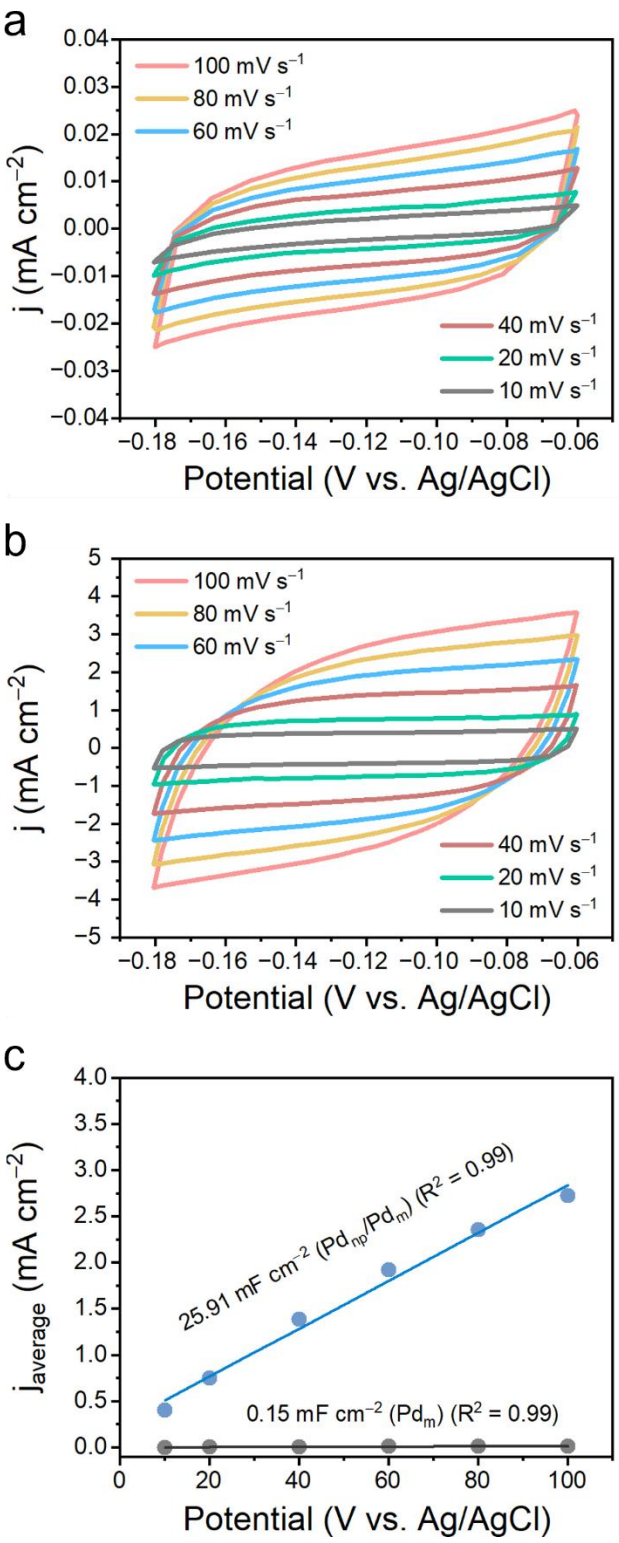

Supplementary Fig. 1. (a) CV curves of the Pd_m electrode collected in the non-Faraday region at different scan rates. (b) CV curves of the Pd_{np}/Pd_m electrode collected in the non-Faraday region at different scan rates. (c) ECSA (electrochemical surface area) of Pd_m and Pd_{np}/Pd_m.

Supplementary Table 1. Current density values from Supplementary Fig. 1a

Scan rate (mV s^{-1})	Average current density (mA cm^{-2})
10	0.0022
20	0.0041
40	0.0075
60	0.0105
80	0.0134
100	0.0157

Supplementary Table 2. Current density values from Supplementary Fig. 1b

Scan rate (mV s^{-1})	Average current density (mA cm^{-2})
10	0.4035
20	0.7529
40	1.3908
60	1.9232
80	2.3570
100	2.7249

2. In Supplementary Figure S2, the open circuit potential varies significantly under different conditions. The authors should provide a more detailed explanation of the factors responsible for these OCP shifts.

Response: As shown in **Supplementary Fig. 3**, the OCP value is governed by two variables: (i) the gas atmosphere (Ar vs CO_2) and (ii) the state of the Pd membrane (metallic Pd vs Pd–H). In the J-Pd_m system, the HER and CO_2ER chambers are operated using electrically independent polarization circuits and are separated by the Pd membrane, and OCP is measured at the CO_2-facing side under open-circuit conditions. Under j_{HER} = 0 mA cm^{-2}, the Pd membrane remains in a predominantly metallic Pd state, giving an OCP of ~0.8–0.9 V vs. RHE. Switching between Ar and CO_2 induces a small OCP shift due to the decrease in solution pH upon CO_2 saturation, consistent with the behavior reported in the literature (Joule 2024, 8, 728–745). When the HER side is polarized at j_{HER} = −10 mA cm^{-2} prior to OCP measurement, hydrogen generated in the HER compartment permeates through the Pd membrane, forming a Pd–H phase, as confirmed by XRD (**Supplementary Fig. 43**). This increases the hydrogen chemical potential within the Pd lattice and shifts the interfacial state at the CO_2-facing side, resulting in a lower OCP approaching ~0 V vs. RHE, consistent with a Pd–H-dominated equilibrium. Therefore, the OCP variations directly reflect the change in the Pd membrane state between metallic Pd and Pd–H, together with minor perturbations from CO_2-induced solution speciation effects. We have clarified this

discussion in the revised Supplementary Information and cited the corresponding reference in the revised manuscript.

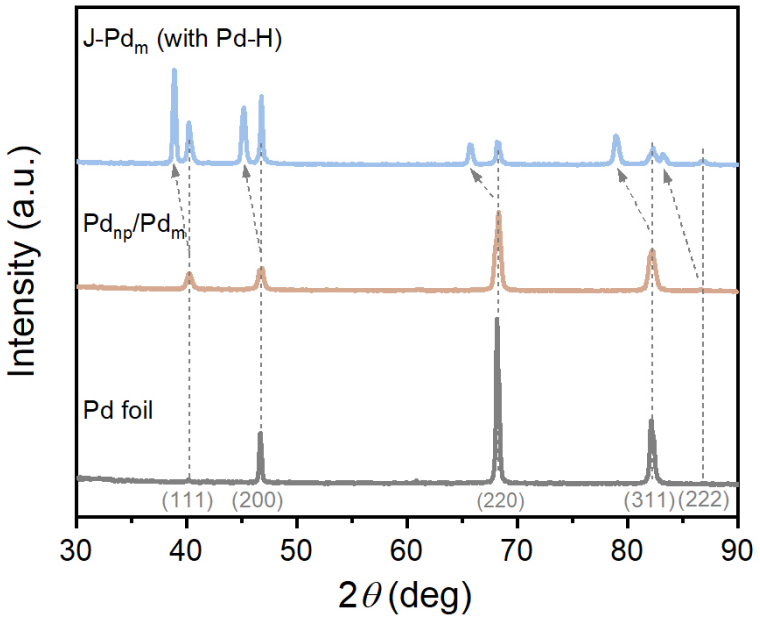

Supplementary Fig. 43. X-ray diffraction patterns of the Pd membrane (Pd_{np}/Pd_m) before and after hydrogen permeation.

3. In lines 162–163, the authors attribute the decrease in formate FE at j_{HER} = −50 mA cm^{-2} to hydrogen bubble accumulation affecting CO_2 transport. However, CO_2RR in H-cells is typically mass transport limited at much lower currents. The reviewer would like to know whether the cell design used in this study has any special features that enable such current densities. If so, the authors should provide either a photograph or a schematic illustration of the experimental setup.

Response: We agree that CO_2 reduction in conventional H-cell configurations is often limited by CO_2 mass transport at relatively low current densities. In the present system, however, the high current densities discussed in the manuscript refer specifically to the HER-side current density (j_{HER}), rather than the effective current density in the CO_2ER compartment. The HER and CO_2ER chambers are separated by the Janus Pd membrane and operated using electrically independent polarization circuits. In this dual-chamber configuration, the HER compartment primarily serves as a hydrogen-source chamber to continuously drive hydrogen permeation through the Pd membrane, thereby sustaining Pd–H species at the CO_2ER-side interface where hydride transfer occurs. Accordingly, the HER-side current density reflects the hydrogen supply rate rather than the effective CO_2 reduction current density at the reaction interface. The corresponding current densities measured in the CO_2ER compartment are also provided in **Supplementary Tables 3, 4 and 7–9**. Under high j_{HER} conditions (e.g., −50 mA cm^{-2}), increased hydrogen permeation and bubble accumulation near the membrane interface can partially hinder local CO_2 transport and electrolyte contact at the CO_2-facing side of the membrane, leading to the observed decrease in formate Faradaic efficiency. To clarify the experimental configuration and operating principle, we have now added detailed annotated schematic illustrations based on photographs of the H-cell setup in the revised Supplementary Information (**Supplementary Figs. 4 and 44**). The revised schematics explicitly illustrate the dual independent polarization circuits, chamber geometry,

membrane configuration, electrode arrangement, and the spatially separated HER and CO_2ER processes in the J-Pd_m system.

Supplementary Table 3. Summary of current density values in Fig. 2b.

Potential (V vs. RHE)	CO_2ER chamber current density (mA cm^{-2})
–0.15	–0.56
–0.25	–2.27
–0.35	–2.48
–0.45	–4.13

Supplementary Table 4. Summary of current density values in Fig. 2d.

j_{HER} (mA cm^{-2})	CO_2ER chamber current density (mA cm^{-2})
–1	–1.48
–5	–2.79
–10	–2.27
–50	–1.36

Supplementary Table 7. Summary of current density values in Fig. 2e.

j_{HER}: 0 mA cm^{-2}		j_{HER}: –10 mA cm^{-2}	
Electrolyte	CO_2ER chamber current density (mA cm^{-2})	Electrolyte	CO_2ER chamber current density (mA cm^{-2})
0.5 M $KHCO_3$	–2.01	0.5 M $KHCO_3$	–3.33
0.5 M $NaClO_4$	–1.27	0.5 M $NaClO_4$	–0.64
50 mM $KHCO_3$, 0.5 M $NaClO_4$	–2.46	50 mM $KHCO_3$, 0.5 M $NaClO_4$	–2.27

Supplementary Table 8. Summary of current density values in Fig. 2f.

j_{HER}: 0 mA cm^{-2}		j_{HER}: –10 mA cm^{-2}	
Electrolyte	CO_2ER chamber current density (mA cm^{-2})	Electrolyte	CO_2ER chamber current density (mA cm^{-2})
50 mM $NaHCO_3$, 0.5 M $NaClO_4$	–2.44	50 mM $NaHCO_3$, 0.5 M $NaClO_4$	–1.00
50 mM $KHCO_3$, 0.5 M $NaClO_4$	–2.46	50 mM $KHCO_3$, 0.5 M $NaClO_4$	–2.27
50 mM $CsHCO_3$, 0.5 M $NaClO_4$	–2.10	50 mM $CsHCO_3$, 0.5 M $NaClO_4$	–1.02

Supplementary Table 9. Summary of current density values in Fig. 3b.

Potential (V vs. RHE)	CO_2ER chamber current density (mA cm^{-2})
–0.15	–0.38
–0.25	–2.58
–0.35	–4.41
–0.45	–3.85

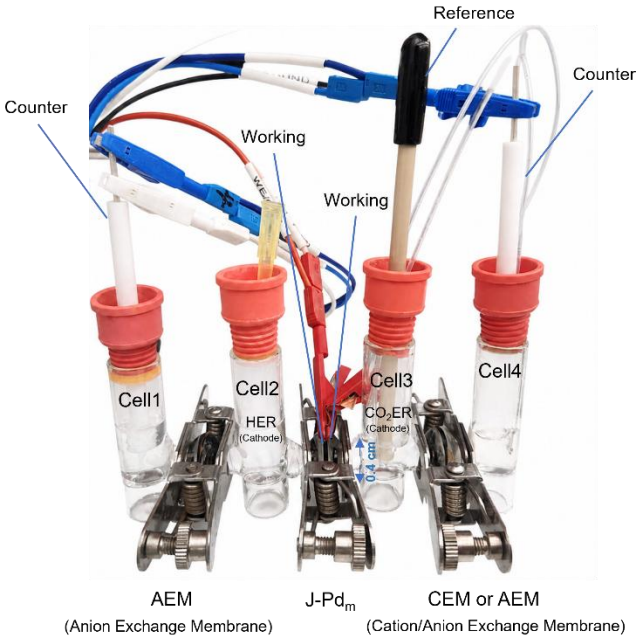

Supplementary Fig. 4. Experimental cell assembly used for the small-area J-Pd_m (0.125 cm^2).

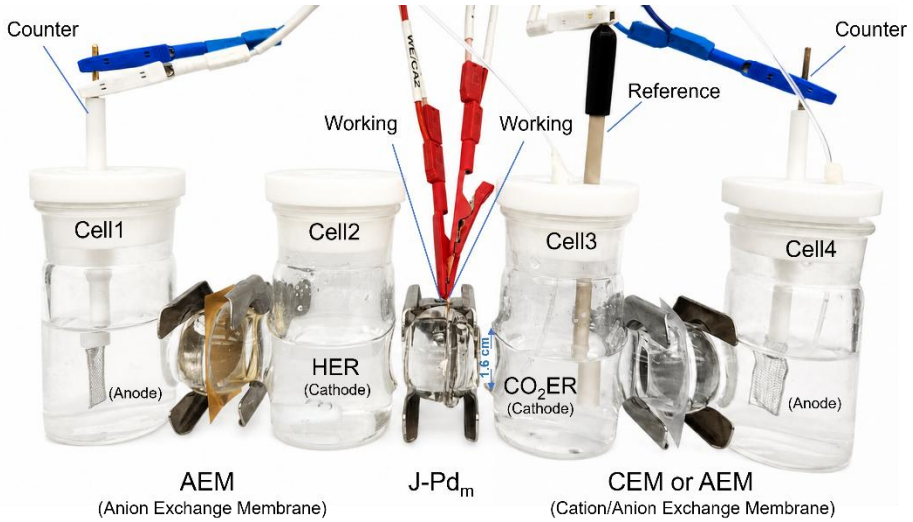

Supplementary Fig. 44. Experimental cell assembly used for the large-area J-Pd_m (2 cm^2).

4. In lines 192–196 (Figure S17), when no potential is applied on the CO_2RR side but j_{HER} = −10 mA cm^{-2} is applied in the HER chamber, almost no formate is produced. The authors should clarify whether Pd-H species exist on the CO_2RR side under this condition. If Pd-H is present, it would be useful to explain why hydride transfer to CO_2 does not occur or what competing processes dominate.

Response: Under the condition where j_{HER} = −10 mA cm^{-2} is applied in the HER chamber while no external potential is applied on the CO_2RR side (essentially as an ePMR configuration), hydrogen generated on the HER side can still permeate through the Pd membrane and populate the CO_2-facing surface with Pd–H species. Therefore, the CO_2-facing Pd surface is indeed expected to remain hydrogen-rich under these conditions. However, the absence of cathodic polarization on the CO_2RR side fundamentally alters the reactivity of these hydrogen species. Previous studies have shown that protic solvents such as water can facilitate disproportionation of surface Pd–H species, enabling limited hydride-transfer reactivity at Pd interfaces (J. Am. Chem. Soc. 2025, 147, 10974−10980; JACS Au 2024, 4, 328−343; Chem. Sci. 2026, 17, 1039–1050). Nevertheless, spontaneous generation of sufficiently hydridic Pd–H species remains inefficient, and hydride transfer to CO_2 is kinetically slow (J. Am. Chem. Soc. 2023, 145, 14316−14323). As a result, although small amounts of formate can still be generated under these open-circuit conditions, the majority of permeated hydrogen species preferentially undergo recombination/desorption to release H_2. Consistent with this interpretation, GC analysis (**Supplementary Fig. 60**) of the CO_2RR chamber confirms substantial H_2 evolution under these conditions in both aqueous electrolyte and acetonitrile, indicating that most permeated hydrogen species are released as H_2 rather than participating in productive hydride transfer to CO_2.

In addition, hydride-mediated CO_2-to-formate conversion is thermodynamically demanding in both aqueous and aprotic media. The hydride transfer to CO_2 is thermodynamically constrained by the hydricity of formate, which is approximately 24.1 kcal mol^{-1} in water and 44 kcal mol^{-1} in acetonitrile, requiring Pd–H species with sufficiently strong hydride-donating ability to enable formate formation (Acc. Chem. Res. 2024, 57, 3488–3499). These considerations highlight that controllable hydride transfer to CO_2 is non-trivial in either solvent environment. A key advantage of the J-Pd_m configuration is that independent polarization of the CO_2-facing interface enables electrochemical tuning of the Pd–H hydricity, thereby substantially enhancing hydride-transfer reactivity and significantly increasing formate production efficiency relative to the unbiased ePMR condition. This distinction becomes even more evident in fully aprotic organic electrolytes. In acetonitrile, spontaneous formation of hydridic Pd–H species is strongly disfavored under open-circuit conditions, and no detectable formate products were observed without polarization on the CO_2RR side. In contrast, the J-Pd_m configuration enables electrochemically controlled hydricity sufficient to drive hydride transfer to CO_2 even in fully aprotic media.

To further support this mechanistic interpretation, we performed additional ePMR control experiments in both aqueous and aprotic electrolytes under conditions where the CO_2RR side remained unpolarized while j_{HER} values of −10, −50, and −100 mA cm^{-2} were applied in the HER chamber (**Supplementary Figs. 47** and **61**). In aqueous electrolytes, small but detectable amounts of formate were observed, whereas no formate was detected in acetonitrile. Together, these results indicate that although Pd–H species are present on the CO_2-facing surface under asymmetric polarization, the absence of independent polarization on the CO_2RR side results in insufficient hydride-transfer reactivity for efficient CO_2 reduction.

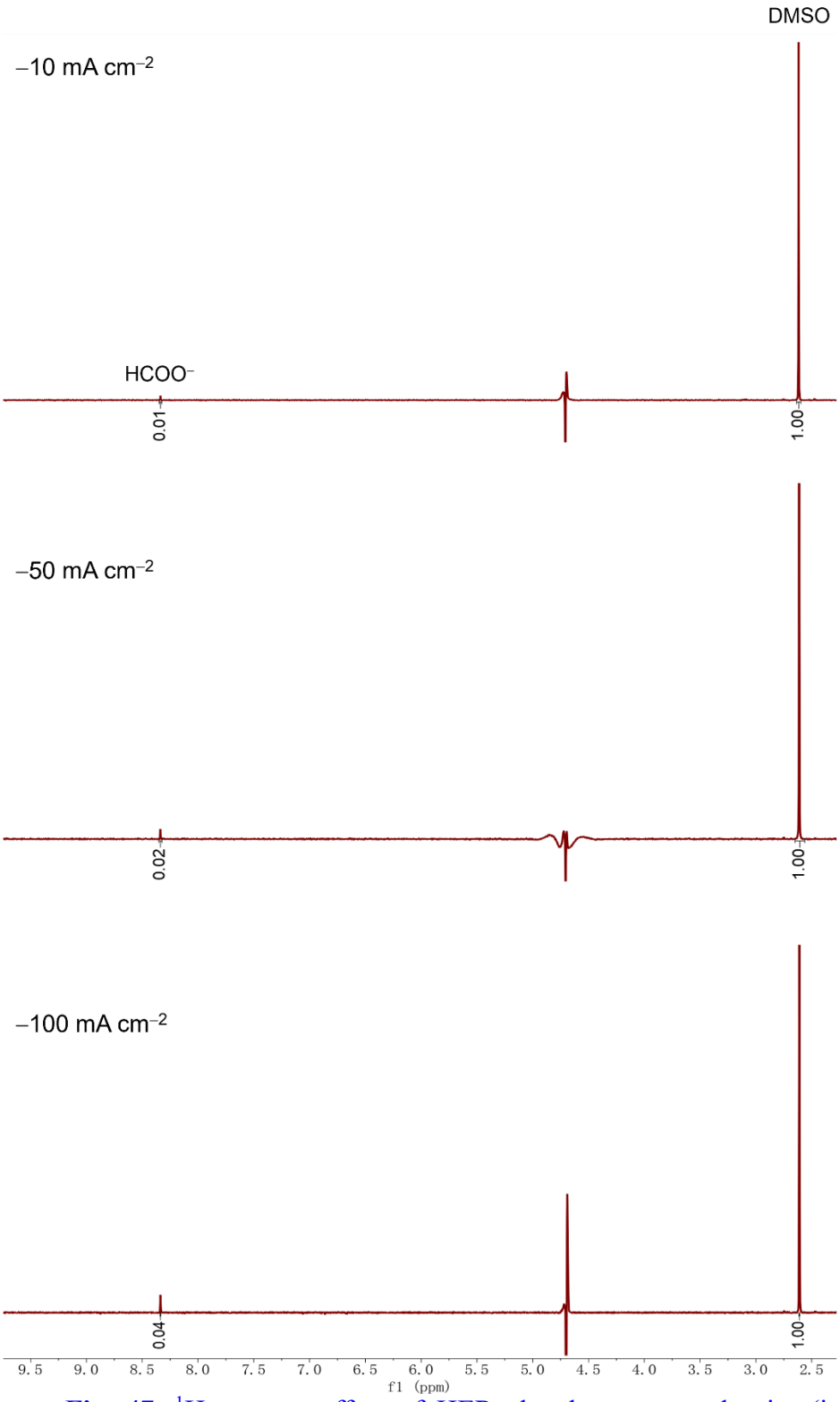

Supplementary Fig. 47. ^{1}H spectra: effect of HER chamber current density (j_{HER}) on CO_2 reduction performance after a 3-h reaction under conditions without potential applied to the CO_2ER chamber with 50 mM $KHCO_3$ and 0.5 M $NaClO_4$ in water (Pd_{np}/Pd_m :2 cm^2).

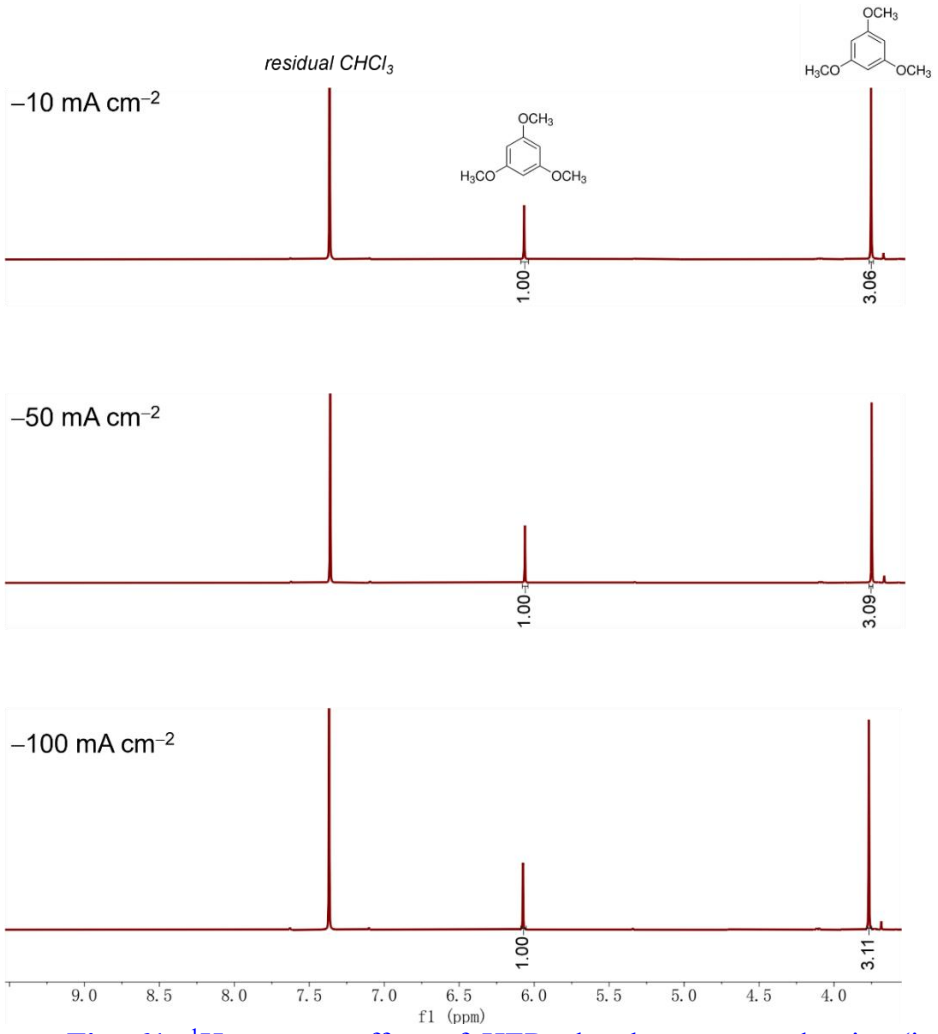

Supplementary Fig. 61. ^{1}H spectra: effect of HER chamber current density (j_{HER}) on CO_2 reduction performance after 6-h reaction under conditions without potential applied to the CO_2ER chamber with 0.1 M $TBABF_4$ inCH_3CN.

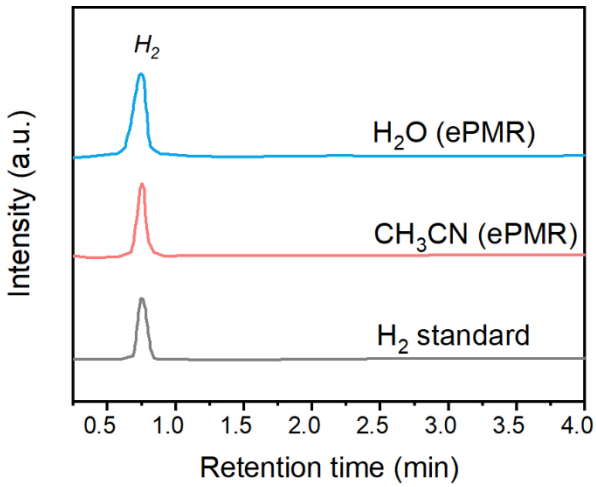

Supplementary Fig. 60. GC detection of H_2 generated in the CO_2ER chamber using the ePMR configuration in H_2O and CH_3CN.

5. In several figures (for example Figure 2b, 2d, 2e, 2f and Figure 3b), only FE values are reported, while the corresponding current densities are not shown. Providing the actual current values would help readers better evaluate the catalytic performance.

Response: In the original manuscript, we primarily focused on Faradaic efficiency to emphasize the selectivity changes associated with the proposed heterogeneous hydride-transfer pathway. However, we agree that the corresponding current densities are also important for assessing the overall catalytic activity and reaction rates. In response to the reviewer's comment, we have now added tables summarizing the corresponding current densities for **Figures 2b, 2d, 2e, 2f,** and **Figure 3b** in the revised Supplementary Information (**Supplementary Tables 3, 4** and **7–9**). These tables include the relevant current density data associated with the reported Faradaic efficiencies and provide a more comprehensive comparison of catalytic performance under different operating conditions.

6. In Figure 3b, the formate FE at −0.15 V appears higher than that reported in Figure 2b, while the value at −0.25 V appears lower. The origin of this discrepancy should be clarified. In addition, because the isotope labeling experiment involves hydrogen and deuterium sources, it would be helpful if the authors could also report the FE of H_2, HD, and D_2.

Response: We thank the reviewer for carefully noting the discrepancy between the formate FE values at −0.15 V in **Fig. 2b** and **Fig. 3b** and for suggesting that the isotope-labeling data be complemented with information on the gaseous products. First, regarding the formate FE at −0.15 V vs RHE, we have repeated the measurements under conditions identical to those used in the isotope-labeling experiments. At −0.15 V, the current density on the CO_2ER side is very low (**Supplementary Table 3**). Under such low-current conditions, if CO_2 is introduced into the CO_2ER chamber before the HER current applied in the HER chamber, transient interfacial accumulation of CO_2 can occur at the Pd membrane surface, which affects the accessibility of interfacial Pd–H species for hydride-transfer reactions. At more negative potentials, where CO_2 consumption is rapid, this effect becomes negligible. To minimize this effect and ensure consistent interfacial conditions, we repeated the −0.15 V experiments by first applying the HER-side current for 10 min to establish steady hydrogen permeation and subsequently introducing CO_2 into the CO_2ER chamber. Under these conditions, the formate Faradaic efficiency at −0.15 V, calculated using the hydride-pathway (one-electron) convention, reaches 89%, in good agreement with the value reported in **Fig. 3b**. We have updated **Fig. 2b** and the corresponding text accordingly.

Second, for the isotope-labeling experiments, ^{2}H NMR (**Fig. 3e** and **Supplementary Fig. 30**) shows that the major liquid product is deuterated formate ($DCOO^-$). Regarding gaseous products, D_2 originates from D_2O reduction in the HER chamber to generate D atoms, which permeate through the Pd membrane and recombine to release D_2 on the CO_2ER side. This process supplies deuterium to the membrane but does not directly participate in CO_2 reduction in the CO_2ER compartment.

On the CO_2-facing side, the relevant competing pathways include (i) coupling between Pd–D species (D^-) and protons (H^+) to form HD, and (ii) direct proton reduction to H_2. To distinguish these pathways, isotope ratio mass spectrometry (IRMS) was performed (**Fig. 4b**). The results show only HD formation with no detectable H_2, indicating that protons preferentially react with Pd–D species rather than undergoing PCET to form H_2.

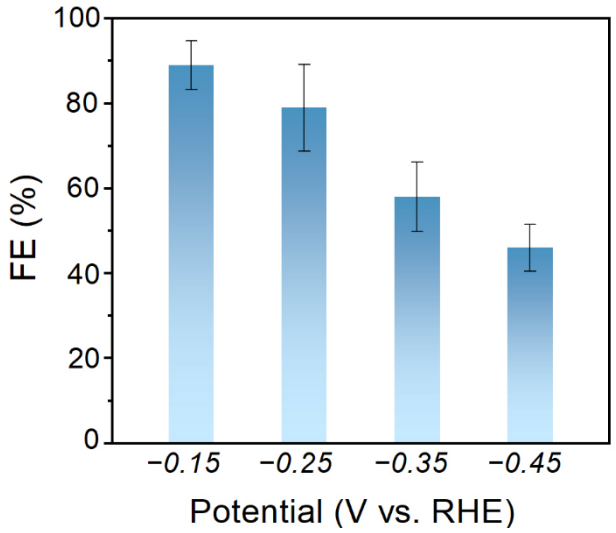

Fig. 2b. Faradaic efficiencies of formate production after 3-h electrolysis at various applied potentials in the CO_2ER chamber with j_{HER} = –10 mA cm^{-2} in the HER chamber.

7. In Figure 5e, the experiments are conducted in acetonitrile. The reviewer would like to know whether any water is present in the electrolyte. If CO is produced through CO_2 reduction, the hydrogen required for the reaction must originate from some source. The authors should clarify the origin of hydrogen in this system. In addition, if hydrogen evolution occurs, the reviewer wonders whether a signal near a retention time of approximately 1 min appears in the GC analysis. In Figure 5f, CO is detected by GC, yet Pd surfaces are known to strongly adsorb CO. The authors should therefore explain why no *CO signal is observed in the IR spectra.

Response: We thank the reviewer for these important questions regarding the role of residual water, the origin of hydrogen in the aprotic acetonitrile system, and the absence of observable *CO signals in the operando IR measurements. First, no water was intentionally added to the acetonitrile electrolyte used in this study. To experimentally evaluate the possible presence and influence of residual water, we performed additional control experiments using acetonitrile electrolytes containing intentionally added 0.1% H_2O and 1% H_2O. Specifically, LSV measurements were conducted in Ar-saturated acetonitrile electrolytes using the original electrolyte, the 0.1% H_2O-containing electrolyte, and the 1% H_2O-containing electrolyte. Upon addition of 0.1% H_2O, noticeably increased cathodic currents were observed, while 1% H_2O produced substantially larger reduction currents at significantly more positive potentials (**Supplementary Fig. 52**). In parallel, ^{1}H NMR spectra of the three electrolyte systems revealed only an extremely weak residual water signal in the original electrolyte, substantially smaller than that observed in the 0.1% H_2O-containing sample (**Supplementary Fig. 53**). Together with the electrochemical results, these observations indicate that the water content in the original acetonitrile electrolyte is negligible and well below the 0.1% level (<1000 ppm).

Regarding the origin of hydrogen in the aprotic CO_2ER chamber, the reactor architecture has now been clarified in **Supplementary Fig. 44**. The experiments were performed using a four-compartment H-cell configuration, where Cells 1 and 2 were used for electrochemical hydrogen generation, while Cells 3 and 4 were used for CO_2 reduction. The Pd membrane separates Cells 2 and 3, with HER occurring on one side of the Pd membrane and CO_2ER occurring on the opposite side. Hydrogen generated from the HER side permeates through the Pd membrane and forms

surface Pd–H species at the CO_2-facing interface. Therefore, the Pd membrane completely separates the aqueous and organic phases while continuously supplying hydrogen species into the aprotic organic electrolyte without direct proton participation, as illustrated in **Fig. 1c**. When no cathodic polarization was applied on the CO_2ER side of the J-Pd_m system, the permeated hydrogen species preferentially recombine and form H_2. Correspondingly, permeated H_2 was directly detected by GC in the CO_2ER chamber (**Supplementary Fig. 59**).

Regarding the absence of observable *CO signals in the operando IR spectra, we agree that CO can strongly adsorb on Pd surfaces under aqueous conditions and poison Pd catalysts. However, previous studies have shown that, in acetonitrile, solvent–Pd interactions substantially weaken CO adsorption on Pd surfaces compared with that in aqueous media (J. Phys. Chem. C 2023, 127, 14518–14527; ACS Catal. 2023, 13, 5780–5786; ACS Catal. 2016, 6, 2382–2392). To further verify this effect, we performed comparative operando IR experiments in aqueous electrolyte and acetonitrile. In both systems, CO was first introduced to saturate the Pd surface, followed immediately by switching to Ar flow. In aqueous electrolyte, the adsorbed CO signal on Pd remained essentially unchanged with time, indicating strong CO adsorption. In contrast, in acetonitrile, the *CO signal continuously decreased with time, demonstrating substantially weaker CO adsorption on the Pd surface (**Supplementary Fig. 64**). This behavior explains why gaseous CO can still be detected by GC during electrolysis, whereas no stable *CO signal is observable in the operando IR spectra under acetonitrile conditions, consistent with previous reports for CO_2 reduction in acetonitrile-based electrolytes (J. Phys. Chem. C 2023, 127, 14518–14527).

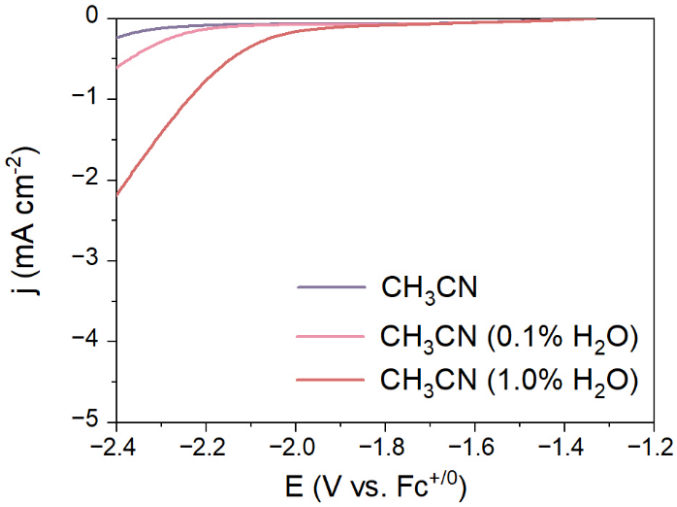

Supplementary Fig. 52. Linear sweep voltammograms of acetonitrile electrolytes with the controlled amounts of water: pristine 0.1 M $TBABF_4/CH_3CN$, with 0.1% H_2O addition, and with 1% H_2O addition.

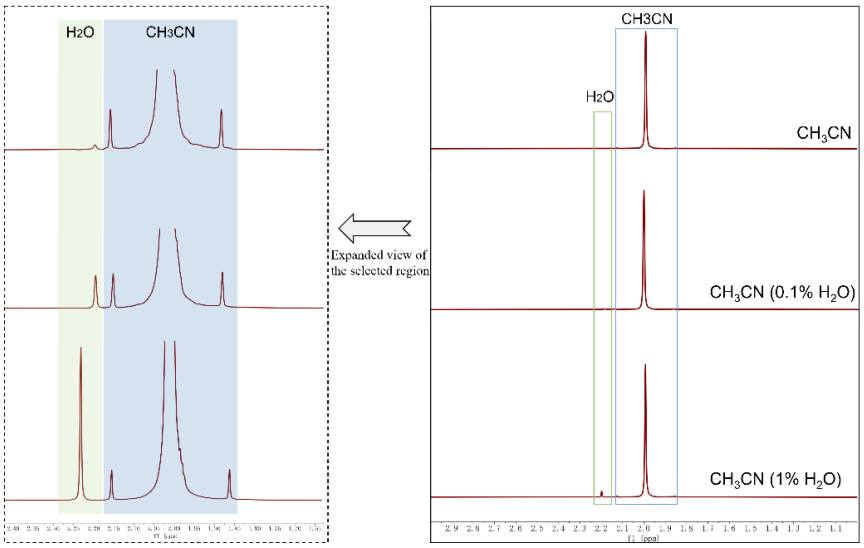

Supplementary Fig. 53. ^{1}H NMR spectra of three acetonitrile electrolytes: pristine 0.1 M $TBABF_4/CH_3CN$, with 0.1% H_2O addition, and with 1% H_2O addition.

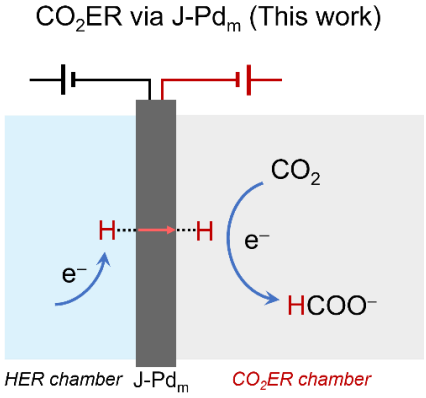

Fig. 1c. Our design of Janus palladium membrane electrode for the selective CO_2 reduction to formate via heterogeneous hydride transfer.

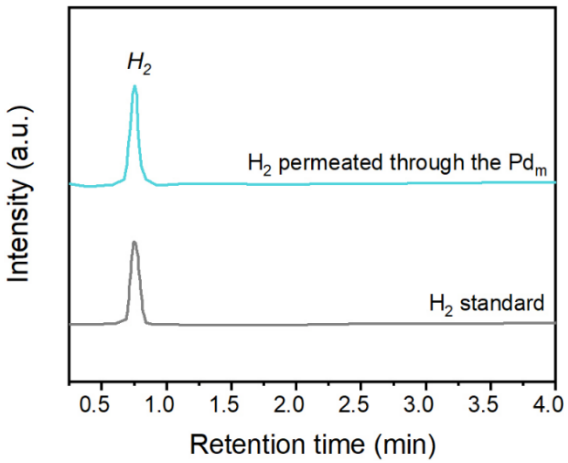

Supplementary Fig. 59. Hydrogen permeation test of a Pd membrane in acetonitrile: GC detection of H_2 in the CO_2ER chamber.

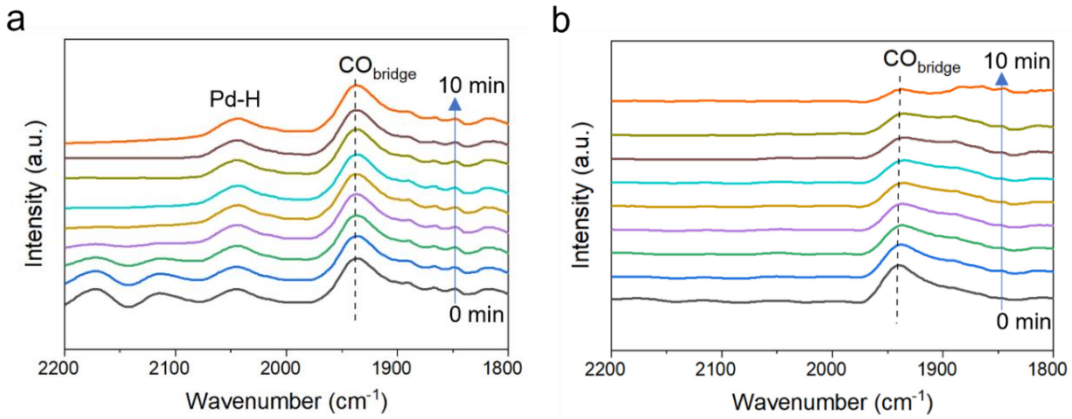

Supplementary Fig. 64. *In situ* ATR-SEIRAS spectra of adsorbed CO species on the Pd electrode in (a) H_2O and (b) CH_3CN.

8. The stability of acetonitrile within the applied potential window should also be discussed. Specifically, the authors should clarify whether acetonitrile remains electrochemically stable in the tested potential range and whether it could react with Pd-H species.

Response: The electrochemical stability of the acetonitrile electrolyte was carefully evaluated under our experimental conditions. As shown in the LSV measurements in **Fig. 5b**, regardless of whether hydrogen permeation was enabled from the HER chamber, no significant cathodic current associated with electrolyte reduction was observed within the potential range employed for CO_2 reduction (−1.65 to −2.05 V vs. $Fc^{+/0}$). To further verify electrolyte stability, additional control potential electrolysis experiments were performed under Ar atmosphere on the CO_2-facing side while maintaining $j_{HER} = -10$ mA cm^{-2} in the HER chamber. Electrolysis was conducted at −1.75, −2.05, −2.25, and −2.45 V vs. $Fc^{+/0}$ (**Supplementary Fig. 57**). Negligible reduction current was observed up to −2.25 V vs. $Fc^{+/0}$, whereas cathodic electrolyte decomposition current only became apparent at −2.45 V vs. $Fc^{+/0}$. These results confirm that the potential window used in **Fig. 5c** lies within the electrochemically stable region of the acetonitrile electrolyte. These results support that acetonitrile remains electrochemically stable and does not interfere with the Pd–H-mediated CO_2-to-formate conversion under the operating conditions employed in this study. We have clarified this discussion and added the corresponding control data in the revised manuscript and Supplementary Information.

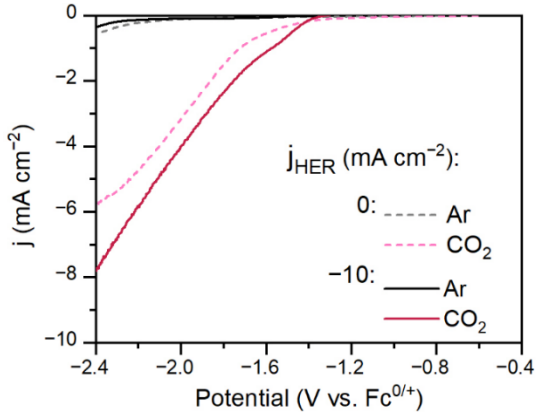

Fig. 5b. Linear sweep voltammograms collected on the CO_2ER side of J-Pd_m in an either Ar- or CO_2-saturated acetonitrile electrolyte, together with or without $j_{HER} = -10$ mA cm^{-2} applied on the HER side.

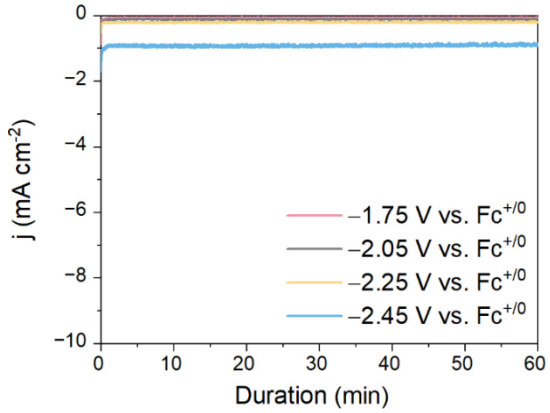

Supplementary Fig. 57. I–t curve for the stability test of the 0.1 M $TBABF_4/CH_3CN$ electrolyte at $j_{HER} = -10$ mA cm^{-2} (Ar).

9. In Supplementary Figure S8, the numbering appears to contain a typographical error and the label "8" is missing.

Response: We thank the reviewer for pointing out this typographical error. We apologize for the oversight. In the original Supplementary Information, "**Supplementary Fig. 7**" was inadvertently written as "Supplementary Fig. S". This typo has now been corrected in the revised Supplementary Information.

10. The manuscript would benefit from a more detailed description of the proposed mechanism for formate formation via Pd-H. In particular, the authors should clarify whether the key elementary step is $H^- + CO_2 \rightarrow HCOO^-$, whether CO_2 adsorption on Pd precedes hydride transfer, and how this pathway differs mechanistically from conventional surface hydrogenation reactions.

Response: We thank the reviewer for this important comment regarding the mechanistic description of the Pd–H-mediated CO_2-to-formate conversion pathway. In the J-Pd_m system, we propose that CO_2-to-formate conversion proceeds through an interfacial Pd–H-mediated heterogeneous hydride transfer process occurring at the polarized CO_2-facing interface. In this heterogeneous regime, "hydride transfer" does not imply the generation of a free solvated H^- species in solution. Rather, consistent with established descriptions of metal–hydride chemistry at electrified interfaces (Nat. Catal. 2023, 6, 351–362), hydrogen is transferred from polarized Pd–H species as a hydride equivalent within the electrical double layer.

In our experiments, hydrogen permeation from the HER side is first established to generate a hydride-rich Pd–H state throughout the Pd membrane prior to CO_2 introduction. CO_2 is then introduced to the CO_2-facing chamber while cathodic polarization is applied at the CO_2-facing interface, with continuous hydrogen supply within the Pd membrane. Under these operating conditions, the reaction therefore occurs at a pre-established Pd–H-rich polarized interface rather than through conventional sequential surface hydrogenation involving independently generated adsorbed H* species. Accordingly, the overall interfacial step may be formally represented as: Pd–H + CO_2 + e^- → $HCOO^-$ + Pd. Importantly, this mechanism differs substantially from conventional surface hydrogenation pathways. In the absence of cathodic polarization on the CO_2-facing side (ePMR), only trace formate formation is observed in aqueous electrolyte, while no detectable formate is observed in aprotic acetonitrile conditions (**Supplementary Figs. 47** and **61**). By contrast, the J-Pd_m system enables efficient CO_2-to-formate conversion under identical

hydrogen-permeation conditions once cathodic polarization is applied at the CO_2-facing interface (**Supplementary Figs. 45, 46, 62** and **63**), highlighting the essential role of polarization-controlled Pd–H hydride-transfer reactivity.

To further substantiate the hydride-transfer capability of the J-Pd_m interface, we investigated the hydrogenation of BIM^+ (1,3-dimethyl-2-phenyl-1H-benzo[d]imidazol-3-ium), a well-established molecular hydride acceptor, using J-Pd_m (**Supplementary Figs. 67** and **68**). Upon hydride transfer, BIM^+ is converted to the corresponding hydride donor BIMH (1,3-dimethyl-2-phenyl-2,3-dihydro-1H-benzo[d]imidazole), which possesses a reported hydricity of approximately 50 kcal mol^{-1} in acetonitrile (*Nat. Catal.*, 2023, 6, 351–362). As shown in the linear sweep voltammograms (**Supplementary Fig. 67**), when no HER current was applied on the HER side of J-Pd_m (j_{HER} = 0 mA cm^{-2}), BIM^+ reduction only commenced at approximately −1.9 V vs. $Fc^+/^0$, corresponding to its direct electron-transfer reduction. In contrast, when a HER current density of −10 mA cm^{-2} was applied on the HER side of J-Pd_m, the onset potential for BIM^+ conversion shifted anodically from approximately −1.9 V to −1.25 V vs. $Fc^+/^0$. This substantial anodic shift indicates that polarized Pd–H species participate directly in BIM^+ hydrogenation, thereby facilitating BIM^+ conversion at substantially less negative potentials. Further scanning toward more negative potentials resulted in a current plateau, consistent with mass-transport limitation of BIM^+ in solution.

To further verify hydride transfer, controlled-potential electrolysis was performed using 10 mM BIM^+ at −1.4 V vs. $Fc^+/^0$ while maintaining a HER current density of −10 mA cm^{-2} on the HER side of J-Pd_m (**Supplementary Fig. 68**). After passing the theoretical charge required for complete conversion of BIM^+ through a one-electron hydride-transfer process in the HRR chamber, BIM^+ was quantitatively converted into BIMH, confirming that polarized Pd–H species are capable of mediating efficient heterogeneous hydride transfer. Importantly, the hydricity of formate in acetonitrile (~44 kcal mol^{-1}, *Acc. Chem. Res.*, 2024, 57, 3488–3499) is comparable to that of BIMH. The ability of J-Pd_m to generate BIMH through hydride transfer therefore supports the feasibility of Pd–H-mediated hydride-equivalent transfer to CO_2 under the conditions employed in this work, consistent with efficient CO_2-to-formate conversion observed in **Fig. 5**. Together, these results support a Pd–H-mediated interfacial hydride-transfer mechanism in the J-Pd_m system.

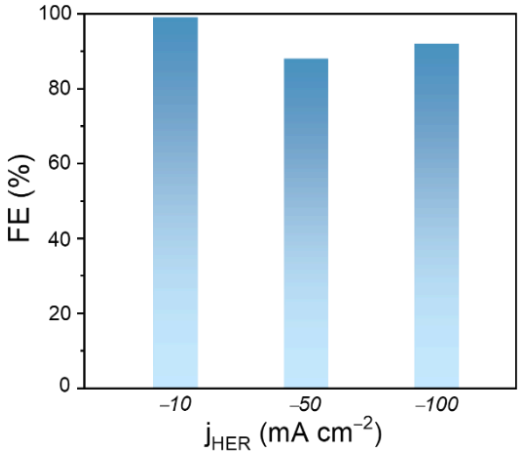

Supplementary Fig. 45. Faradaic efficiency of formate formation: effect of HER chamber current density (j_{HER}) on CO_2 reduction performance after a 3-h reaction at –0.25 V vs. RHE in the CO_2ER chamber (J-Pd_m system, 50 mM $KHCO_3$ + 0.5 M $NaClO_4$ (aq)), with Pd_{np}/Pd_m (2 cm^2).

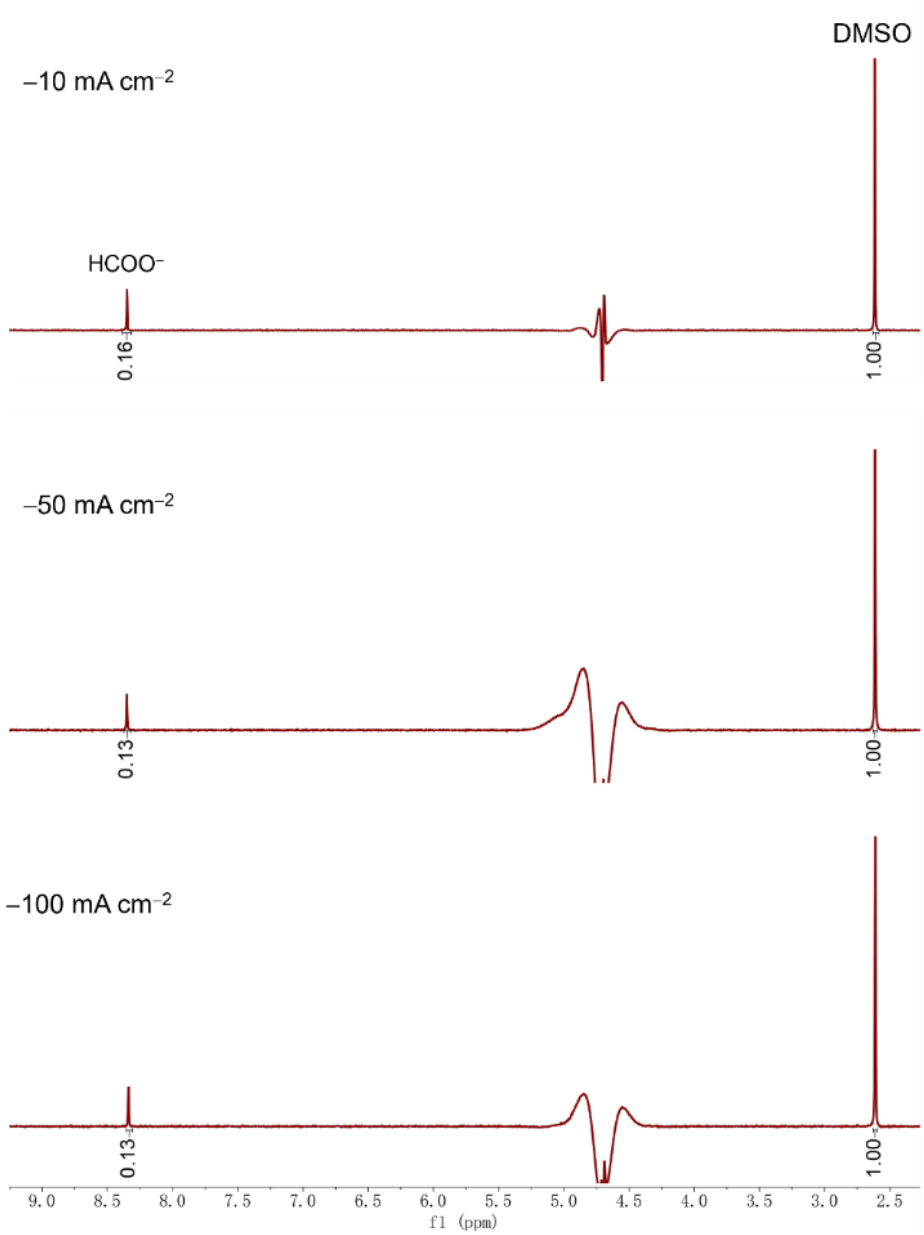

Supplementary Fig. 46. ^{1}H spectra: effect of HER chamber current density (j_{HER}) on CO_2 reduction performance after a 3-h reaction at –0.25 V vs. RHE in the CO_2ER chamber (J-Pd_m system, 50 mM $KHCO_3$ + 0.5 M $NaClO_4$ (aq)), with Pd_{np}/Pd_m (2 cm^2).

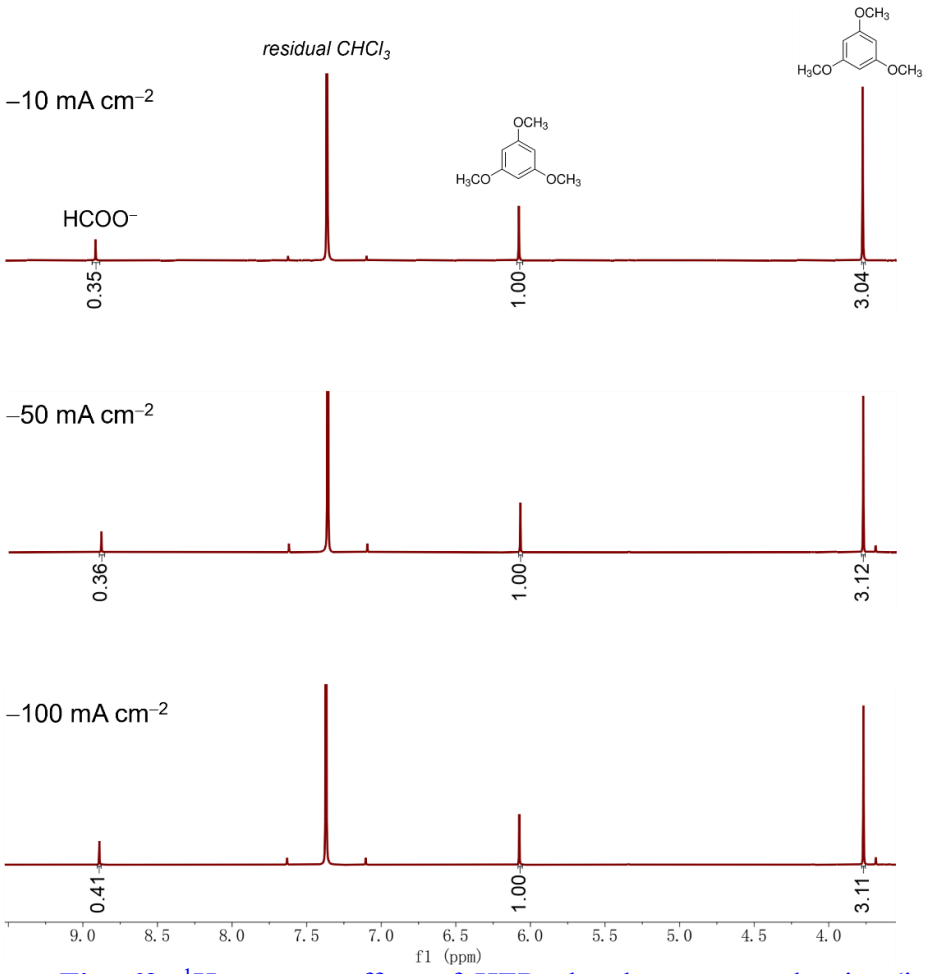

Supplementary Fig. 62. ^{1}H spectra: effect of HER chamber current density (j_{HER}) on CO_2 reduction performance for 6-h electrolysis at –1.75 V vs. $Fc^{+/0}$ in the CO_2ER chamber (J-Pd_m system, 0.1 M $TBABF_4/CH_3CN$).

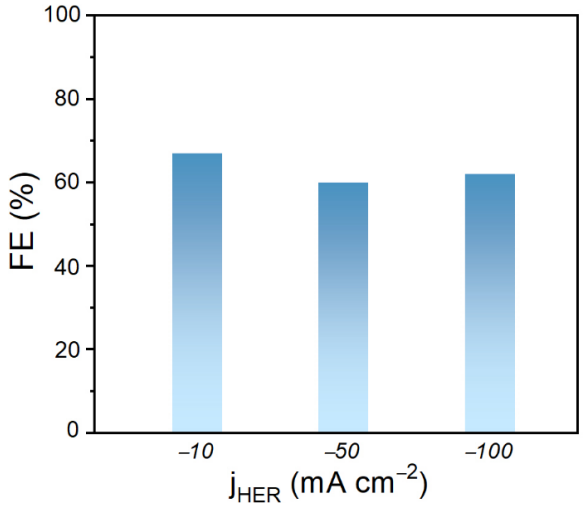

Supplementary Fig. 63. Faradaic efficiency of formate formation: effect of HER chamber current density (j_{HER}) on CO_2 reduction performance for 6-h electrolysis at –1.75 V vs. $Fc^{+/0}$ in the CO_2ER chamber (J-Pd_m system, 0.1 M $TBABF_4/CH_3CN$).

11. The supplementary materials provide SEM images of the electrode surface. To better illustrate the structural characteristics of the Janus design, the authors are encouraged to include cross-sectional SEM images of the electrode. Such images would help reveal the thickness of the deposited Pd layer and the structural relationship between the deposited Pd nanoparticles and the underlying Pd membrane.

Response: Following the reviewer's recommendation, we have added cross-sectional SEM characterization of the J-Pd_m electrode in the revised Supplementary Information (**Supplementary Fig. 2**). The cross-sectional images clearly reveal the structural relationship between the electrodeposited Pd nanoparticles and the underlying Pd foil substrate. The Pd foil possesses a thickness of approximately 25 μm, while the electrodeposited Pd nanoparticles are uniformly distributed on the Pd foil surface, forming a continuous and porous catalyst layer with a thickness of approximately 7–13 μm.

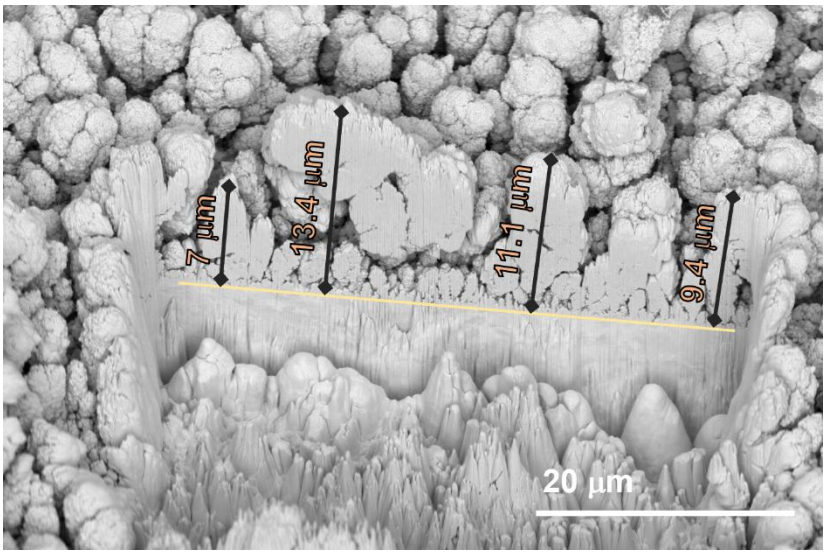

Supplementary Fig. 2. Cross-sectional SEM image of the J-Pd_m membrane, illustrating the porous layer of electrodeposited Pd nanoparticles on the dense Pd foil.

Reviewer #2

This manuscript by Sun and co-workers reports on a Janus palladium membrane electrode (J-Pd_m) that spatially separates hydrogen generation from CO_2 reduction and enables selective CO_2-to-formate conversion via heterogeneous hydride transfer. The authors claim that electrochemically tunable Pd–H hydricity allows the reaction to bypass the conventional proton-coupled electron transfer (PCET) paradigm. This concept is potentially innovative and interesting. However, several mechanistic claims do not have rigorous substantiation, and certain interpretations may be overstated relative to the evidence provided. Hence, this manuscript does not meet the requirement for publication in Nature Chemistry.

Response: We thank the reviewer for the careful evaluation of our work and for recognizing that this concept is potentially innovative and interesting. We appreciate the reviewer's comments regarding the mechanistic interpretation and the need for further clarification and more detailed substantiation. In response, we have revised the manuscript, added additional control experiments and quantitative analyses, and refined the mechanistic discussion to improve its consistency with the experimental evidence. We believe these revisions improve the clarity and consistency of the mechanistic description while maintaining the core experimental findings. Detailed point-by-point responses to each comment are provided below.

Specific questions and concerns are listed below.

1. Authors claim upon cathodic polarization on this CO_2-facing side of J-Pd_m, those permeated hydrogen atoms are reduced to hydride species that can undergo direct transfer to CO_2, leading to the production of formate.

A key mechanistic ambiguity arises from the fact that the observed reactivity does not necessarily require a true hydride transfer mechanism. Specifically, the authors propose that CO_2 reduction proceeds via direct hydride transfer from Pd–H^- to CO_2: Pd–H^- + CO_2 → $HCOO^-$. However, the experimental observations presented in the manuscript cannot rule out an alternative pathway in which hydrogenation occurs through a coupled electron–proton process involving neutral surface hydrogen: Pd–H + CO_2 + e^- → $HCOO^-$. In this scenario, the hydrogen atom originates from surface Pd–H, while the additional electron required for formate formation is directly from the electrode to electrochemically activated CO_2. As a result, the process would correspond to a surface hydrogenation coupled with electron transfer, rather than a genuine hydride transfer.

Because both pathways could produce identical isotopic labeling results and similar electrochemical signatures, the current evidence does not unambiguously distinguish between: hydride transfer: Pd–H^- + CO_2 → $HCOO^-$ and electron-assisted hydrogenation: Pd–H + CO_2 + e^- → $HCOO^-$. That is, an alternative mechanism involving neutral Pd–H reacting with an electrochemically activated CO_2 intermediate cannot be ruled out. Therefore, additional mechanistic evidence would be required to conclusively establish the proposed heterogeneous hydride transfer mechanism.

Response: We appreciate the reviewer's comment regarding the mechanistic distinction between a true hydride transfer process and an alternative electron-assisted hydrogenation pathway. To directly address whether hydride transfer and electron transfer occur as sequential steps, we performed control experiments in aprotic acetonitrile, where no proton-coupled electron transfer is possible. We employed two stepwise protocols: (i) CO_2-facing polarization at −1.75 V vs. $Fc^{+/0}$ for a defined period to enable electron transfer, followed by termination of this step, after which

hydrogen permeation from the HER chamber (ePMR, −10 mA cm^{-2}) was carried out for an equivalent time window (**Supplementary Fig. 65**); (ii) hydrogen permeation from the HER chamber (ePMR, −10 mA cm^{-2}) for a defined period, followed by termination of hydrogen permeation, after which the system was reconfigured using a fresh Pd membrane and electrochemical polarization at −1.75 V vs. $Fc^{+}/^{0}$ was applied for an equivalent time window (**Supplementary Fig. 66**). In both cases, no detectable formate formation was observed, indicating that CO_2 reduction does not occur via any stepwise pathway involving sequential electron and hydrogen transfer in either order.

In this context, we describe the CO_2-to-formate conversion as proceeding via a Pd–H-mediated heterogeneous hydride-transfer process at the J-Pd_m interface. In this heterogeneous regime, "hydride transfer" does not imply the release of a free solvated H^- species, but rather a surface-mediated interfacial hydride-transfer process in which hydrogen is transferred from Pd–H as a hydride equivalent, consistent with established descriptions of metal–hydride chemistry at electrified interfaces (Nat. Catal. 2023, 6, 351–362). Formally, this process can be expressed as $Pd–H + CO_2 + e^- \rightarrow HCOO^- + Pd$, which should be interpreted as an interfacial hydride-equivalent transfer rather than a stepwise sequence.

To further substantiate the hydride-transfer capability of the J-Pd_m interface, we investigated the hydrogenation of BIM^+ (1,3-dimethyl-2-phenyl-1H-benzo[d]imidazol-3-ium), a well-established molecular hydride acceptor, using J-Pd_m (**Supplementary Figs. 67** and **68**). Upon hydride transfer, BIM^+ is converted to the corresponding hydride donor BIMH (1,3-dimethyl-2-phenyl-2,3-dihydro-1H-benzo[d]imidazole), which possesses a reported hydricity of approximately 50 kcal mol^{-1} in acetonitrile (*Nat. Catal.*, 2023, 6, 351–362). As shown in the linear sweep voltammograms (**Supplementary Fig. 67**), when no HER current was applied on the HER side of J-Pd_m (j_{HER} = 0 mA cm^{-2}), BIM^+ reduction only commenced at approximately −1.9 V vs. $Fc^{+}/^{0}$, corresponding to its direct electron-transfer reduction. In contrast, when a HER current density of −10 mA cm^{-2} was applied on the HER side of J-Pd_m, the onset potential for BIM^+ conversion shifted anodically from approximately −1.9 V to −1.25 V vs. $Fc^{+}/^{0}$. This substantial anodic shift indicates that polarized Pd–H species participate directly in BIM^+ hydrogenation, thereby facilitating BIM^+ conversion at substantially less negative potentials. Further scanning toward more negative potentials resulted in a current plateau, consistent with mass-transport limitation of BIM^+ in solution.

To further verify hydride transfer, controlled-potential electrolysis was performed using 10 mM BIM^+ at −1.4 V vs. $Fc^{+}/^{0}$ while maintaining a HER current density of −10 mA cm^{-2} on the HER side of J-Pd_m (**Supplementary Fig. 68**). After passing the theoretical charge required for complete conversion of BIM^+ through a one-electron hydride-transfer process in the HRR chamber, BIM^+ was quantitatively converted into BIMH, confirming that polarized Pd–H species are capable of mediating efficient heterogeneous hydride transfer. Importantly, the hydricity of formate in acetonitrile (~44 kcal mol^{-1}, *Acc. Chem. Res.*, 2024, 57, 3488–3499) is comparable to that of BIMH. The ability of J-Pd_m to generate BIMH through hydride transfer therefore supports the feasibility of Pd–H-mediated hydride-equivalent transfer to CO_2 under the conditions employed in this work, consistent with efficient CO_2-to-formate conversion observed in **Fig. 5**. Together, these results support a Pd–H-mediated interfacial hydride-transfer mechanism in the J-Pd_m system.

2. Regardless of the specific mechanism, once Pd–H species generated on the HER side are involved, the conversion of CO_2 to formate on the CO_2-facing side effectively corresponds to a one-electron electrochemical step, rather than the conventional two-electron CO_2 reduction process assumed in the Faradaic efficiency analysis.

Response: In the original manuscript (**Fig. 2**), FE values were calculated using the conventional two-electron proton-coupled electron transfer (PCET) assumption for CO_2-to-formate conversion, and therefore represent apparent Faradaic efficiencies. Under this normalization, the calculated FE values can exceed 100%, which initially prompted us to further examine the underlying reaction mechanism. This apparent inconsistency motivated the mechanistic investigation presented in **Fig. 3**. Through isotope-labeling experiments, we were able to distinguish formate generated via hydride transfer from Pd–H species (deuterated formate) and that arising from the conventional PCET pathway (non-deuterated formate). Based on this analysis, we quantified the respective contributions of the two pathways. These results clearly indicate that CO_2 reduction in the J-Pd_m system is dominated by a Pd–H-mediated hydride transfer pathway originating from the HER side, rather than a conventional PCET process alone.

We agree with the reviewer that, given the mechanistic nature of this system, a hydride-transfer-based electron-counting framework provides a more physically meaningful representation of the reaction. We have therefore revised all FE values in **Fig. 2** and the corresponding discussions using a one-electron hydride-transfer basis. This revision better reflects the intrinsic efficiency of the dominant reaction pathway and is fully consistent with the mechanistic conclusions drawn from **Fig. 3**. Importantly, it does not affect the observed experimental trends. All updated calculations, figures, and corresponding discussions have been revised in the manuscript and Supplementary Information.

3. The observed cation effect on the CO_2-facing side also raises questions about the proposed mechanism. Alkali metal cations are well known to influence the structure of the electrical double layer and the local electrochemical environment. The fact that the catalytic performance varies with the identity of the cation could suggest that the reaction likely involves electrochemical steps occurring within the double layer. Consequently, a mechanism involving neutral Pd–H reacting with CO_2 coupled with a single electron transfer ($Pd–H + CO_2 + e^- \rightarrow HCOO^-$) cannot be excluded.

Response: We fully agree that alkali metal cations play an important role in structuring the electrical double layer and modulating the local interfacial electrochemical environment. Such effects are well established in electrochemical CO_2 reduction and are expected to influence reaction kinetics at polarized interfaces. In the present J-Pd_m system, CO_2-to-formate conversion occurs at the CO_2-facing interface via a Pd–H-mediated heterogeneous hydride-type transfer process. As discussed above, this terminology follows the established description of metal–hydride chemistry at electrified interfaces, where a polarization-dependent surface-bound Pd–H species delivers hydrogen as a "hydride equivalent" in concert with electron flow from the electrode (Nat. Catal. 2023, 6, 351–362), rather than through a free solvated hydride intermediate. Within this framework, the cation effect can be attributed to modulation of the interfacial electric field and double-layer structure at the reaction interface, which in turn regulates the reactivity of Pd–H species toward CO_2 and the kinetics of the hydride-transfer step. The observed cation dependence is therefore consistent with field-controlled modulation of an interfacial Pd–H-mediated hydride-transfer process, rather than suggesting a distinct electron-transfer pathway for CO_2 reduction.

4. The role of $KHCO_3$ in the CO_2-facing electrolyte also requires clarification. The authors show that formate production is negligible in pure $NaClO_4$ but increases substantially when $KHCO_3$ is present, indicating that bicarbonate plays a critical role in the reaction. It is therefore unclear whether the improved performance arises from enhanced CO_2 buffering, or changes in local pH. The possible influence of electrolyte pH and interfacial electrochemical processes on the CO_2 reduction pathway should be more carefully examined.

Response: We agree that the role of $KHCO_3$ in the CO_2-facing electrolyte and the influence of the local interfacial environment on the hydride-transfer-mediated CO_2 reduction pathway require further clarification. $NaClO_4$ serves solely as an inert supporting electrolyte, providing ionic conductivity and enabling stable electrochemical polarization without participating in CO_2 conversion chemistry or acid–base equilibria. To establish the interfacial electrolyte environment, we first measured the pH values before and after CO_2 saturation (**Supplementary Tables 5** and **6**). Distinct pH variations were observed across 0.5 M $NaClO_4$, $KHCO_3$ + $NaClO_4$, and 0.5 M $KHCO_3$, confirming fundamentally different CO_2/HCO_3^- equilibrium conditions in each electrolyte system. Electrochemical measurements show a clear performance trend of 0.5 M $NaClO_4$ < 0.5 M $KHCO_3$ < $KHCO_3$ + $NaClO_4$, indicating that neither pure buffering nor purely inert electrolyte conditions are optimal for formate formation (**Supplementary Fig. 22**).

In $KHCO_3$-containing electrolytes, the CO_2/HCO_3^- equilibrium enhances local CO_2 availability at the Pd–H interface, whereas $NaClO_4$ provides high ionic conductivity but lacks such CO_2 buffering capability. However, excessively high $KHCO_3$ concentration leads to reduced effective CO_2 availability and increased interfacial ion crowding. In contrast, the mixed electrolyte provides a more favorable interfacial environment that simultaneously enhances CO_2 availability and maintains sufficient ionic conductivity, thereby maximizing formate production. These observations are consistent with previous reports on electrolyte-mediated CO_2 hydrogenation, where the CO_2/HCO_3^- equilibrium and interfacial buffering capacity were shown to strongly influence catalytic performance and polarization-driven reaction pathways (J. Am. Chem. Soc. 2020, 142, 13384−13390). Under j_{HER} = −10 mA cm^{-2}, controlled-potential electrolysis experiments without CO_2 saturation produced no detectable formate in 0.5 M $KHCO_3$ or 50 mM $KHCO_3$ + 0.5 M $NaClO_4$ electrolytes (**Supplementary Figs. 23** and **24**), confirming that dissolved CO_2 is the essential carbon source, while bicarbonate species primarily function to regulate the interfacial CO_2 equilibrium rather than directly participating as reactants.

Overall, the reaction outcome is governed by competitive consumption of Pd–H species at the CO_2-facing interface, where CO_2 and protons act as competing acceptors. The mixed electrolyte optimizes this interfacial competition by simultaneously enhancing CO_2 accessibility while maintaining favorable polarization conditions, leading to preferential hydride transfer to CO_2 over hydride consumption by protons to form H_2.

5. The article lacks a lot of critical information, such as the H_2 production rate and potentials on the HER side; the currents, as well as the FE and production rate of H_2 on the CO_2 side.

Response: We thank the reviewer for this important comment. We agree that additional quantitative information regarding hydrogen generation, permeation, and product distribution is essential for a complete understanding of the system, and we have therefore performed a set of

new control experiments to provide a more comprehensive electrochemical and mass-balance description of the J-Pd_m platform.

To quantify hydrogen generation on the HER side, we first evaluated the Faradaic efficiency of hydrogen evolution in a conventional H-cell configuration by immersing the Pd membrane in 1 M KOH electrolyte under different applied current densities (−10, −25, and −50 mA cm^{-2}). Hydrogen was collected by water displacement, and the measured H_2 amounts closely matched the theoretical values, confirming an H_2 Faradaic efficiency close to unity (**Supplementary Figs. 5** and **6**). We further quantified hydrogen permeation through the Pd membrane by placing the membrane between two compartments and independently measuring the evolved hydrogen on both sides. Under increasing current densities (−10, −25, and −50 mA cm^{-2}), the hydrogen permeation efficiencies were determined to be approximately 80%, 58%, and 54%, respectively (**Supplementary Fig. 37**). These results provide a quantitative measure of hydrogen transport across the membrane under operating conditions. In this configuration, the HER chamber primarily serves as a controllable hydrogen reservoir, continuously supplying permeated hydrogen species to the CO_2-facing interface.

To further validate the chemical identity and reactivity of the permeated hydrogen species, we introduced a hydrogenation probe molecule (maleic acid) into the CO_2-facing chamber. In the absence of CO_2, the addition of maleic acid significantly enhanced the driving force for hydrogen consumption at the CO_2-facing interface, thereby increasing the effective hydrogen permeation efficiencies from 80%, 58%, and 54% to 100%, 90%, and 79% under the corresponding current densities, consistent with efficient hydrogenation to succinic acid (**Supplementary Figs. 37** and **39**). This confirms that permeated hydrogen is chemically accessible and can be directed toward subsequent hydrogenation reactions. In parallel, CO_2-side current densities have now been explicitly provided in the revised manuscript to improve the reporting of electrochemical behavior at the CO_2-facing compartment (**Supplementary Tables 3, 4** and **7–9**). Importantly, isotope-labeling experiments (H_2O/D_2O exchange) in the HER chamber (**Fig. 3**) already demonstrate that the hydrogen incorporated into formate originates from the hydrogen-supplying side, yielding predominantly $DCOO^-$ under D_2O conditions. In addition, newly added isotope ratio mass spectrometry (IRMS) analysis provides direct evidence that under J-Pd_m operating conditions, only HD is detected on the CO_2-facing side, with no detectable H_2 formation (**Fig. 4b**). This indicates that the Pd surface at the CO_2 interface is hydrogen-enriched in a form consistent with membrane-derived hydrogen, and that the reaction pathway does not proceed via conventional proton-coupled electron transfer or H_2 evolution, but instead is governed by hydride transfer processes at the interface.

Collectively, these results establish a quantitative and mechanistic picture in which (i) hydrogen is generated with near-unity efficiency at the HER side, (ii) the generated hydrogen efficiently permeates through the Pd membrane to provide a continuous hydrogen supply to the CO_2-facing interface, and (iii) the fate of the permeated hydrogen is governed by the interfacial state of the CO_2-facing electrode, where electrochemical polarization enables efficient heterogeneous hydride transfer to CO_2, while in its absence hydrogen is diverted toward non-productive release pathways.

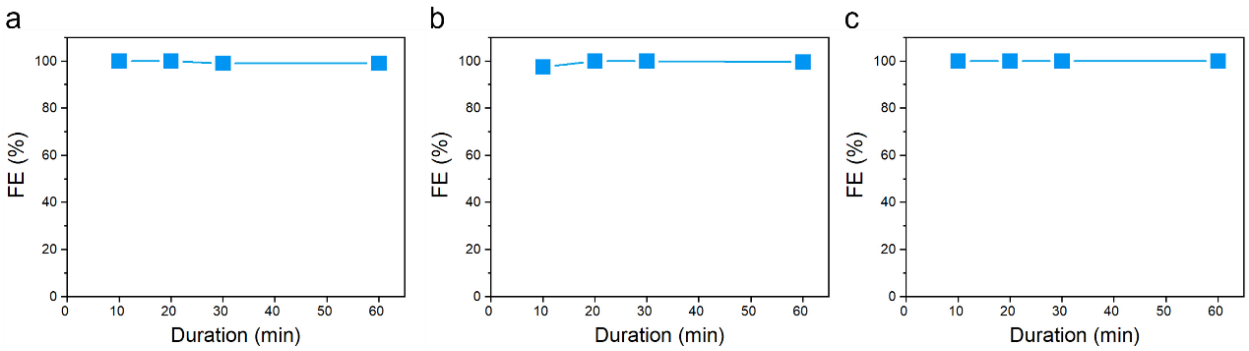

Supplementary Fig. 5. Hydrogen generation capability of an immersed Pd membrane (1 M KOH) as a function of time at different current densities, measured by H_2 collection via water displacement. (a) –10 mA cm^{-2}; (b) –25 mA cm^{-2}; (c) –50 mA cm^{-2}.

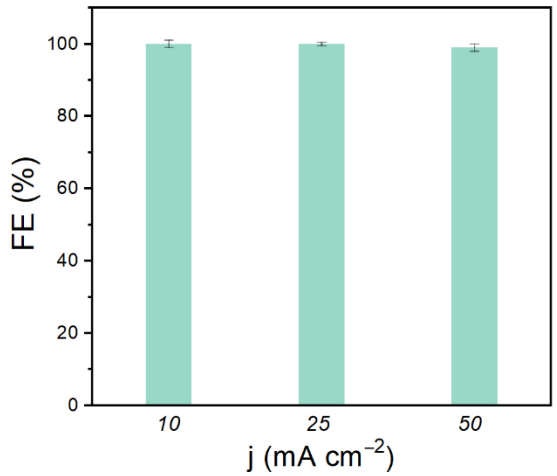

Supplementary Fig. 6. Pd membrane immersed in electrolyte (1 M KOH): hydrogen generation capability on the Pd membrane at different current densities, measured by H_2 collection via water displacement.

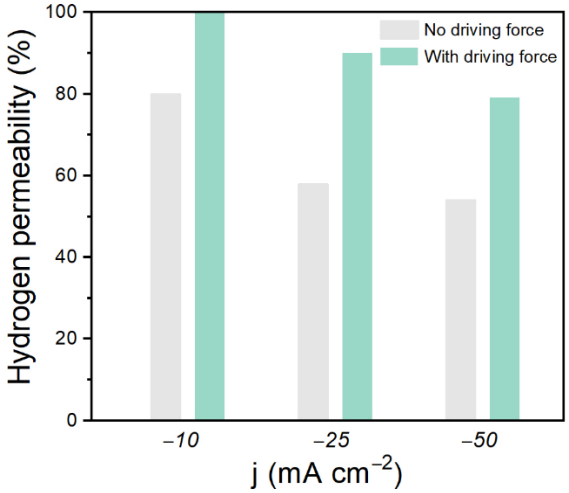

Supplementary Fig. 37. Hydrogen permeation behavior of fresh Pd_{np}/Pd_m with and without maleic acid as the driving force.

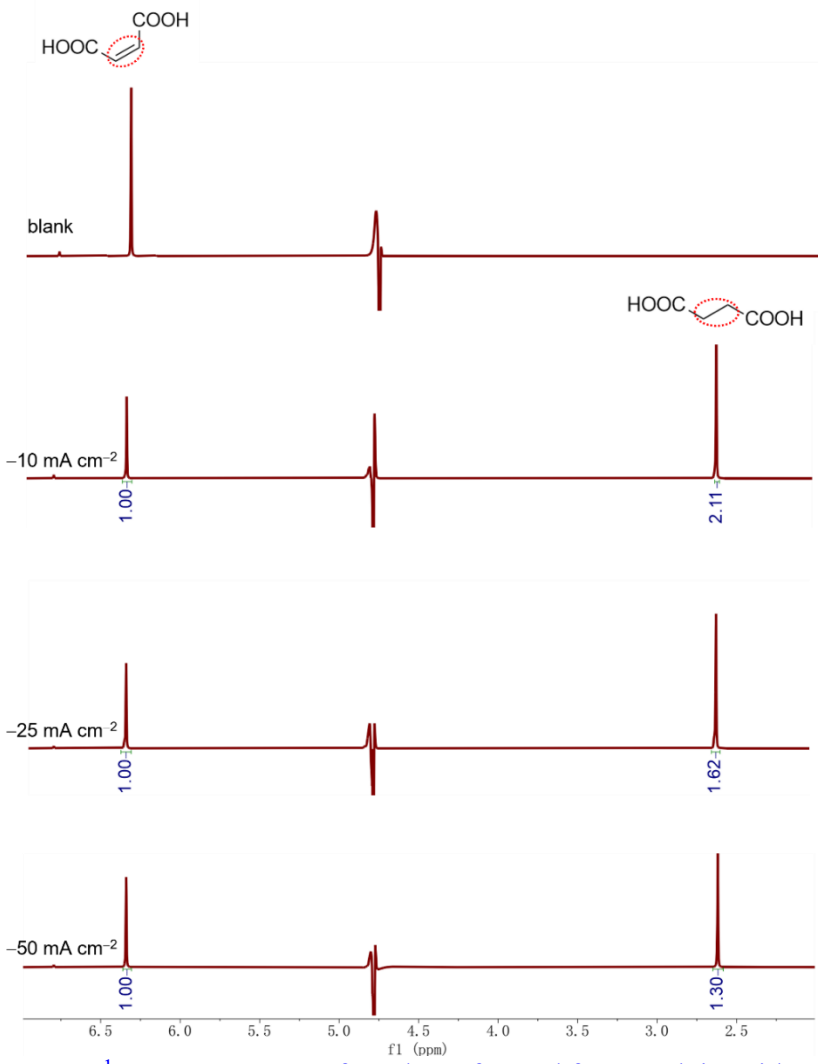

Supplementary Fig. 39. ^{1}H NMR spectra of products formed from maleic acid used as a hydrogen probe in a hydrogen permeation experiment through fresh Pd_{np}/Pd_{m}.

6. In an aprotic organic electrolyte, the performance data for ePMR is absent. Moreover, how do ePMR and J-Pd_m behave when the current on the HER side is varied in the organic system?

Response: We thank the reviewer for this insightful comment. To address this point, we have now systematically investigated both ePMR conditions (with the CO_2RR side left unpolarized) and J-Pd_m operating conditions in acetonitrile while varying the HER-side current density from −10 to −50 and −100 mA cm^{-2}. Under ePMR conditions in acetonitrile, no detectable formate products were observed across all HER-side current densities investigated, despite continuous hydrogen permeation through the Pd membrane (**Supplementary Fig. 61**). Gas analysis of the CO_2RR chamber confirmed the presence of permeated hydrogen under these conditions (**Supplementary Fig. 59**), indicating that, in the absence of cathodic polarization on the CO_2RR side, the permeated hydrogen species are unable to efficiently generate sufficiently hydridic Pd–H species for productive hydride transfer to CO_2. In contrast, under J-Pd_m operating conditions with cathodic polarization of the CO_2RR interface, appreciable formate production was consistently observed across the investigated HER-side current densities, while the Faradaic efficiency for formate remained relatively stable (**Supplementary Figs. 62** and **63**). These results further support that

electrochemical polarization of the CO_2-facing interface enables electrochemical tuning of Pd–H hydricity, thereby generating sufficiently hydridic Pd–H species for efficient heterogeneous hydride transfer to CO_2 in fully aprotic media.

7. The caption for Figure S7 is wrong.
Response: We thank the reviewer for pointing this out. In the original Supplementary Information, "**Supplementary Fig. 7**" was inadvertently written as "Supplementary Fig. S". This typographical error has now been corrected in the revised Supplementary Information.

8. There are two data for –1.85 V in Figure S25. At the same time, I'm curious why the formate signals in the NMR are very different at –1.85 V and –1.95 V, while the production rates in Fig. 5c are similar?
Response: We thank the reviewer for carefully examining the data and for raising this point. In the original **Supplementary Fig. 25** (**Supplementary Fig. 56** in the revised Supplementary Information), the reaction times were indicated on the corresponding NMR spectra. Specifically, the two spectra shown at −1.85 V vs. $Fc^{+/0}$ corresponded to two separate 3 h electrolysis experiments, whereas the spectra at the other potentials were obtained after continuous 6 h electrolysis. Therefore, the actual 6 h formate production at −1.85 V should be interpreted as the sum of the formate amounts obtained from the two independent 3 h experiments. Nevertheless, we greatly appreciate the reviewer for pointing out that this presentation could potentially lead to confusion when comparing the NMR spectra with the production rates shown in **Fig. 5c**. To provide a more direct and internally consistent comparison across different potentials, we have now repeated the −1.85 V experiment using a continuous 6 h electrolysis protocol under identical conditions. The newly collected NMR spectra have been added in the revised Supplementary Information, and the corresponding formate production rate in **Fig. 5c** has also been revised accordingly. Importantly, the overall trend in formate production remains unchanged.

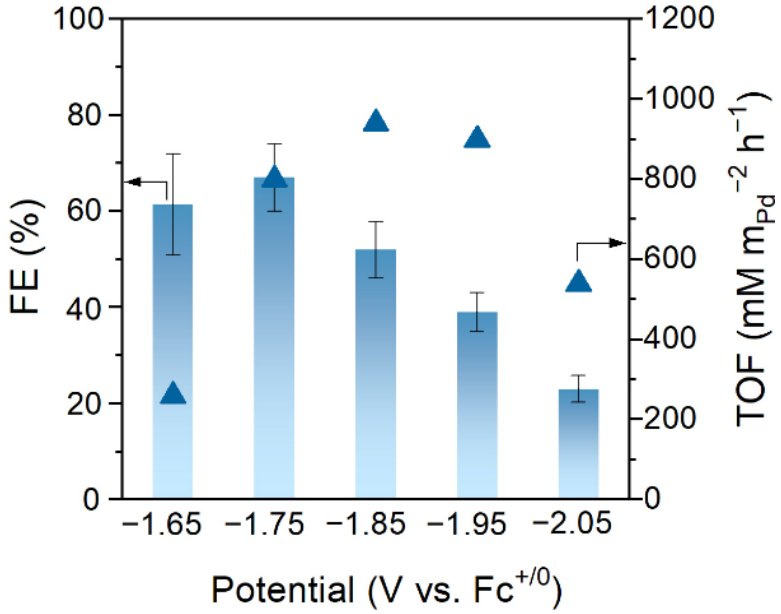

Fig. 5c. Faradaic efficiencies and turnover frequencies of formate production after 6-h electrolysis in acetonitrile at various applied potentials in the CO_2ER chamber with j_{HER} = –10 mA cm^{-2} in the HER chamber.

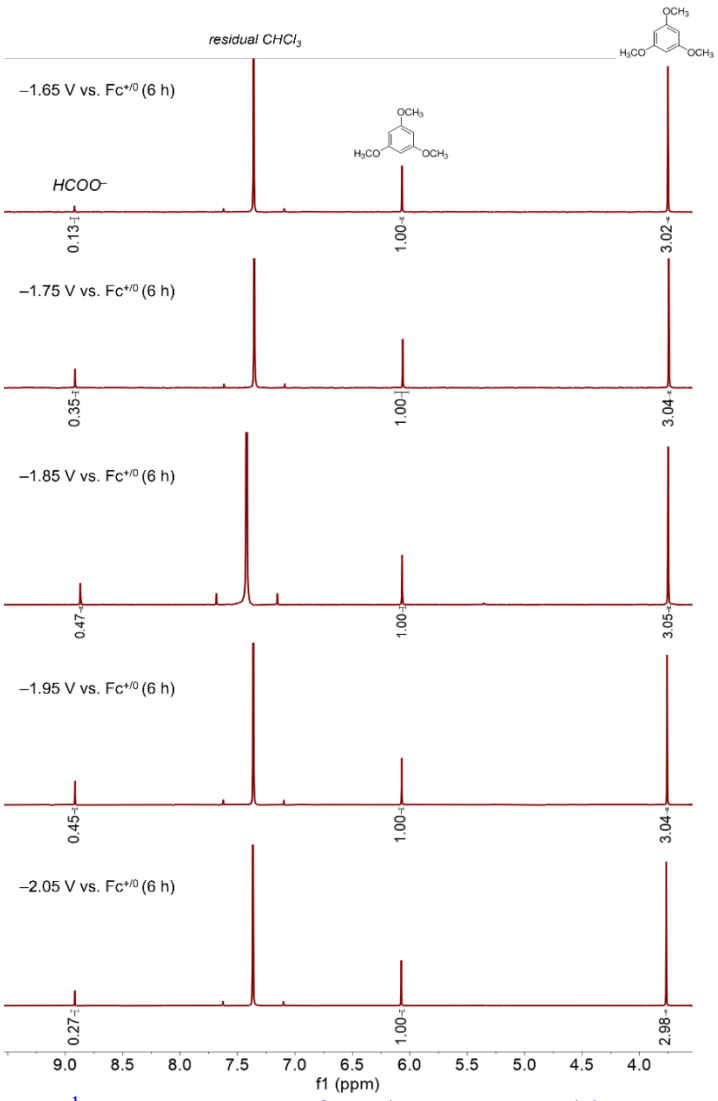

Supplementary Fig. 56. ^{1}H NMR spectra of products generated in CH_3CN at different CO_2ER potentials in the CO_2ER chamber with j_{HER} = –10 mA cm^{-2} in the HER chamber.

9. For Fig. 2d and Figure S4, the formate FE approaching 160% at j_{HER} = −10 mA cm^{-2}. Nevertheless, further increasing jHER to −50 mA cm^{-2} resulted in a lower formate FE of 130%. However, the relative peak areas for formate in NMR are 0.21 and 0.11, respectively. The results indicate that the current density on CO_2ER side at j_{HER} = −50 mA cm^{-2} is much smaller than the current density on CO_2ER side at j_{HER} = −10 mA cm^{-2}. This trend is opposite to that in Fig. 2c.

Response: As correctly noted by the reviewer, the relative formate peak area in the ^{1}H NMR spectra at j_{HER} = −50 mA cm^{-2} is smaller than that at j_{HER} = −10 mA cm^{-2}, despite the CO_2ER-side LSV in **Fig. 2c** showing a larger cathodic current response at higher HER-side current density. It should be noted that the cathodic current measured on the CO_2ER side does not exclusively correspond to hydride transfer to CO_2 and formate production, but instead reflects the combined contribution of multiple interfacial processes.

In the J-Pd_m system, the HER chamber primarily functions as a controllable hydrogen reservoir that continuously supplies permeated hydrogen species to the CO_2-facing interface. Once the Pd

membrane is transformed into the Pd–H phase, as evidenced by the XRD results (**Supplementary Fig. 43**), the overall rate of formate production becomes increasingly governed by the catalytic activity and interfacial environment at the CO_2-facing interface, rather than by the HER-side hydrogen supply rate. This interpretation is further supported by the comparison between smooth Pd foil and Pd nanoparticle-modified Pd membranes. As shown by the ECSA and CO-stripping measurements (**Supplementary Figs. 1 and 14**), electrodeposition of Pd nanoparticles significantly increases the electrochemically accessible surface area and the density of active interfacial sites at the CO_2-facing interface. In contrast, smooth Pd foil exhibits very limited cathodic current and no quantifiable formate production under otherwise identical conditions (**Supplementary Figs. 10** and **11**), indicating that, once the Pd membrane is converted into the Pd–H phase, the availability of active interfacial sites at the CO_2-facing interface becomes a dominant factor governing efficient formate generation.

At higher HER-side current densities (e.g., $j_{HER} = -50$ mA cm^{-2}), hydrogen permeation through the Pd membrane is further increased. However, after formation of the Pd–H phase, excess permeated hydrogen species preferentially undergo recombination/desorption to release H_2. The increased local hydrogen accumulation near the Pd surface can also hinder effective CO_2 access to interfacial active sites, which is unfavorable for hydride transfer to CO_2 and lowering the formate production rate. Moreover, because the electrolysis is performed in CO_2-saturated aqueous electrolyte, polarized Pd–H species can also transfer hydrogen to protons in the electrolyte to generate H_2, which constitutes a major hydrogen-consumption pathway under these conditions. Therefore, the larger cathodic current observed in the CO_2ER-side LSV at $j_{HER} = -50$ mA cm^{-2} reflects the combined contribution of CO_2-involved interfacial processes and hydrogen-related surface processes, rather than exclusively representing current associated with formate production. This interpretation is further supported by the LSV measurements in **Fig. 2a**. Under Ar atmosphere, a pronounced cathodic current is observed, corresponding to intrinsic hydrogen evolution on the Pd membrane surface. Upon introducing CO_2, additional cathodic current arises beyond the HER baseline, indicating that the cathodic current under CO_2 in **Fig. 2c** includes contributions from both CO_2-involved interfacial processes and hydrogen-related surface processes.

To further examine the influence of local interfacial transport effects, we expanded the Pd membrane area from 0.125 cm^2 to 2 cm^2 while simultaneously increasing the H-cell volume. Under these conditions, the highest formate Faradaic efficiency was still observed at $j_{HER} = -10$ mA cm^{-2}. Increasing the HER-side current density to -50 mA cm^{-2} resulted in decreased formate FE and formate production rates, while further increasing the HER-side current density to -100 mA cm^{-2} led to little additional change, with both the FE and formate production remaining relatively stable (**Supplementary Figs. 45** and **46**). This trend is consistent with that observed for the smaller-area Pd membrane. Importantly, the substantially higher FE achieved with the larger-area Pd membrane suggests that increasing the interfacial area can partially alleviate local transport limitations associated with excessive hydrogen permeation, thereby helping maintain more efficient hydride transfer to CO_2.

Overall, these results indicate that once sufficient hydrogen supply is established to form the Pd–H phase, the hydride-transfer-mediated CO_2 reduction process becomes primarily governed by the catalytic activity and interfacial environment at the CO_2-facing side, rather than by continuously

increasing the HER-side current density. Accordingly, excessively high HER-side current densities do not further enhance formate production efficiency.

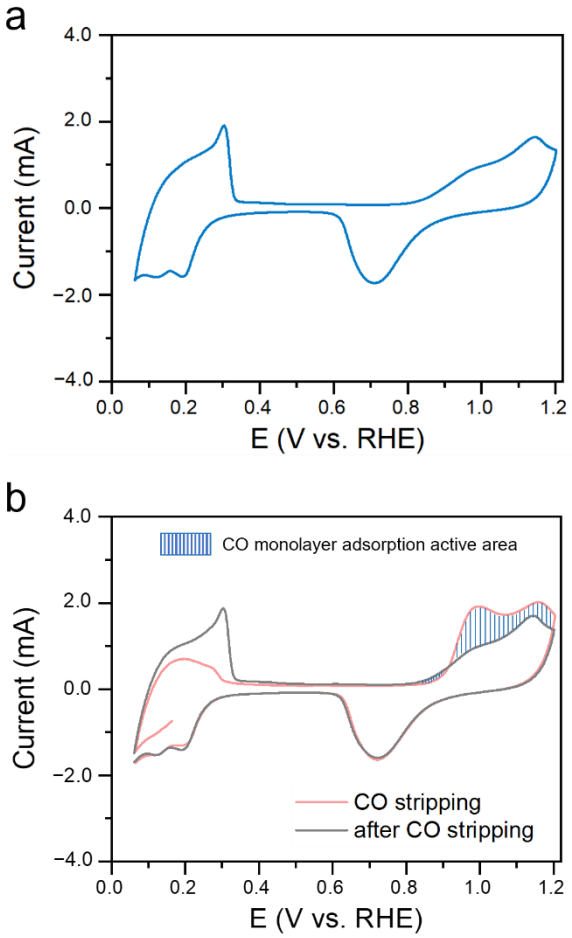

Supplementary Fig. 14. CO stripping tests. (a) Background; (b) CO-stripping curves. In (b), the red curve represents the CO-stripping measurement and the black curve shows the signal after CO-stripping.

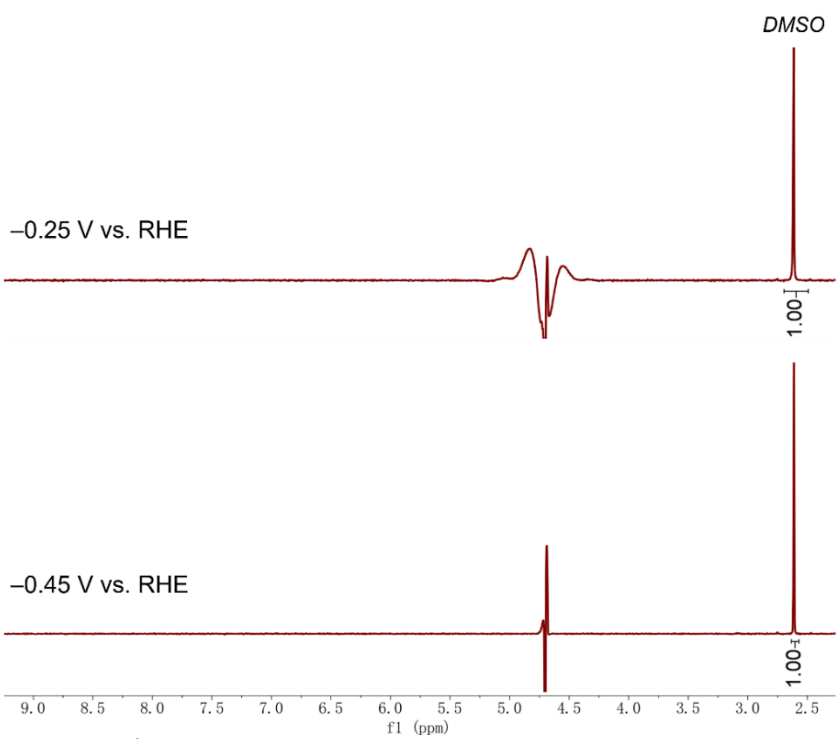

Supplementary Fig. 10. ^{1}H NMR spectra of products generated in aqueous solution (50 mM $KHCO_3$ + 0.5 M $NaClO_4$) at different CO_2ER potentials for 3 h in the CO_2ER chamber, with j_{HER} = –10 mA cm^{-2} in the HER chamber, using a smooth Pd foil.

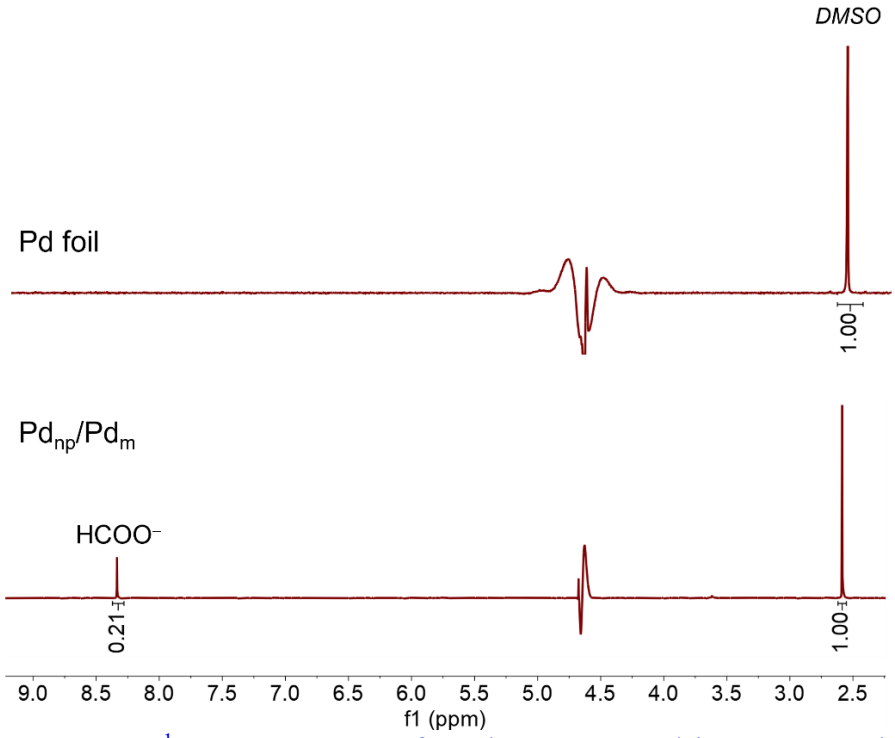

Supplementary Fig. 11. ^{1}H NMR spectra of products generated in aqueous solution (50 mM $KHCO_3$ + 0.5 M $NaClO_4$) at −0.25 V vs. RHE for 3 h in the CO_2ER chamber, with j_{HER} = –10 mA cm^{-2} in the HER chamber, using (a) a smooth Pd foil and (b) Pd_{np}/Pd_m.

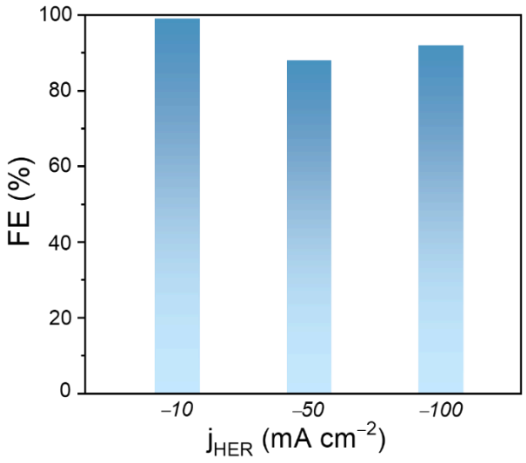

Supplementary Fig. 45. Faradaic efficiency of formate formation: effect of HER chamber current density (j_{HER}) on CO_2 reduction performance after a 3-h reaction at –0.25 V vs. RHE in the CO_2ER chamber (J-Pd_m system, 50 mM $KHCO_3$ + 0.5 M $NaClO_4$ (aq)), with Pd_{np}/Pd_m (2 cm^2).

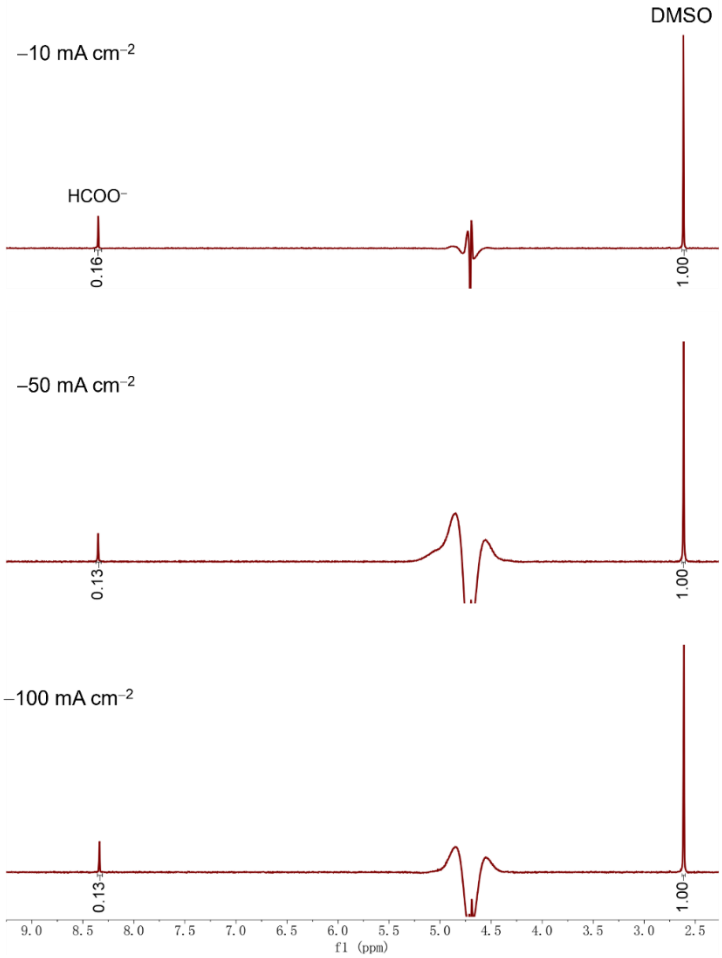

Supplementary Fig. 46. ^1H spectra: effect of HER chamber current density (j_{HER}) on CO_2 reduction performance after a 3-h reaction at –0.25 V vs. RHE in the CO_2ER chamber (J-Pd_m system, 50 mM $KHCO_3$ + 0.5 M $NaClO_4$ (aq)), with Pd_{np}/Pd_m (2 cm^2).

10. Why must the CO_2 reduction side require electrodeposition of high surface area Pd? Are the results substantially different with a smooth flat Pd surface?

Response: The electrodeposition of high-surface-area Pd on the CO_2RR side was primarily introduced to increase the density of accessible catalytic active sites at the CO_2-facing interface. As shown by the electrochemical surface area (ECSA) measurements (**Supplementary Fig. 1**) and CO-stripping experiments (**Supplementary Fig. 14**), electrodeposition of Pd nanoparticles on the Pd membrane leads to a dramatic increase in both the electrochemically accessible surface area and the effective active surface area, by nearly two orders of magnitude compared with the smooth Pd foil.

Following the reviewer's suggestion, we additionally performed electrolysis experiments using a smooth Pd foil without electrodeposited Pd nanoparticles under otherwise identical conditions to those used for the Pd nanoparticle-modified membrane electrode (Pd_{np}/Pd_m) reported in the manuscript. Due to the limited density of accessible active sites, the smooth Pd foil exhibited only very small reduction currents. Moreover, after 3 h of electrolysis at both −0.25 V vs. RHE and −0.45 V vs. RHE, no quantifiable formate products were detected by ^{1}H NMR analysis. The corresponding ^{1}H NMR spectra have been included in the revised Supplementary Information for comparison with the Pd_{np}/Pd_m system (**Supplementary Figs. 10** and **11**). In contrast, as shown in **Fig. 2** of the revised manuscript, the Pd_{np}/Pd_m electrode with electrodeposited Pd nanoparticles exhibits substantially enhanced formate production activity under the same operating conditions. These results indicate that increasing the density of accessible Pd active sites is critical for achieving efficient CO_2-to-formate conversion in the J-Pd_m system.

Reviewer #3

In this manuscript, Hu et. al. reported a Janus palladium membrane electrode, affording CO_2-to-formate conversion via hydride transfer mechanism, rather than conventional PCET mechanism. This was achieved by tuning the hydricity of Pd–H species via external polarization. The key point of the study is very clear, and I believe the tunable hydricity in the Pd-membrane provides great insights for more reaction systems for value-added chemicals synthesis. Therefore, I support its publication, and have the following concerns for the authors.

Response: We sincerely thank the reviewer for the positive evaluation of our work and for recognizing the significance of tunable hydricity in the Janus Pd membrane system for hydride-transfer-mediated CO_2 conversion. We are encouraged by the reviewer's interest in the broader implications of this strategy for future electrosynthetic transformations and appreciate the constructive comments provided below.

1. The calculation of FE in this work is significant but not clarified, especially in regard to the FE higher than 100%. According to the Figure 2e and 2f, it is speculated that the total charge used in the FE calculation formula only contains that of the CO_2ER chamber. Considering that the applied polarization circuits at the HER and CO_2ER chamber are independent, it is theoretically impossible for total FE more than 100%. Hence, the detailed calculation process on FE should be provided and re-checked.

Response: We appreciate the reviewer's insightful comment regarding the electron-counting basis used for Faradaic efficiency (FE) analysis. As pointed out by the reviewer, the polarization circuits used in the HER and CO_2ER compartments are electrically independent, and the current from the HER compartment is not included in the Faradaic efficiency calculation for the CO_2ER compartment. In the original manuscript (**Fig. 2**), FE values were calculated using the conventional two-electron proton-coupled electron transfer (PCET) assumption for CO_2-to-formate conversion, and therefore represent apparent Faradaic efficiencies. Under this normalization, the calculated FE values can exceed 100%, which initially prompted us to further examine the underlying reaction mechanism. This apparent inconsistency motivated the mechanistic investigation presented in **Fig. 3**. Through isotope-labeling experiments, we were able to distinguish formate generated via hydride transfer from Pd–H species (deuterated formate) and that arising from the conventional PCET pathway (non-deuterated formate). Based on this analysis, we quantified the respective contributions of the two pathways. These results clearly indicate that CO_2 reduction in the J-Pd_m system is dominated by a Pd–H-mediated hydride transfer pathway originating from the HER side, rather than a conventional PCET process alone. Accordingly, we agree with the reviewer that, given the hydride-transfer-dominated reaction mechanism established in this work, FE values should not be interpreted using the conventional two-electron PCET stoichiometry and should not exceed 100% under a physically consistent definition. We have therefore revised all FE values in **Fig. 2** and the corresponding discussions using a one-electron hydride-transfer basis. This revision ensures consistency with the mechanistic picture established in **Fig. 3** and does not affect the observed experimental trends.

2. According to the previous study (Joule 2024, 8, 728-745), the OCP value at the $^*H/H^+$ polarization interface is significantly influenced by the solution pH. Hence, the more positive OCP values after introducing CO_2 should be discussed thoroughly regarding the change of solution pH.

Response: We thank the reviewer for pointing out the influence of solution pH on OCP behavior and for providing the relevant reference (Joule 2024, 8, 728–745). Following the reviewer's

suggestion, we measured the electrolyte pH before and after CO_2 saturation, and the results are now included in **Supplementary Tables 5** and **6**. The electrolyte pH changes from 8.65 under Ar to 6.44 after CO_2 saturation. Consistent with the literature report, the decrease in solution pH correspondingly induces a positive shift in the observed OCP.

In our J-Pd_m system, the OCP is governed by two controlled variables: (i) the gas atmosphere (Ar vs CO_2) and (ii) the state of the Pd membrane (metallic Pd vs Pd–H). Under j_{HER} = 0 mA cm^{-2}, the Pd membrane remains in a predominantly metallic Pd state, giving an OCP of ~0.8–0.9 V vs. RHE. Switching between Ar and CO_2 induces a small OCP shift due to the decrease in solution pH upon CO_2 saturation, consistent with the behavior reported in the literature (Joule 2024, 8, 728–745). When the HER side is polarized at j_{HER} = −10 mA cm^{-2} prior to OCP measurement, hydrogen generated in the HER compartment permeates through the Pd membrane, forming a hydrogen-rich Pd–H phase, as confirmed by XRD (**Supplementary Fig. 43**). This increases the hydrogen chemical potential within the Pd lattice and shifts the interfacial state on the CO_2-facing side, resulting in a lower OCP approaching ~0 V vs. RHE, consistent with a Pd–H-dominated equilibrium. Therefore, the OCP variations directly reflect the change in Pd membrane state between metallic Pd and Pd–H, together with minor perturbations from CO_2-induced solution speciation effects. We have clarified this discussion in the revised Supplementary Information and cited the corresponding reference in the revised manuscript.

3. Hunt et al. (J. Am. Chem. Soc. 2023, 145, 14316−14323) proposed that the hydrogenation thermodynamics of CO_2 in Pd membrane reactor is significantly affected by HER chamber current density and almost no product at low current density. Therefore, I think that it is more reasonable to compare the CO_2 hydrogenation efficiency of different reaction modes (ePMR, conventional CO_2ER and Janus CO_2ER) under higher HER chamber's current density.

Response: In response to the reviewer's suggestion, we have added additional ePMR and J-Pd_m control experiments under a range of HER-side current densities (−10, −50, and −100 mA cm^{-2}) in aqueous electrolyte, together with the corresponding comparison data. In the ePMR configuration, the absence of cathodic polarization on the CO_2-facing side limits the reactivity of permeated hydrogen species. Although previous studies have shown that protic media such as water can promote disproportionation of surface Pd–H species, enabling limited hydride-transfer reactivity at Pd interfaces (J. Am. Chem. Soc. 2025, 147, 10974–10980; JACS Au 2024, 4, 328–343; Chem. Sci. 2026, 17, 1039–1050), the spontaneous formation of sufficiently hydridic Pd–H species remains inefficient, and hydride transfer to CO_2 is kinetically unfavorable under these open-circuit conditions (FE ≈ 0.06%) (J. Am. Chem. Soc. 2023, 145, 14316–14323). Consequently, although trace formate formation can still be observed (**Supplementary Fig. 47**), majority of the permeated hydrogen species preferentially undergo recombination/desorption to produce H_2.

In contrast, the J-Pd_m configuration enables independent polarization of the CO_2-facing interface, allowing electrochemical regulation of Pd–H hydricity. This enhances the hydride-transfer capability of the interfacial Pd–H species and leads to higher formate formation compared to the corresponding ePMR conditions. Importantly, at identical HER-side current densities, J-Pd_m consistently shows improved catalytic performance (**Supplementary Figs. 45** and **46**), highlighting the role of interfacial polarization in enabling efficient CO_2-to-formate conversion. This distinction becomes even more pronounced in aprotic acetonitrile electrolyte. In the absence

of protic species, spontaneous formation of hydridic Pd–H is strongly suppressed, and no detectable formate is observed under open-circuit conditions (**Supplementary Fig. 61**). By contrast, the J-Pd_m configuration enables electrochemically driven hydride transfer to CO_2 under fully aprotic conditions, leading to efficient formate formation (**Supplementary Figs. 62** and **63**).

4. As a more comprehensive evaluation, the FE corresponding to the H_2 evolution in the HER chamber and CO_2ER chamber should also be provided to demonstrate the respective distributions of electrons in the two circuits.

Response: We appreciate the reviewer's suggestion to provide a more comprehensive evaluation of electron distribution across both compartments. In response, we have now quantified the Faradaic efficiency for H_2 evolution in both the HER and CO_2ER chambers to provide a complete description of electron partitioning in the dual-circuit system. When the Pd membrane electrode is immersed in the electrolyte (not act as a membrane electrode), H_2 evolution was quantified by gas collection using a water-displacement method, and a near-unity H_2 Faradaic efficiency (~100%) was obtained across the applied current range (**Supplementary Figs. 5** and **6**), confirming that electrons in this compartment are exclusively consumed for H_2 evolution, which serves as a continuous hydrogen reservoir to maintain sufficient Pd–H coverage on the CO_2-facing side of the membrane.

In the CO_2ER chamber, additional control and isotope-labeling experiments further clarify the electron utilization pathways. When D_2O was used as the hydrogen source in the hydride-transfer experiments (**Fig. 3**), deuterated formate was quantified by ^{2}H NMR spectroscopy, whereas HD as the gaseous product was identified by isotope ratio mass spectrometry (IRMS) (**Fig. 4b**). The results confirmed the formation of deuterated formate together with HD as the only gaseous hydrogen-containing product, with no H_2 observed. This indicates that, under hydride-transfer conditions for CO_2 reduction, proton–hydride recombination to form H_2 is the primary competing pathway for electron consumption. Consistently, GC measurements performed during CO_2 reduction electrolysis in CO_2-saturated electrolytes also confirm the presence of H_2 as a side-product in the CO_2ER compartment (**Supplementary Fig. 27**), demonstrating that electrons in this chamber are distributed between CO_2-to-formate conversion and H_2 evolution via hydride-transfer-mediated pathways.

Taken together, these results provide a complete picture of electron partitioning in the J-Pd_m system: the HER chamber functions exclusively as a hydrogen-generation reservoir, while in the CO_2ER chamber electrons are partitioned between CO_2-to-formate conversion via hydride transfer and competitive proton–hydride coupling leading to H_2 evolution.

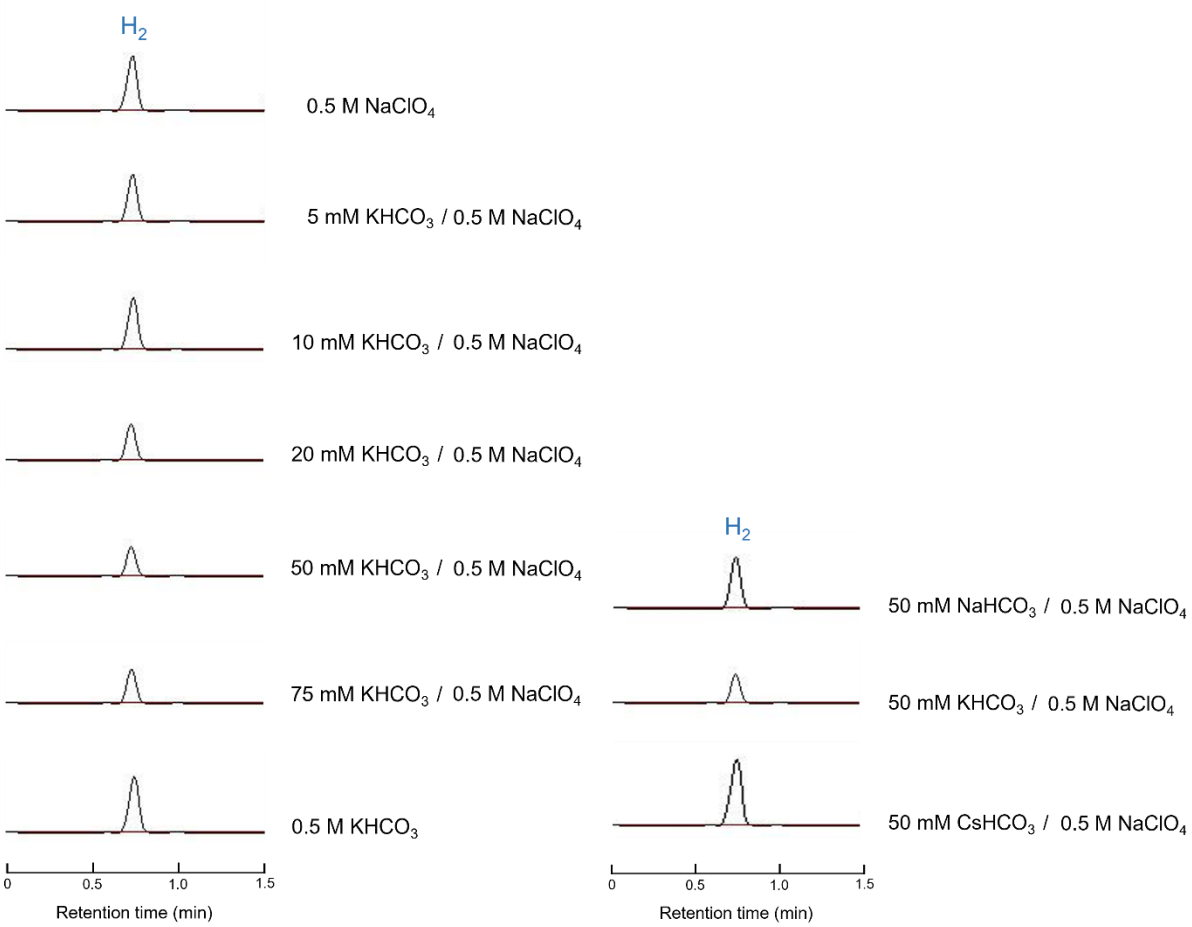

Supplementary Fig. 27. GC analysis after 3-h electrolysis at −0.25 V vs. RHE in the CO_2ER chamber using different electrolytes (j_{HER} = −10 mA cm^{-2}).

5. The Janus hydrogenation system features two independent circuits and their respective polarization effects on hydrogen species. However, whether a synergistic interaction exists between these two circuits remains unexplored. This study (Chem Catal. 2026, https://doi.org/10.1016/j.checat.2025.101602) aims to address this gap.

Response: We appreciate the reviewer for raising the point regarding the possible synergistic interaction between the two independently polarized circuits in the Janus hydrogenation system. We agree that the interplay between hydrogen generation, transmembrane hydrogen transport, and interfacial hydrogen utilization is fundamentally important in Pd-membrane-based hydrogenation systems. As highlighted in the recent Chem Catalysis study suggested by the reviewer (Chem Catal. 2026, https://doi.org/10.1016/j.checat.2025.101602), independently polarized interfaces can exhibit cooperative effects arising from the distinct kinetic roles of bulk hydrogen species and surface hydrogen species. In our J-Pd_m system, although the HER and CO_2ER chambers operate using electrically independent circuits, they are intrinsically coupled through Pd–H generation, hydrogen permeation, and hydride consumption across the Pd membrane. Specifically, the HER chamber continuously supplies hydrogen species to maintain sufficient Pd–H coverage on the CO_2-facing side of the membrane, whereas the CO_2ER chamber governs the subsequent utilization pathways of Pd–H species, including hydride transfer to CO_2 and competing proton–hydride coupling leading to H_2 evolution. This coupling behavior is reflected in the HER-current-

dependent experiments presented in this work (**Fig. 2d** and **Supplementary Figs. 45–47**). At low HER-side current densities, insufficient hydrogen supply limits Pd–H availability at the CO_2-facing interface. In contrast, increasing the HER-side current density beyond an optimal range does not further improve formate production, indicating that the hydrogen utilization process at the CO_2ER interface rather than hydrogen supply itself becomes the dominant limitation. While the primary focus of the present work is the hydride-transfer-mediated CO_2 reduction mechanism enabled by the Janus Pd membrane architecture, the reviewer's comment and the recent Chem Catalysis study provide important perspectives for understanding interfacial coupling and cooperative hydrogen regulation in dual-circuit Pd membrane systems.

6. In the Figure 1b, it is proposed that HCOOH production in aprotic solvents is forbidden in ePMR. The CO_2 hydrogenation experimental results without the CO_2ER polarization in aprotic solvents should be provided as a response.

Response: We appreciate the reviewer for pointing out the need for experimental verification of the proposed behavior shown in **Fig. 1b**. In response, we performed additional ePMR control experiments in CO_2-saturated acetonitrile without applying CO_2ER-side polarization. HER-side current densities of −10, −50, and −100 mA cm^{-2} were examined, and no detectable formate product was observed under all tested conditions (**Supplementary Fig. 61**). These results indicate that, although hydrogen permeation through the Pd membrane can still occur under aprotic conditions, CO_2 hydrogenation to formate was not observed in the absence of CO_2ER-side electrochemical polarization. The corresponding experimental results and related discussion have been incorporated into the revised manuscript and Supplementary Information.

7. I noticed that when applying a more negative potential at the chemical compartment, FE of formate reduced under different conditions (Fig. 2b, Fig. 3b, Fig. 5c). The reason for this observation under specific conditions requires further explanation, more than simply attribute it to the competition of HER. I assumed that delta G of Pd-H species should be larger at more negative potential, making it easier for CO_2RR. In addition, since the current density at electrochemical chamber is fixed, leading to a similar migrated H species amount and thus H species coverage at Pd surface in the chemical chamber, the recombination of H species to give H_2 may not be more competitive.

Response: We thank the reviewer for this insightful comment regarding the potential-dependent variation in formate Faradaic efficiency. We agree that applying more negative polarization at the CO_2-facing side can, in principle, increase the thermodynamic driving force associated with hydride transfer from Pd–H species. However, the observed decrease in formate Faradaic efficiency at more negative potentials indicates that the overall selectivity is not determined solely by hydride transfer thermodynamics, but by the balance between interfacial hydride-transfer kinetics and competing surface processes at the CO_2-facing electrode, which become increasingly significant under stronger polarization conditions.

In aqueous electrolytes, the primary competing pathway to CO_2 hydride transfer is proton–hydride recombination ($H^+ + H^- \rightarrow H_2$). This is directly supported by isotopic labeling experiments. When H_2O in the HER chamber is replaced by D_2O, the hydride species transported to the CO_2ER side is converted to D^-. In addition to the formation of $DCOO^-$ (**Fig. 3**), the only gaseous product detected is HD, with no H_2 observed (**Fig. 4b**), confirming that the dominant competing pathway is hydride–proton coupling rather than conventional D_2 (or H_2) evolution at the CO_2-facing

interface. As reported in the literature (Acc. Chem. Res. 2024, 57, 3488–3499), in aqueous media proton–hydride recombination to form H_2 is thermodynamically more favorable than hydride transfer to CO_2 to form formate, with the corresponding hydricity thresholds required for Pd–H species estimated at 34.2 and 24.1 kcal mol^{-1}, respectively (**Fig. R1**). In our $KHCO_3/NaClO_4$ mixed electrolyte system, the CO_2/HCO_3^- equilibrium together with interfacial buffering capacity (J. Am. Chem. Soc. 2020, 142, 13384–13390) enhances CO_2 availability while maintaining favorable interfacial polarization conditions. This optimized interfacial environment shifts the reaction competition such that hydride transfer to CO_2 is favored over proton consumption to form H_2. At more negative applied potentials, however, stronger driving forces induce local CO_2 mass-transport limitations and partial disruption of the buffering equilibrium. Under these conditions, the polarized Pd–H species increasingly undergo competing reactions with protons, leading to decreased formate Faradaic efficiency.

In aprotic acetonitrile, proton-mediated H_2 evolution is absent. However, Pd exhibits strong CO_2 adsorption and can catalyze direct electron-transfer pathways leading to CO formation and carbonate species (CO_3^{2-}) (ACS Catal. 2023, 13, 5780–5786), consistent with our LSV results in **Fig. 5b**. Even under conditions where no current is applied on the HER side, Pd alone can promote CO_2 reduction, and both CO and CO_3^{2-} are detected experimentally (**Fig. 5e, f**). At more negative potentials, this direct CO_2 reduction pathway is further enhanced. The generated CO strongly adsorbs on Pd, partially blocking active sites and thereby reducing the accessibility of interfacial Pd–H species. This site-blocking effect suppresses hydrogen permeation and limits exposure of Pd–H active sites, ultimately decreasing hydride transfer to CO_2 and reducing formate Faradaic efficiency.

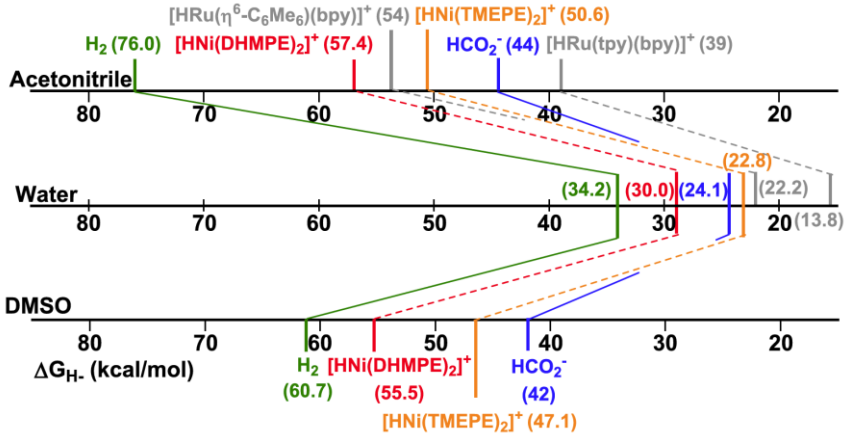

Fig. R1. Hydricity values of formate and H_2 in different solvents, reflecting the relative thermodynamic favorability of hydride transfer reactions involving CO_2 reduction and proton reduction. (Acc. Chem. Res. 2024, 57, 3488−3499.)

Reviewer #4

This manuscript by Sun and Hu presents an original and potentially impactful concept for CO_2 reduction using a Janus palladium membrane electrode that spatially separates hydrogen generation from the CO_2-reduction interface supported by an additional electrochemical bias. The study is scientifically interesting, and the combination of isotopic labelling, SEIRAS and experiments in aprotic media make the work promising. However, in its current form, the manuscript still feels somewhat premature to me. Several central claims are intriguing but not yet supported with sufficient rigor or require clearer discussion. I therefore recommend reconsideration after major revisions. The following points deserve attention:

Response: We sincerely thank the reviewer for the thoughtful and constructive evaluation of our manuscript and for recognizing the originality and potential impact of the Janus palladium membrane concept for spatially decoupled CO_2 reduction. We appreciate the reviewer's overall assessment that the manuscript would benefit from further clarification and strengthening of several key mechanistic and interpretative aspects. We have carefully addressed all comments point-by-point and have substantially revised the manuscript to improve clarity, rigor, and mechanistic support of the central claims.

The reported formate Faradaic efficiencies above 100%, especially at the beginning, are central to the paper but are not yet resolved rigorously enough. Beyond very initial measurements there should not be any FE beyond 100% here. Since the authors are clearly aware of this issue, the manuscript should provide a more transparent charge balance and clearly distinguish between compartment-specific values and overall device-level efficiencies.

Response: We appreciate the reviewer's insightful comment regarding the reported formate Faradaic efficiencies (FE), particularly the values exceeding 100% at early stages. As correctly noted, the HER and CO_2ER compartments in the J-Pd_m system operate using electrically independent polarization circuits, and the current in the HER compartment is not included in the Faradaic efficiency calculation for CO_2 reduction, which is defined exclusively based on the CO_2ER compartment. In the original manuscript (**Fig. 2**), formate Faradaic efficiencies were calculated using the conventional two-electron stoichiometry for CO_2-to-formate conversion. Under this conventional PCET-based electron-counting framework, the reported values represent apparent efficiencies and may exceed 100% in a system where CO_2 reduction is predominantly governed by a one-electron-equivalent hydride-transfer pathway.

To address this point, we have revised the FE analysis and explicitly clarified the electron-counting convention in the revised manuscript and Supplementary Information. The full FE calculation procedure, including charge definitions for the CO_2ER compartment, has been provided to ensure transparency and reproducibility. Accordingly, all Faradaic efficiency values have been recalculated based on a one-electron hydride-transfer-consistent framework, resulting in values that are not exceeding 100% while preserving the observed experimental trends. To further support a complete description of electron utilization, hydrogen evolution in both compartments has been quantified. In the HER chamber, hydrogen evolution was measured by gas collection using a water-displacement method, and a near-unity H_2 Faradaic efficiency (~100%) was obtained across the investigated current range (**Supplementary Figs. 5** and **6**), confirming exclusive electron consumption for hydrogen generation and sustained Pd–H supply at the CO_2-facing membrane interface.

When D_2O is used as the hydrogen source, ^2H NMR spectroscopy confirms deuterated formate formation, while isotope ratio mass spectrometry (IRMS) reveals HD as the dominant gaseous product with no detectable H_2 (**Figs. 3e** and **4b**). These results support a Pd–H-mediated reaction network involving CO_2-to-formate conversion and a competing proton–hydride coupling pathway. This provides a direct view of electron distribution within the CO_2ER compartment. Importantly, all formate Faradaic efficiencies reported in the revised **Fig. 2** are now calculated strictly based on the CO_2ER compartment charge using a physically consistent electron-counting framework. This removes ambiguity associated with apparent FE values above 100% while preserving all experimental trends.

The long-term data are still rather superficial. A 20 h stability test is encouraging, but still limited for such a central claim. In addition, Fig. S28 appears to show noticeable structural changes of the Pd electrode, which are not discussed in sufficient detail. Longer measurements and more thorough structural post-analysis would be needed to support the durability claims.

Response: We thank the reviewer for this important comment regarding long-term stability and the structural evolution of the Pd-based membrane electrode. To address the durability concern, we performed extended stability tests in a flow-cell configuration. The J-Pd_m system exhibited robust long-term operational stability, maintaining formate Faradaic efficiencies above 75% over 105 h of continuous operation (**Fig. 4e** and **Supplementary Fig. 36**). During this period, the formate concentration steadily increased, demonstrating sustained product accumulation under continuous-flow conditions. To further evaluate the functional integrity of the Pd membrane, we conducted hydrogen permeation measurements using a water-displacement method before and after electrolysis. The results show that the Pd_{np}/Pd_m electrode maintains excellent hydrogen permeation capability after operation, with no significant degradation observed (**Supplementary Figs. 38–40**). Post-reaction structural characterization was performed using SEM, XRD, and ECSA analysis. SEM images reveal morphological evolution of the electrode surface, including growth and restructuring of electrodeposited Pd nanoparticles (**Supplementary Fig. 42**). However, XRD patterns confirm that the characteristic Pd–H phase is preserved after electrolysis, indicating that the hydride-forming capability of the membrane remains intact (**Supplementary Fig. 43**). Consistently, ECSA measurements show a decrease relative to the fresh electrode, but still retain approximately 71% of the initial electrochemically active surface area after operation (**Supplementary Fig. 41**). Importantly, despite these morphological changes, both hydrogen permeation behavior and catalytic performance remain largely unaffected, indicating that the observed structural evolution does not compromise the functional integrity of the Pd membrane. These results suggest that the Pd-based system undergoes dynamic surface restructuring under operating conditions while maintaining its key hydrogen transport functionality.

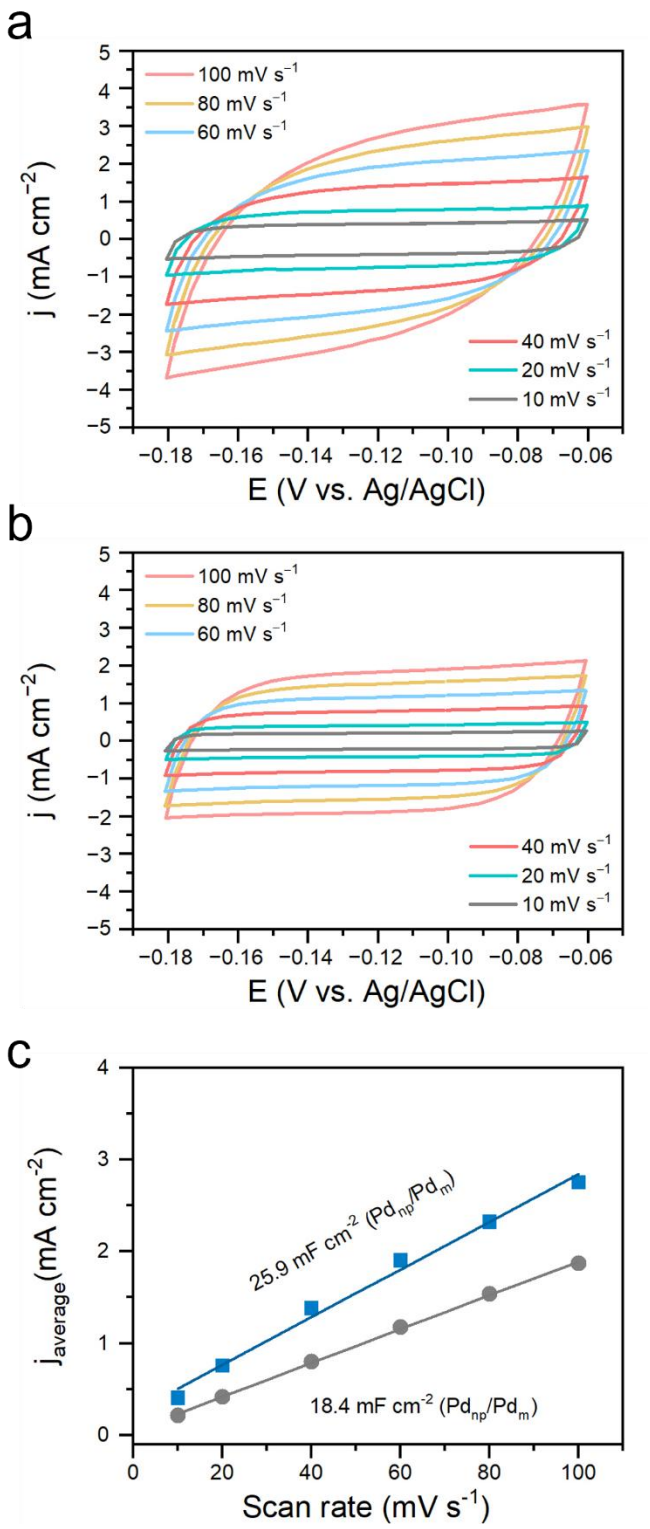

Supplementary Fig. 41. (a) CV curves of the fresh Pd_{np}/Pd_m electrode collected in the non-Faradaic region at different scan rates. (b) CV curves of the Pd_{np}/Pd_m electrode after stability testing collected in the non-Faradaic region at different scan rates. (c) ECSA (electrochemical surface area) of fresh Pd_{np}/Pd_m and Pd_{np}/Pd_m after stability testing.

The experimental setup and its scalability should be discussed more clearly.
The cell design/configuration is important for the mechanistic argument, but the setup is not described in enough detail. A clearer schematic and more information on chamber dimensions and cell geometry would be helpful. Moreover, the active area appears very small, and the use of a 25 μm Pd foil raises obvious questions regarding scalability and capital cost. A brief discussion of larger-area operation or the possible use of alternatives would improve the practical relevance of the study.
Response: We thank the reviewer for these valuable comments regarding the experimental configuration, device geometry, and practical scalability of the J-Pd_m system. In addition to the original 0.125 cm^2 membrane configuration, we further expanded the active membrane area to 2 cm^2. The large-area J-Pd_m system maintained efficient CO_2-to-formate conversion and exhibited even higher formate Faradaic efficiencies (**Fig. 2d** and **Supplementary Figs. 45 and 46**), which we attribute to alleviated CO_2 mass-transport limitations under the larger-area configuration. These results demonstrate that the Janus hydride-transfer architecture is extendable beyond the initial small-area proof-of-concept system.

To evaluate scalability under practical operating conditions, we also implemented a flow-cell configuration, which is now included in the revised manuscript. In this system, a 1 cm^2 Pd-based membrane electrode was employed, and stable operation was maintained for 105 h with formate Faradaic efficiency remaining above 75% (**Fig. 4e** and **Supplementary Fig. 35**). These results demonstrate the feasibility of extending the J-Pd_m architecture from batch H-cell operation to continuous-flow electrolysis, significantly improving its practical relevance.

To address the reviewer's concern regarding the Pd cost, we replaced the pure Pd membrane with a PdAg alloy membrane (Pd:Ag = 75:25 wt%, 25 μm thickness). Hydrogen permeation measurements showed hydrogen-transfer behavior comparable to that of the pure Pd membrane, while the Faradaic efficiency for hydride-transfer-mediated CO_2-to-formate conversion remained essentially unchanged (**Supplementary Figs. 48–51**). These results indicate that the Janus membrane architecture is not restricted to pure Pd membranes and can be extended to alloy membrane systems with reduced noble-metal content.

In addition, we note that further engineering strategies may provide additional opportunities for scalable fabrication. Physical vapor deposition methods such as magnetron sputtering or thermal evaporation on porous or polymer-supported substrates (e.g., PTFE-based supports) could, in principle, enable the fabrication of Pd-, PdAg-, or PdX-based thin films with controllable thickness and tunable alloy composition. Such approaches may offer a versatile platform for further reducing noble-metal use and expanding membrane design flexibility.

To improve clarity of the experimental setup and device geometry, we have added photographs and annotated schematics of the electrochemical cells in the revised Supplementary Information, including both the original and large-area H-cell configurations as well as the flow-cell configuration (**Supplementary Figs. 4**, **35** and **44**). The revised Supplementary Information now explicitly provides chamber geometry, membrane dimensions, exposed membrane area, electrode arrangement, and other relevant cell parameters to improve reproducibility and clarify the configuration of the dual-chamber system.

These results collectively demonstrate that the J-Pd_m architecture can be extended from small-area H-cell operation to large-area configurations and continuous-flow electrolysis, while also being compatible with PdAg alloy membrane. Together, these results support the scalability and practical relevance of the system beyond the initial proof-of-concept design.

The claim of "tunable hydricity" is currently very strong. Although it is one of the most interesting ideas in the manuscript, at present it is not yet quantitatively established. The authors should either weaken this claim or explain more clearly what range of tuning is actually implied, how it is supported experimentally, and what broader reactivity consequences may realistically follow from it.

Response: We thank the reviewer for this important comment regarding the description of "tunable hydricity" in our manuscript. We appreciate the opportunity to further clarify and strengthen the experimental basis of this concept.

In this work, the term "tunable hydricity" is used to describe the ability of polarized Pd–H to function as a hydride source toward acceptors with different thermodynamic hydride affinities. This reflects a polarization-dependent modulation of the effective hydride-donor strength of Pd–H at the electrified interface. Importantly, this concept is not intended to imply a modification of molecular intrinsic hydricity, but rather reflects how cathodic polarization enables Pd–H to access hydride-transfer reactivity across different energetic requirements.

To further verify this heterogeneous hydride-transfer capability, we have expanded our experimental investigation using BIM^+ as an additional molecular hydride acceptor (**Supplementary Figs. 67–68**). BIM^+ is a well-established hydride acceptor, and its reduced form BIMH (1,3-dimethyl-2-phenyl-2,3-dihydro-1H-benzo[d]imidazole) has a reported hydricity of approximately 50 kcal mol^{-1} in acetonitrile (*Nat. Catal.*, 2023, 6, 351–362).

As shown in the linear sweep voltammograms (**Supplementary Fig. 67**), when no HER current was applied on the HER side of J-Pd_m (j_{HER} = 0 mA cm^{-2}), BIM^+ reduction only commenced at approximately −1.9 V vs. $Fc^{+/0}$, corresponding to direct electron-transfer reduction. In contrast, when a HER current density of −10 mA cm^{-2} was applied on the HER side, the onset potential for BIM^+ conversion shifted anodically to approximately −1.25 V vs. $Fc^{+/0}$. This pronounced shift indicates that polarized Pd–H species can mediate hydride-equivalent transfer to BIM^+ under cathodic polarization conditions, enabling its conversion at substantially less negative potentials. Further controlled-potential electrolysis (−1.4 V vs. $Fc^{+/0}$, j_{HER} = −10 mA cm^{-2}) confirms that BIM^+ is quantitatively converted to BIMH after passing the theoretical charge required for a one-electron hydride-transfer process (**Supplementary Fig. 68**), demonstrating efficient heterogeneous hydride transfer at the J-Pd_m interface.

Importantly, hydricity provides a thermodynamic scale to benchmark hydride-transfer reactions. In general, lower hydricity values correspond to stronger hydride-donor ability, reflecting a greater thermodynamic driving force for hydride transfer. In this context, the hydricity of formate in acetonitrile (~44 kcal mol^{-1}) is comparable to that of BIMH (~50 kcal mol^{-1}), while the corresponding value in water is ~24.1 kcal mol^{-1} (*Acc. Chem. Res.*, 2024, 57, 3488–3499; Nat. Catal. 2023, 6, 351–362). Together, these observations establish the experimentally accessible

range of hydride-donor reactivity of polarized Pd–H in hydride-transfer processes within the J-Pd_m system.

Minor points:
There appear to be inconsistencies in how the isotope experiments are described. In the main text and Fig. 3 caption, the experiment is presented as a potential-dependent study and the HER chamber is specified as 1.0 M KOH in D_2O. In the SI methods, the HER chamber is described as 1.0 M $NaClO_4$ in D_2O, and the electrolysis is described at −0.35 V vs. RHE, which reads as a single-point experiment rather than the broader potential series.
Response: We thank the reviewer for carefully identifying the inconsistencies in the description of the isotope-labeling experiments. We confirm that the isotope experiments were performed under a potential-dependent study, rather than at a single fixed potential. This has been corrected in the Supplementary Information Methods section to accurately reflect the experimental conditions. In addition, we note that the electrolyte used for the isotope-labeling experiments is 1.0 M $NaClO_4$ in D_2O, and the **Fig. 3** caption was incorrectly described as 1.0 M KOH in D_2O. This has now been corrected in the revised manuscript.

The aprotic electrolyte should be characterized more rigorously, for example by Karl Fischer titration, to assess residual water.
Response: We thank the reviewer for this valuable suggestion regarding residual water in the aprotic electrolyte system. We experimentally evaluated the influence of residual water using both electrochemical measurements and ^1H NMR analysis. Specifically, linear sweep voltammetry (LSV) measurements were conducted in Ar-saturated acetonitrile electrolytes containing the original electrolyte, 0.1% added H_2O, and 1% added H_2O. Upon addition of 0.1% H_2O, noticeably increased cathodic current was observed, while 1% H_2O produced substantially larger reduction current in the same potential window (**Supplementary Fig. 52**). In parallel, ^1H NMR spectra of the three electrolyte systems revealed only a very weak residual water signal in the original electrolyte, which was substantially smaller than that observed in the 0.1% H_2O-containing electrolyte (**Supplementary Fig. 53**). These results indicate that the residual water content in the aprotic electrolyte is well below the 0.1% level (<1000 ppm). Importantly, no detectable formate product was observed in the ePMR system under aprotic conditions without CO_2ER-side polarization (**Supplementary Fig. 61**), further supporting that the hydride-transfer-mediated CO_2 reduction behavior observed in the J-Pd_m system cannot be attributed to residual water alone.

I am not fully convinced by the use of DMSO as an internal standard for NMR quantification, especially given its hygroscopic nature and the use of solvent suppression. The authors should clarify whether specific precautions were taken to ensure quantitative accuracy.
Response: We agree that the use of DMSO as an internal standard for quantitative ^1H NMR analysis requires careful control because of its hygroscopic nature, particularly when solvent suppression methods are employed. To minimize potential errors associated with moisture uptake, the DMSO internal standard solution was freshly prepared immediately prior to use. The DMSO solvent was purified using a solvent purification system (SPS) and further dried over molecular sieves activated at 300 °C before use. We also note that DMSO has been commonly employed as an internal standard for quantitative ^1H NMR analysis in electrochemical CO_2 reduction literature. (Angew. Chem. Int. Ed. 2026, e3692505; Nat. Commun. 2018, 9, 3828; Nat. Commun. 2019, 10, 5186; Nat. Nanotechnol. 2024, 19, 311–318.)

For the ^{1}H NMR measurements, 50 μL of the reaction solution and 50 μL of an internal standard solution containing a fixed concentration of DMSO in the corresponding electrolyte were mixed with 400 μL of D_2O. Water suppression was applied primarily to suppress the residual water signal introduced from the small amount of electrolyte in the sample. Importantly, the DMSO resonance used for quantification is well separated from the suppressed water region and was therefore not affected by the solvent suppression method. To further evaluate the robustness of the quantification procedure, we additionally compared spectra collected with and without water suppression using the same sample and observed negligible differences in the integrated DMSO and formate signals. Repeated measurements of the same sample also showed nearly identical integrations and quantified formate concentrations (**Supplementary Fig. 8**). In addition, quantitative analysis using an alternative aqueous internal standard (maleic acid) yielded results consistent with those obtained using DMSO (**Supplementary Fig. 9**). Together, these control experiments support the reliability and reproducibility of the quantitative NMR analysis reported in this work.

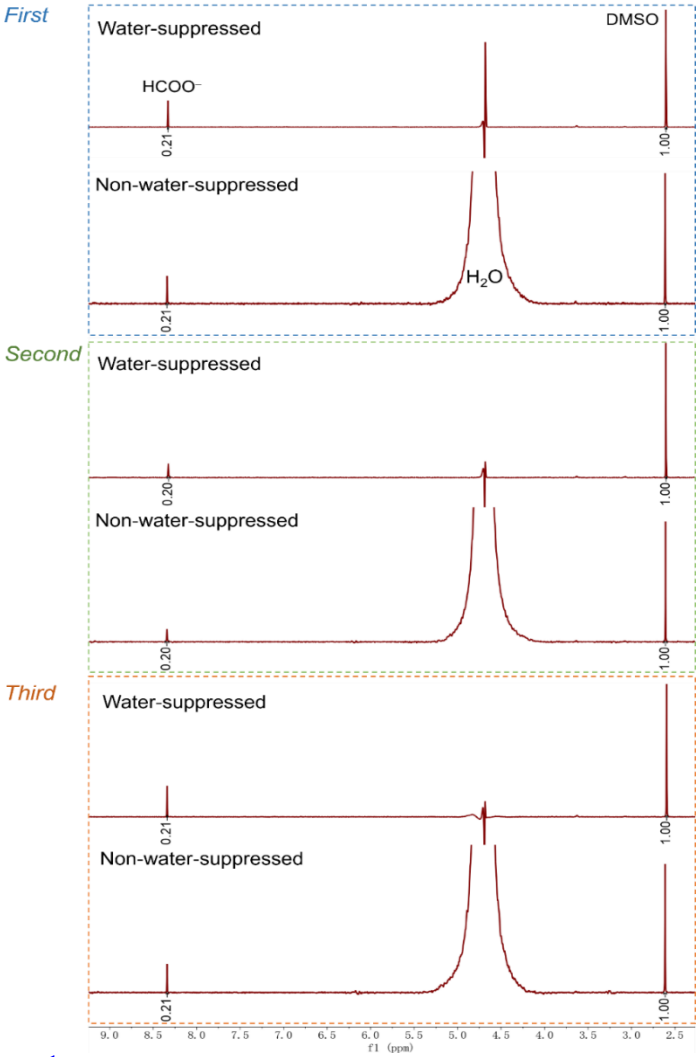

Supplementary Fig. 8. ^{1}H NMR spectra using DMSO as an internal standard under water-suppressed and non-water-suppressed conditions in aqueous solution (50 mM $KHCO_3$ + 0.5 M $NaClO_4$) at −0.25 V vs. RHE for 3 h in the CO_2ER chamber with j_{HER} = −10 mA cm^{-2} in the HER chamber.

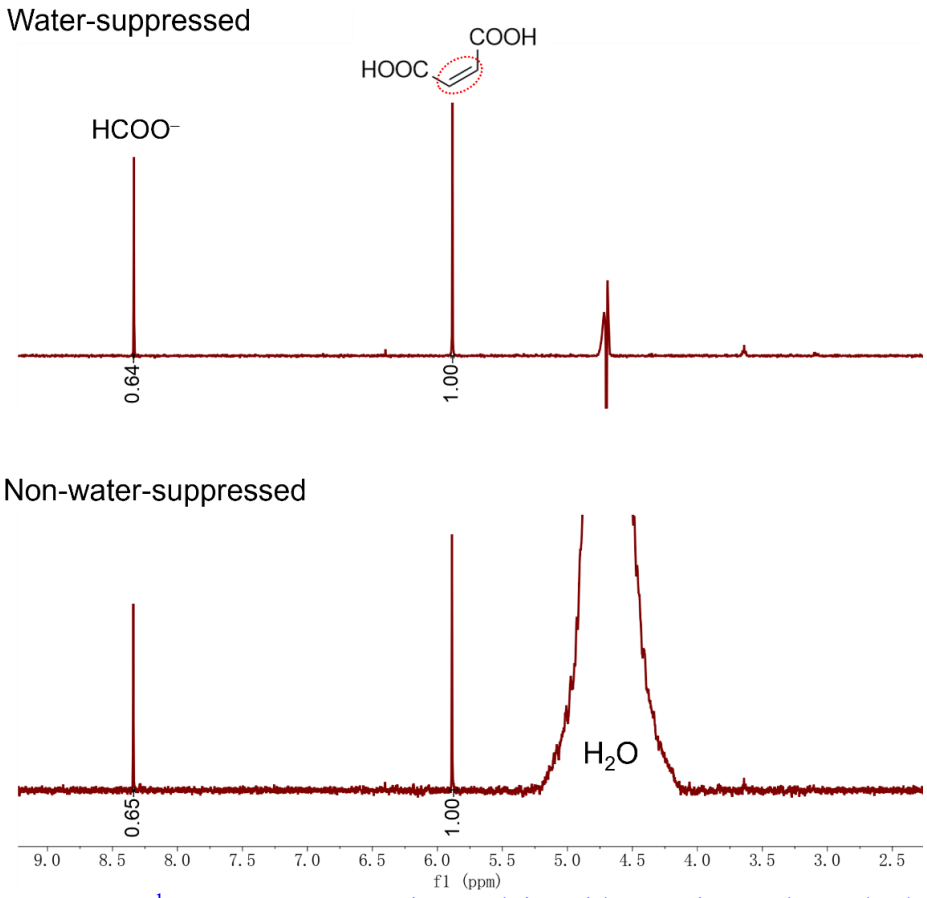

Supplementary Fig. 9. ^{1}H NMR spectra using maleic acid as an internal standard under water-suppressed and non-water-suppressed conditions in aqueous solution (50 mM $KHCO_3$ + 0.5 M $NaClO_4$) at −0.25 V vs. RHE for 3 h in the CO_2ER chamber with j_{HER} = −10 mA cm^{-2} in the HER chamber.

Point-by-Point Response to Reviewer Comments (Round 2)

Reviewer #1

Authors have satisfactorily addressed my comments raised in the last round.

Response: We sincerely thank the reviewer for the positive evaluation and are pleased that the comments raised in the previous round have been satisfactorily addressed.

Reviewer #2

Authors have addressed the Reviewer comments quite comprehensively and I am happy to support publication.

Response: We sincerely thank the reviewer for the positive evaluation and for supporting the publication of our revised manuscript.

Reviewer #3

The authors provide a detailed response to my questions, but I think the authors do not fully understand and response my questions. Therefore, I think further substantial revision is still required, with the following concerns shown below:

Response: We sincerely thank the reviewer for the detailed evaluation of our previous responses. We appreciate the concerns raised regarding clarity and presentation. In the responses below, we have carefully restructured and clarified each point to ensure that all comments are addressed in a direct and explicit manner. Detailed point-by-point responses are provided below.

1. When reading the response letter, I felt deeply confused because the authors almost did not directly provide any revision figures corresponding to their descriptions in the response to my questions. Although I know that the authors have made revisions in the manuscript and SI and even displayed them in the responses to the other reviewers, this has not improved my reading experience. I am not obliged to manually match the descriptions with the corresponding figures in SI that are embedded in a long and cumbersome text during the review process. This should be the authors' work. I hope that the responses to each reviewer can receive equal attention.

Response: We sincerely apologize for the inconvenience caused by the presentation of the previous response letter. In the 1st-round response letter, we adopted a unified formatting strategy across all reviewers, in which figures and supporting data were presented only once within the overall point-by-point response letter to avoid unnecessary repetition. However, we understand the reviewer's concern that this format reduced readability if a reviewer does not read the whole letter from the beginning and made it more difficult to directly associate specific revisions with individual comments.

In this revision round, we have reorganized the 1st-round point-by-point responses to Reviewer #3 and placed them at the end of this 2nd-round response document. All relevant figures, tables, and datasets are now directly embedded within each response item to improve clarity, navigation, and ease of evaluation.

2. Regarding Q2 in my previous comment, the authors explained the influence of pH variation before and after the CO_2 saturation in the interfacial potential of CO_2 chamber. The authors attributed the major reasons of potential variation to the change of Pd phase during electrolysis. However, the applied current density can not only increase the bulk hydrogen concentration to

vary PdH_x phase, but also increase the interfacial hydrogen coverage at the CO_2ER chamber side. In fact, the pH effect influences the EOCP values via the chemical polarization of interfacial $^*H/H^+$ equilibrium. Hence, the role of interfacial H coverage should also be taken into consideration.

Response: We thank the reviewer for this insightful follow-up comment regarding Q2 and for highlighting the role of interfacial hydrogen coverage and $^*H/H^+$ equilibrium in determining E_{OCP} behavior. We agree that our previous description did not sufficiently emphasize the contribution of interfacial hydrogen coverage on the CO_2ER chamber side.

Following the reviewer's original suggestion, we quantified the electrolyte pH before and after CO_2 saturation, and the pH values are provided in **Supplementary Tables 5** and **6**. The bulk pH is significantly lower after CO_2 saturation, and this decrease in solution pH induces a positive shift in the observed OCP, consistent with the pH dependence of the interfacial $^*H/H^+$ equilibrium reported in *Joule 2024, 8, 728–745*. In addition, the XRD characterization of the Pd membrane (**Supplementary Fig. 43**) confirms the formation of a hydrogen-rich Pd–H phase under HER polarization, indicating an increase in the lattice hydrogen chemical potential during electrolysis.

As the reviewer points out, the applied current density can not only increase the bulk hydrogen concentration and drive Pd → PdH_x phase evolution, but also increase the interfacial hydrogen coverage ($^*H$) at the CO_2-facing Pd surface. The interfacial $^*H/H^+$ equilibrium is sensitive to the local proton activity at the interface; therefore, changes in interfacial hydrogen coverage together with changes in the local proton environment can contribute to the observed E_{OCP} behavior through chemical polarization effects.

In our J-Pd_m system, bulk Pd/PdH_x evolution establishes the lattice hydrogen chemical potential, while the interfacial $^*H/H^+$ equilibrium and local solution environment define the proton activity at the CO_2-facing interface. The observed E_{OCP} variations should therefore be understood as arising from a coupled bulk–interfacial hydrogen response, in which Pd/PdH_x phase evolution and interfacial hydrogen coverage ($^*H$) jointly define the hydrogen state of the electrode, while the chemical polarization of the interfacial $^*H/H^+$ equilibrium governs how this hydrogen state is reflected in the measured equilibrium potential. We have revised the corresponding discussion in the **Supplementary Information (Page 12)** to reflect this coupled bulk–interfacial mechanism and to explicitly incorporate the role of interfacial hydrogen coverage and $^*H/H^+$ equilibrium, in line with the reviewer's recommendation.

Supplementary Table 5. Summary of electrolyte pH values.

Electrolyte	H_2O	0.5 M $NaClO_4$	5 mM $KHCO_3$, 0.5 M $NaClO_4$	10 mM $KHCO_3$, 0.5 M $NaClO_4$	20 mM $KHCO_3$, 0.5 M $NaClO_4$	50 mM $KHCO_3$, 0.5 M $NaClO_4$	75 mM $KHCO_3$, 0.5 M $NaClO_4$	0.5 M $KHCO_3$
pH	6.91±0.06	6.47±0.04	8.36±0.01	8.48±0.01	8.52±0.01	8.65±0.01	8.68±0.01	8.87±0.02

Supplementary Table 6. Summary of electrolyte pH values after CO_2 saturation

Electrolyte	H_2O	0.5 M $NaClO_4$	5 mM $KHCO_3$, 0.5 M $NaClO_4$	10 mM $KHCO_3$, 0.5 M $NaClO_4$	20 mM $KHCO_3$, 0.5 M $NaClO_4$	50 mM $KHCO_3$, 0.5 M $NaClO_4$	75 mM $KHCO_3$, 0.5 M $NaClO_4$	0.5 M $KHCO_3$
pH	4.03±0.02	3.97±0.02	5.46±0.02	5.75±0.01	6.01±0.01	6.44±0.02	6.58±0.02	7.45±0.01

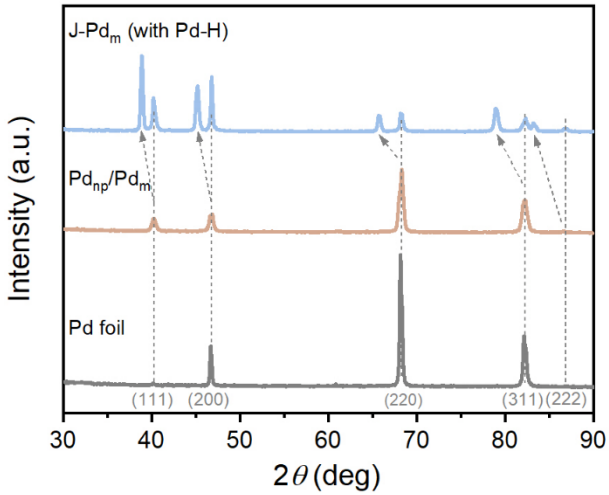

Supplementary Fig. 43. X-ray diffraction patterns of the Pd membrane (Pd_{np}/Pd_m) before and after hydrogen permeation.

3. Regarding Q3 in my previous comment, the authors did not provide additional performance data on the conventional CO_2ER system just like the work J. Am. Chem. Soc. 2019, 141, 7815−7821. And please explain why the authors did not response to it.

Response: We thank the reviewer for this comment and apologize that this point was not explicitly addressed in our previous response. Following the reviewer's suggestion, we have now added conventional CO_2ER control experiments in aqueous electrolyte at current densities of −10, −50, and −100 mA cm^{-2} (**Supplementary Fig. 48**). Under these conditions, formate production is extremely limited. The formate Faradaic efficiency was below 1% at −10 and −50 mA cm^{-2}, and no detectable formate was observed at −100 mA cm^{-2} within the analytical detection limit. These results indicate that, as increasingly negative potentials are required to achieve higher current densities in the conventional CO_2ER configuration, hydrogen evolution becomes increasingly competitive and substantially suppresses CO_2-to-formate conversion. We therefore consider that comparison between conventional CO_2ER and the J-Pd_m system is more appropriately performed under a matched-potential regime where CO_2 reduction remains observable. Accordingly, the comparison shown in **Fig. 2e** and **Supplementary Table 7** was carried out under these conditions to evaluate differences in CO_2-to-formate conversion performance, while the newly added data in **Supplementary Fig. 48** provides the conventional CO_2ER performance at higher current densities requested by the reviewer.

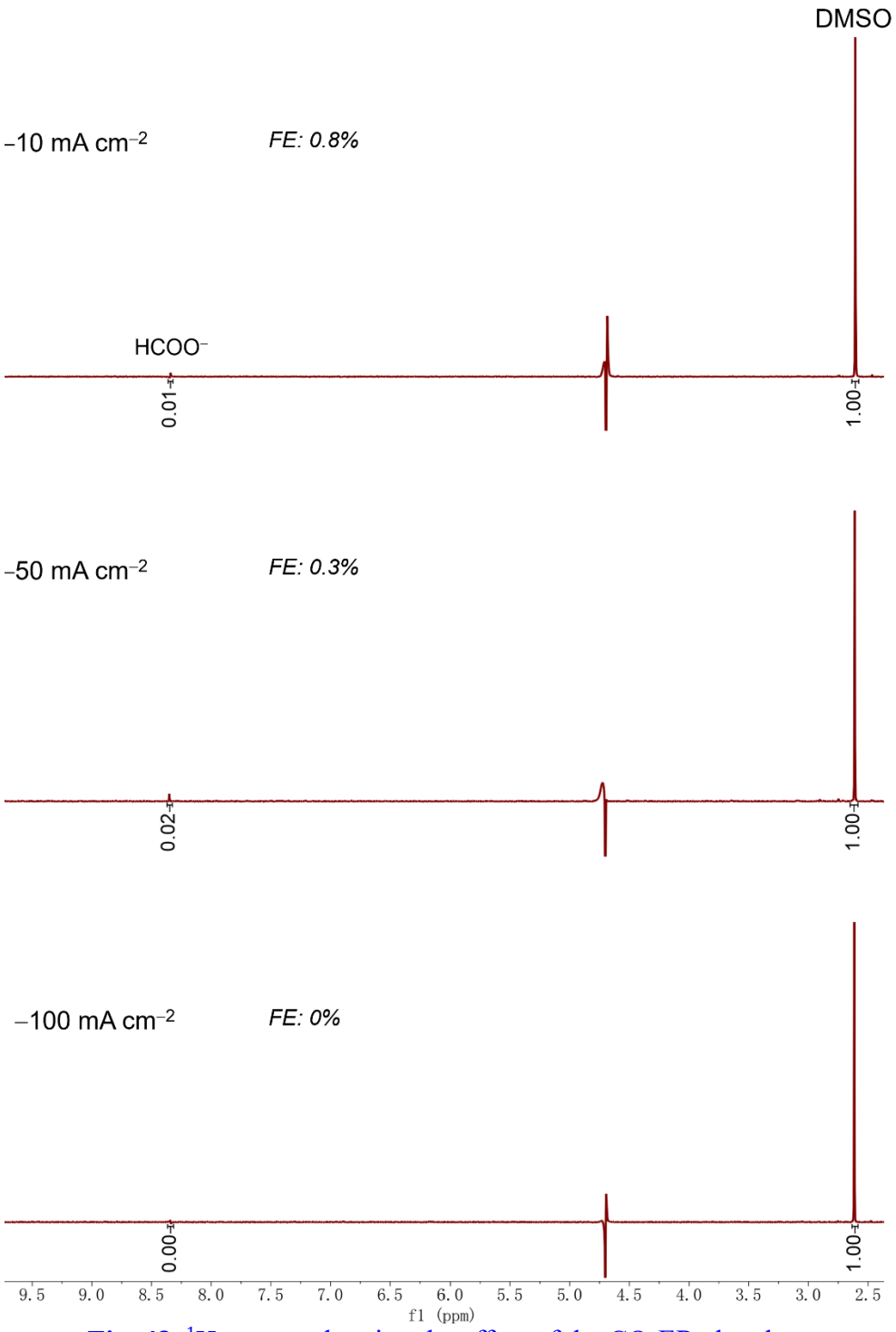

Supplementary Fig. 48. ^{1}H spectra showing the effect of the CO_2ER chamber current density on CO_2 reduction performance after a 3-h reaction under conditions where no current was applied to the HER chamber (conventional CO_2ER). CO_2ER chamber electrolyte: 50 mM $KHCO_3$ and 0.5 M $NaClO_4$ in water.

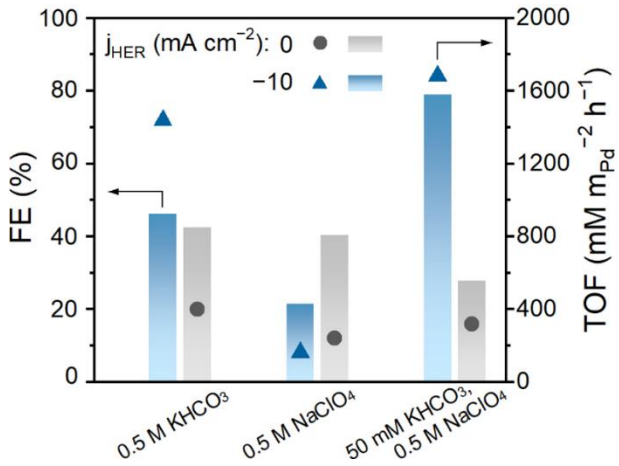

Fig. 2e. Performance comparison of CO_2ER after 3-h electrolysis at –0.25 V vs. RHE in the CO_2ER chamber with j_{HER} of 0 versus –10 mA cm^{-2} in various electrolytes of the CO_2ER chamber. The HER chamber electrolyte was 1.0 M KOH in H_2O.

Supplementary Table 7. Summary of current density values in Fig. 2e.

j_{HER}: 0 mA cm^{-2}		j_{HER}: –10 mA cm^{-2}	
Electrolyte	CO_2ER chamber current density (mA cm^{-2})	Electrolyte	CO_2ER chamber current density (mA cm^{-2})
0.5 M $KHCO_3$	–2.01	0.5 M $KHCO_3$	–3.33
0.5 M $NaClO_4$	–1.27	0.5 M $NaClO_4$	–0.64
50 mM $KHCO_3$, 0.5 M $NaClO_4$	–2.46	50 mM $KHCO_3$, 0.5 M $NaClO_4$	–2.27

4. Regarding the response to Q3, I have an additional question that the performance data in the Supplementary Figs. 45 and 46 do not match well. In Supplementary Fig. 45, it is demonstrated that FE values of reaction systems with j_{HER} of –10 mA/cm^2 and –100 mA/cm^2 are almost equal (~100% vs. ~90%). However, according to the raw data in Supplementary Fig. 46, the relative peak area of reaction systems with j_{HER} of –10 mA/cm^2 and –100 mA/cm^2 are also almost equal (0.16 vs. 0.13), which is confusing. Considering a difference of 10 times between their total charges, the FE with j_{HER} of –10 mA/cm^2 and –100 mA/cm^2 should also differ by ~10 times. Or there is another possibility that the author did not change their FE calculation method as they promised in the response to Q1? But this issue also substantially reduces confidence in the care with which the manuscript was prepared.

Response: The current densities discussed in the manuscript refer specifically to the HER-side current density (j_{HER}), rather than the effective current density in the CO_2ER compartment. The HER and CO_2ER chambers are separated by the Janus Pd membrane and operated using electrically independent polarization circuits. In this dual-chamber configuration, the HER compartment serves as a hydrogen-source chamber that continuously drives hydrogen permeation through the Pd membrane, thereby sustaining Pd–H species at the CO_2ER-side interface where hydride transfer occurs. Accordingly, j_{HER} reflects the hydrogen supply rate rather than the effective CO_2 reduction current density at the CO_2ER interface.

To avoid possible ambiguity in data interpretation, we have now explicitly added the corresponding HER- and CO_2ER-side current density tables associated with **Supplementary Figs.**

45 and **46** in the revised Supplementary Information (**Supplementary Table 10**). In addition, the CO_2ER-side current densities for all experiments discussed in the manuscript are also provided in **Supplementary Tables 3**, **4**, and **7–9**. We further clarify that variations in j_{HER} do not translate into proportional changes in the CO_2ER-side current density, as the CO_2 reduction process in this dual-chamber configuration is primarily governed by interfacial kinetics at the CO_2-facing side. Therefore, a simple scaling relationship between HER-side current input and CO_2ER-side response is not expected in this electrochemically decoupled membrane system.

We further clarify that the Faradaic efficiency (FE) is determined based on the charge passed in the CO_2ER compartment, and the detailed FE calculation procedure, including the definition of the CO_2ER-side charge, has been explicitly described in the Experimental Section of the **Supplementary Information** (**Page 8**).

Supplementary Table 3. Summary of current density values in Fig. 2b.

Potential (V vs. RHE)	CO_2ER chamber current density (mA cm^{-2})
–0.15	–0.56
–0.25	–2.27
–0.35	–2.48
–0.45	–4.13

Supplementary Table 4. Summary of current density values in Fig. 2d.

j_{HER} (mA cm^{-2})	CO_2ER chamber current density (mA cm^{-2})
–1	–1.48
–5	–2.79
–10	–2.27
–50	–1.36

Supplementary Table 7. Summary of current density values in Fig. 2e.

j_{HER}: 0 mA cm^{-2}		j_{HER}: –10 mA cm^{-2}	
Electrolyte	CO_2ER chamber current density (mA cm^{-2})	Electrolyte	CO_2ER chamber current density (mA cm^{-2})
0.5 M $KHCO_3$	–2.01	0.5 M $KHCO_3$	–3.33
0.5 M $NaClO_4$	–1.27	0.5 M $NaClO_4$	–0.64
50 mM $KHCO_3$, 0.5 M $NaClO_4$	–2.46	50 mM $KHCO_3$, 0.5 M $NaClO_4$	–2.27

Supplementary Table 8. Summary of current density values in Fig. 2f.

j_{HER}: 0 mA cm^{-2}		j_{HER}: −10 mA cm^{-2}	
Electrolyte	CO_2ER chamber current density (mA cm^{-2})	Electrolyte	CO_2ER chamber current density (mA cm^{-2})
50 mM $NaHCO_3$, 0.5 M $NaClO_4$	−2.44	50 mM $NaHCO_3$, 0.5 M $NaClO_4$	−1.00
50 mM $KHCO_3$, 0.5 M $NaClO_4$	−2.46	50 mM $KHCO_3$, 0.5 M $NaClO_4$	−2.27
50 mM $CsHCO_3$, 0.5 M $NaClO_4$	−2.10	50 mM $CsHCO_3$, 0.5 M $NaClO_4$	−1.02

Supplementary Table 9. Summary of current density values in Fig. 3b.

Potential (V vs. RHE)	CO_2ER chamber current density (mA cm^{-2})
−0.15	−0.38
−0.25	−2.58
−0.35	−4.41
−0.45	−3.85

Supplementary Table 10. Summary of current values in Supplementary Fig. 45

j_{HER} (mA cm^{-2})	CO_2ER chamber current density (mA cm^{-2})
−10	−1.13
−50	−1.27
−100	−1.21

Reviewer #4

The authors have addressed my major concerns in a satisfactory manner. In particular, the revised Faradaic-efficiency analysis, the additional flow-cell stability data, and the added controls substantially strengthen the manuscript. I still consider the term “tunable hydricity” somewhat strong. However, this point should not prevent publication. I therefore support the acceptance of the manuscript.

Response: We sincerely thank the reviewer for the positive evaluation and for acknowledging that the revised analyses, stability data, and controls substantially strengthen the manuscript. We appreciate the reviewer’s recommendation for publication.

Restructured Point-by-Point Response to Reviewer #3's Comments (Round 1)

Reviewer #3

In this manuscript, Hu et. al. reported a Janus palladium membrane electrode, affording CO_2-to-formate conversion via hydride transfer mechanism, rather than conventional PCET mechanism. This was achieved by tuning the hydricity of Pd–H species via external polarization. The key point of the study is very clear, and I believe the tunable hydricity in the Pd-membrane provides great insights for more reaction systems for value-added chemicals synthesis. Therefore, I support its publication, and have the following concerns for the authors.

Response: We sincerely thank the reviewer for the positive evaluation of our work and for recognizing the significance of tunable hydricity in the Janus Pd membrane system for hydride-transfer-mediated CO_2 conversion. We are encouraged by the reviewer's interest in the broader implications of this strategy for future electrosynthetic transformations and appreciate the constructive comments provided below.

1. The calculation of FE in this work is significant but not clarified, especially in regard to the FE higher than 100%. According to the Figure 2e and 2f, it is speculated that the total charge used in the FE calculation formula only contains that of the CO_2ER chamber. Considering that the applied polarization circuits at the HER and CO_2ER chamber are independent, it is theoretically impossible for total FE more than 100%. Hence, the detailed calculation process on FE should be provided and re-checked.

Response: We appreciate the reviewer's insightful comment regarding the electron-counting basis used for Faradaic efficiency (FE) analysis. As pointed out by the reviewer, the polarization circuits used in the HER and CO_2ER compartments are electrically independent, and the current from the HER compartment is not included in the Faradaic efficiency calculation for the CO_2ER compartment. In the original manuscript (**Fig. 2**), FE values were calculated using the conventional two-electron proton-coupled electron transfer (PCET) assumption for CO_2-to-formate conversion, and therefore represent apparent Faradaic efficiencies. Under this normalization, the calculated FE values can exceed 100%, which initially prompted us to further examine the underlying reaction mechanism. This apparent inconsistency motivated the mechanistic investigation presented in **Fig. 3**. Through isotope-labeling experiments, we were able to distinguish formate generated via hydride transfer from Pd–H species (deuterated formate) and that arising from the conventional PCET pathway (non-deuterated formate). Based on this analysis, we quantified the respective contributions of the two pathways. These results clearly indicate that CO_2 reduction in the J-Pd_m system is dominated by a Pd–H-mediated hydride transfer pathway originating from the HER side, rather than a conventional PCET process alone. Accordingly, we agree with the reviewer that, given the hydride-transfer-dominated reaction mechanism established in this work, FE values should not be interpreted using the conventional two-electron PCET stoichiometry and should not exceed 100% under a physically consistent definition. We have therefore revised all FE values in **Fig. 2** and the corresponding discussions using a one-electron hydride-transfer basis. This revision ensures consistency with the mechanistic picture established in **Fig. 3** and does not affect the observed experimental trends.

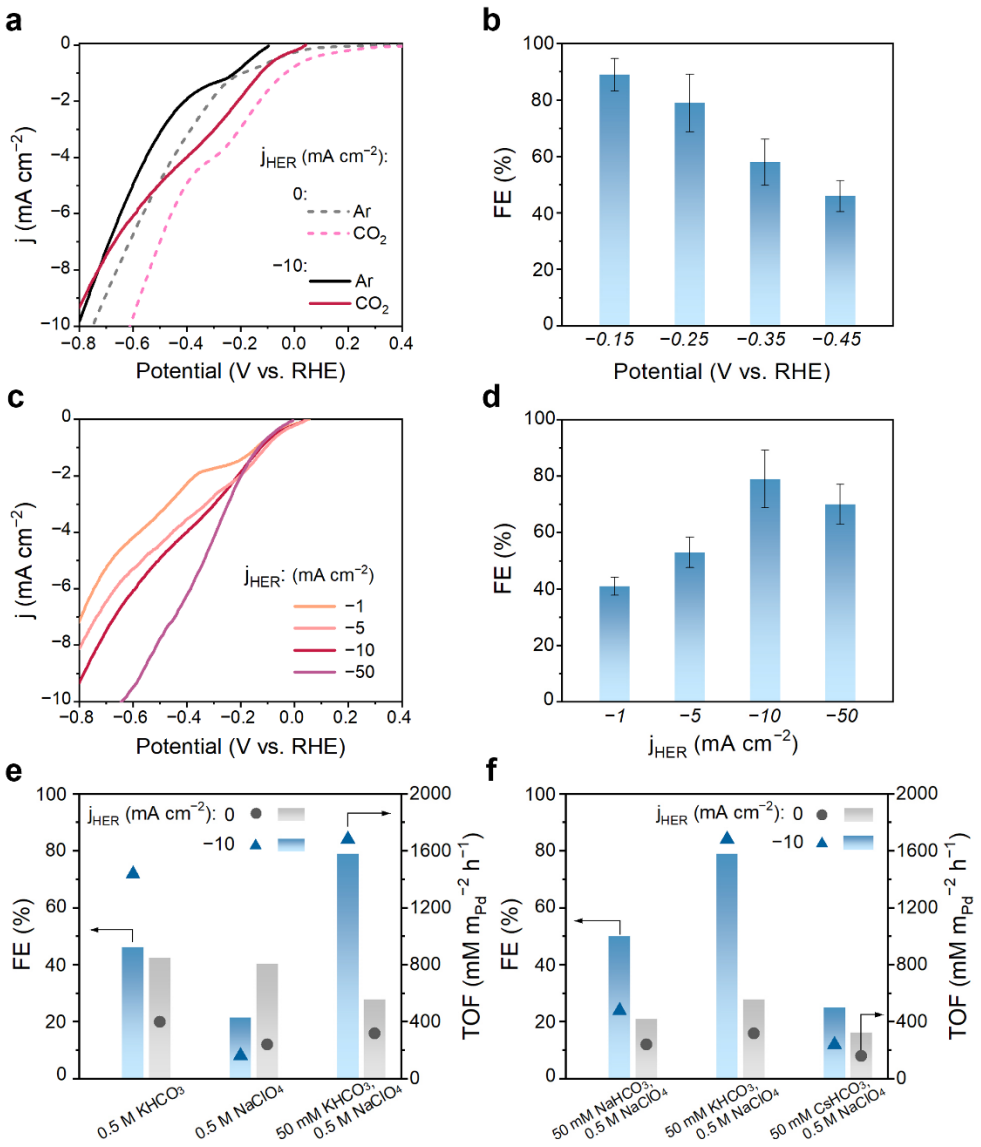

Fig. 2 | Performance of CO_2ER using J-Pd_m under various conditions. a, Linear sweep voltammograms collected on the CO_2ER side of J-Pd_m in the absence or presence of CO_2, together with or without j_{HER} = –10 mA cm^{-2} applied on the HER side. **b**, Faradaic efficiencies of formate production after 3-h electrolysis at various applied potentials in the CO_2ER chamber with j_{HER} = –10 mA cm^{-2} in the HER chamber. **c**, Linear sweep voltammograms collected on the CO_2ER side of J-Pd_m in the presence of CO_2 together with varying j_{HER}. **d**, Faradaic efficiencies of formate production after 3-h electrolysis at –0.25 V vs. RHE in the CO_2ER chamber with varying j_{HER}. **e**, Performance comparison of CO_2ER after 3-h electrolysis at –0.25 V vs. RHE in the CO_2ER chamber with j_{HER} of 0 versus –10 mA cm^{-2} in various electrolytes of the CO_2ER chamber. **f**, Cation effect comparison of CO_2ER after 3-h electrolysis at –0.25 V vs. RHE in the CO_2ER chamber with j_{HER} of 0 versus –10 mA cm^{-2}. In **a**–**f**, the HER chamber electrolyte was 1.0 M KOH in H_2O. In **a**–**d**, the CO_2ER chamber electrolyte was 50 mM $KHCO_3$ and 0.5 M $NaClO_4$ in H_2O.

2. According to the previous study (Joule 2024, 8, 728-745), the OCP value at the $^{*}H/H^{+}$ polarization interface is significantly influenced by the solution pH. Hence, the more positive OCP values after introducing CO_2 should be discussed thoroughly regarding the change of solution pH.
Response: We thank the reviewer for pointing out the influence of solution pH on OCP behavior and for providing the relevant reference (Joule 2024, 8, 728–745). Following the reviewer's suggestion, we measured the electrolyte pH before and after CO_2 saturation, and the results are now included in **Supplementary Tables 5** and **6**. The electrolyte pH changes from 8.65 under Ar to 6.44 after CO_2 saturation. Consistent with the literature report, the decrease in solution pH correspondingly induces a positive shift in the observed OCP.

In our J-Pd_m system, the OCP is governed by two controlled variables: (i) the gas atmosphere (Ar vs CO_2) and (ii) the state of the Pd membrane (metallic Pd vs Pd–H). Under j_{HER} = 0 mA cm^{-2}, the Pd membrane remains in a predominantly metallic Pd state, giving an OCP of ~0.8–0.9 V vs. RHE. Switching between Ar and CO_2 induces a small OCP shift due to the decrease in solution pH upon CO_2 saturation, consistent with the behavior reported in the literature (Joule 2024, 8, 728–745). When the HER side is polarized at j_{HER} = −10 mA cm^{-2} prior to OCP measurement, hydrogen generated in the HER compartment permeates through the Pd membrane, forming a hydrogen-rich Pd–H phase, as confirmed by XRD (**Supplementary Fig. 43**). This increases the hydrogen chemical potential within the Pd lattice and shifts the interfacial state on the CO_2-facing side, resulting in a lower OCP approaching ~0 V vs. RHE, consistent with a Pd–H-dominated equilibrium. Therefore, the OCP variations directly reflect the change in Pd membrane state between metallic Pd and Pd–H, together with minor perturbations from CO_2-induced solution speciation effects. We have clarified this discussion in the revised Supplementary Information and cited the corresponding reference in the revised manuscript.

Supplementary Table 5. Summary of electrolyte pH values.

Electrolyte	H_2O	0.5 M $NaClO_4$	5 mM $KHCO_3$, 0.5 M $NaClO_4$	10 mM $KHCO_3$, 0.5 M $NaClO_4$	20 mM $KHCO_3$, 0.5 M $NaClO_4$	50 mM $KHCO_3$, 0.5 M $NaClO_4$	75 mM $KHCO_3$, 0.5 M $NaClO_4$	0.5 M $KHCO_3$
pH	6.91±0.06	6.47±0.04	8.36±0.01	8.48±0.01	8.52±0.01	8.65±0.01	8.68±0.01	8.87±0.02

Supplementary Table 6. Summary of electrolyte pH values after CO_2 saturation

Electrolyte	H_2O	0.5 M $NaClO_4$	5 mM $KHCO_3$, 0.5 M $NaClO_4$	10 mM $KHCO_3$, 0.5 M $NaClO_4$	20 mM $KHCO_3$, 0.5 M $NaClO_4$	50 mM $KHCO_3$, 0.5 M $NaClO_4$	75 mM $KHCO_3$, 0.5 M $NaClO_4$	0.5 M $KHCO_3$
pH	4.03±0.02	3.97±0.02	5.46±0.02	5.75±0.01	6.01±0.01	6.44±0.02	6.58±0.02	7.45±0.01

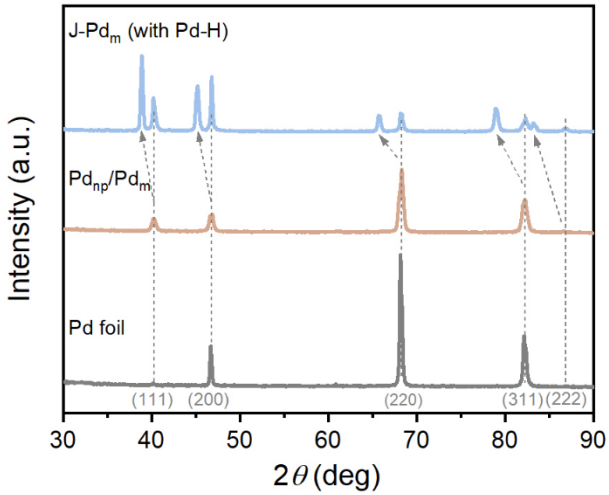

Supplementary Fig. 43. X-ray diffraction patterns of the Pd membrane (Pd_{np}/Pd_m) before and after hydrogen permeation.

3. Hunt et al. (J. Am. Chem. Soc. 2023, 145, 14316−14323) proposed that the hydrogenation thermodynamics of CO_2 in Pd membrane reactor is significantly affected by HER chamber current density and almost no product at low current density. Therefore, I think that it is more reasonable to compare the CO_2 hydrogenation efficiency of different reaction modes (ePMR, conventional CO_2ER and Janus CO_2ER) under higher HER chamber's current density.

Response: In response to the reviewer's suggestion, we have added additional ePMR and J-Pd_m control experiments under a range of HER-side current densities (−10, −50, and −100 mA cm^{-2}) in aqueous electrolyte, together with the corresponding comparison data. In the ePMR configuration, the absence of cathodic polarization on the CO_2-facing side limits the reactivity of permeated hydrogen species. Although previous studies have shown that protic media such as water can promote disproportionation of surface Pd–H species, enabling limited hydride-transfer reactivity at Pd interfaces (J. Am. Chem. Soc. 2025, 147, 10974–10980; JACS Au 2024, 4, 328–343; Chem. Sci. 2026, 17, 1039–1050), the spontaneous formation of sufficiently hydridic Pd–H species remains inefficient, and hydride transfer to CO_2 is kinetically unfavorable under these open-circuit conditions (FE ≈ 0.06%) (J. Am. Chem. Soc. 2023, 145, 14316–14323). Consequently, although trace formate formation can still be observed (**Supplementary Fig. 47**), majority of the permeated hydrogen species preferentially undergo recombination/desorption to produce H_2.

In contrast, the J-Pd_m configuration enables independent polarization of the CO_2-facing interface, allowing electrochemical regulation of Pd–H hydricity. This enhances the hydride-transfer capability of the interfacial Pd–H species and leads to higher formate formation compared to the corresponding ePMR conditions. Importantly, at identical HER-side current densities, J-Pd_m consistently shows improved catalytic performance (**Supplementary Figs. 45** and **46**), highlighting the role of interfacial polarization in enabling efficient CO_2-to-formate conversion. This distinction becomes even more pronounced in aprotic acetonitrile electrolyte. In the absence of protic species, spontaneous formation of hydridic Pd–H is strongly suppressed, and no detectable formate is observed under open-circuit conditions (**Supplementary Fig. 62**). By contrast, the J-Pd_m configuration enables electrochemically driven hydride transfer to CO_2 under fully aprotic conditions, leading to efficient formate formation (**Supplementary Figs. 63** and **64**).

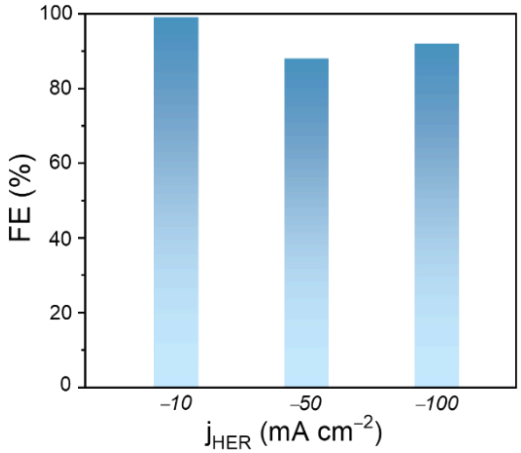

Supplementary Fig. 45. Faradaic efficiency of formate formation: effect of HER chamber current density (j_{HER}) on CO_2 reduction performance after a 3-h reaction at –0.25 V vs. RHE in the CO_2ER chamber (J-Pd_m system, 50 mM $KHCO_3$ + 0.5 M $NaClO_4$ (aq)), with Pd_{np}/Pd_m (2 cm^2).

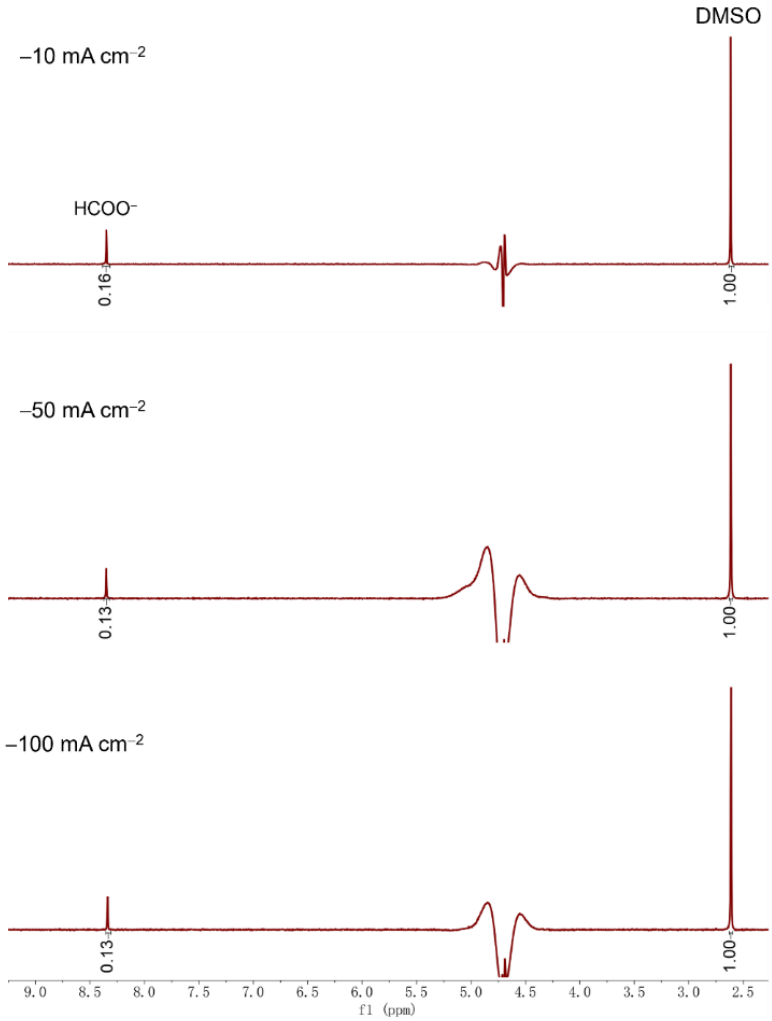

Supplementary Fig. 46. ^1H spectra: effect of HER chamber current density (j_{HER}) on CO_2 reduction performance after a 3-h reaction at –0.25 V vs. RHE in the CO_2ER chamber (J-Pd_m system, 50 mM $KHCO_3$ + 0.5 M $NaClO_4$ (aq)), with Pd_{np}/Pd_m (2 cm^2).

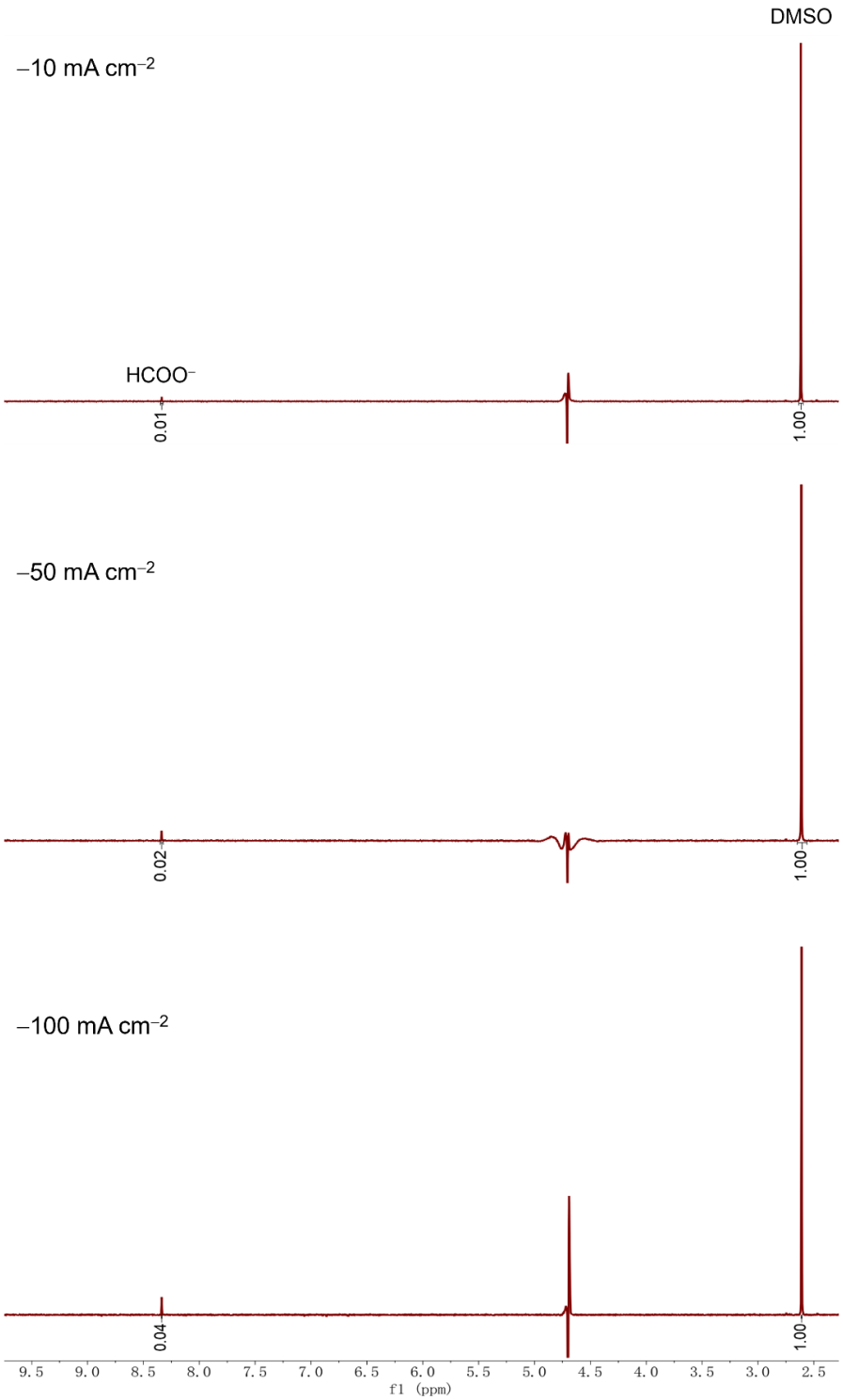

Supplementary Fig. 47. ^{1}H spectra: effect of HER chamber current density (j_{HER}) on CO_2 reduction performance after a 3-h reaction under conditions without potential applied to the CO_2ER chamber with 50 mM $KHCO_3$ and 0.5 M $NaClO_4$ in water (ePMR system, Pd_{np}/Pd_m: 2 cm^2).

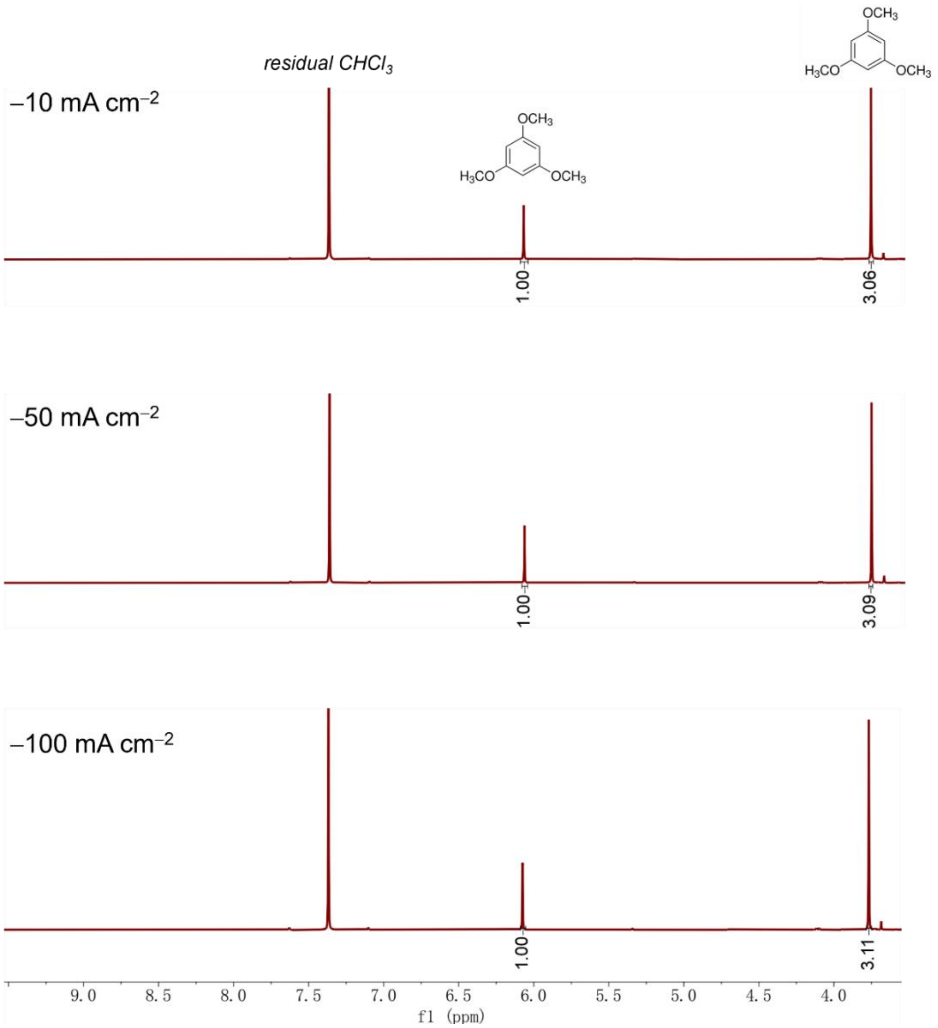

Supplementary Fig. 62. ^{1}H spectra: effect of HER chamber current density (j_{HER}) on CO_2 reduction performance after 6-h reaction under conditions without potential applied to the CO_2ER chamber with 0.1 M $TBABF_4$ in CH_3CN (ePMR system).

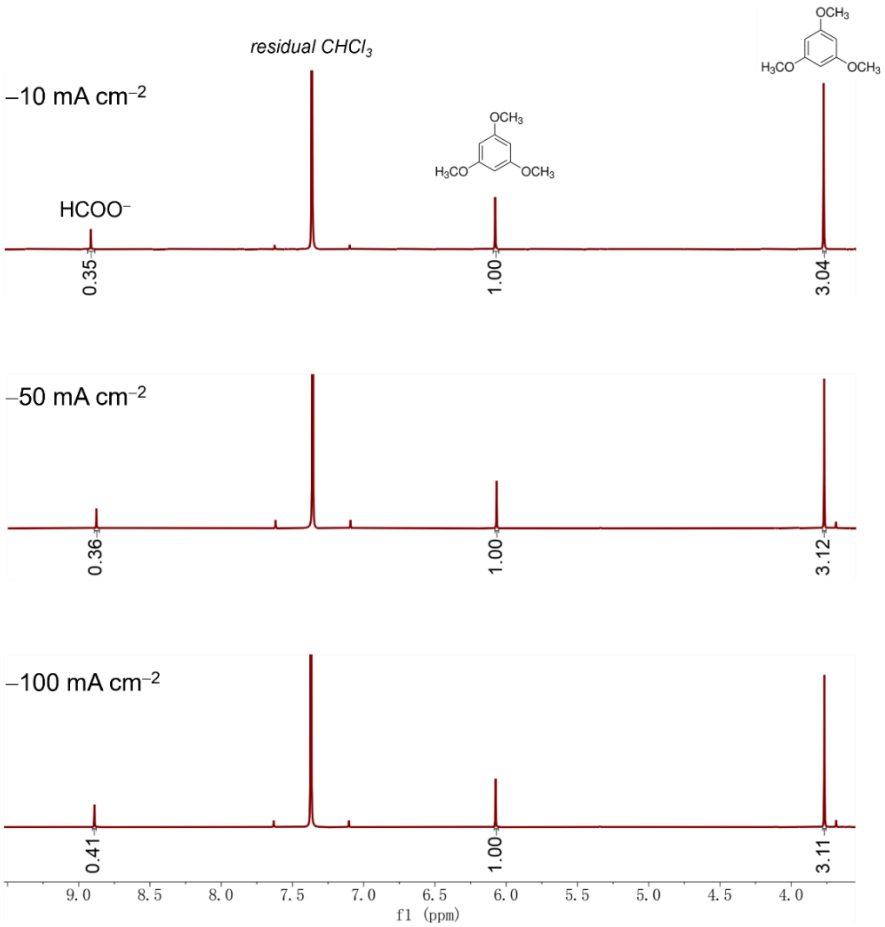

Supplementary Fig. 63. ^{1}H spectra: effect of HER chamber current density (j_{HER}) on CO_2 reduction performance for 6-h electrolysis at –1.75 V vs. $Fc^{+/0}$ in the CO_2ER chamber (J-Pd_m system, 0.1 M $TBABF_4/CH_3CN$).

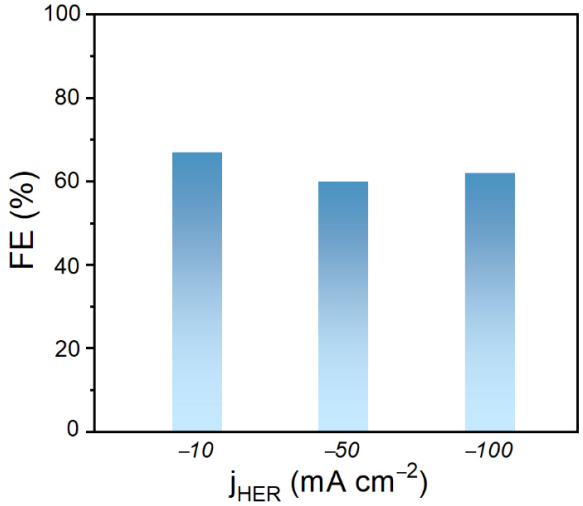

Supplementary Fig. 64. Faradaic efficiency of formate formation: effect of HER chamber current density (j_{HER}) on CO_2 reduction performance for 6-h electrolysis at –1.75 V vs. $Fc^{+/0}$ in the CO_2ER chamber (J-Pd_m system, 0.1 M $TBABF_4/CH_3CN$).

4. As a more comprehensive evaluation, the FE corresponding to the H_2 evolution in the HER chamber and CO_2ER chamber should also be provided to demonstrate the respective distributions of electrons in the two circuits.

Response: We appreciate the reviewer's suggestion to provide a more comprehensive evaluation of electron distribution across both compartments. In response, we have now quantified the Faradaic efficiency for H_2 evolution in both the HER and CO_2ER chambers to provide a complete description of electron partitioning in the dual-circuit system. When the Pd membrane electrode is immersed in the electrolyte (not act as a membrane electrode), H_2 evolution was quantified by gas collection using a water-displacement method, and a near-unity H_2 Faradaic efficiency (~100%) was obtained across the applied current range (**Supplementary Figs. 5** and **6**), confirming that electrons in this compartment are exclusively consumed for H_2 evolution, which serves as a continuous hydrogen reservoir to maintain sufficient Pd–H coverage on the CO_2-facing side of the membrane.

In the CO_2ER chamber, additional control and isotope-labeling experiments further clarify the electron utilization pathways. When D_2O was used as the hydrogen source in the hydride-transfer experiments (**Fig. 3**), deuterated formate was quantified by ^{2}H NMR spectroscopy, whereas HD as the gaseous product was identified by isotope ratio mass spectrometry (IRMS) (**Fig. 4b**). The results confirmed the formation of deuterated formate together with HD as the only gaseous hydrogen-containing product, with no H_2 observed. This indicates that, under hydride-transfer conditions for CO_2 reduction, proton–hydride recombination to form H_2 is the primary competing pathway for electron consumption. Consistently, GC measurements performed during CO_2 reduction electrolysis in CO_2-saturated electrolytes also confirm the presence of H_2 as a side-product in the CO_2ER compartment (**Supplementary Fig. 27**), demonstrating that electrons in this chamber are distributed between CO_2-to-formate conversion and H_2 evolution via hydride-transfer-mediated pathways.

Taken together, these results provide a complete picture of electron partitioning in the J-Pd_m system: the HER chamber functions exclusively as a hydrogen-generation reservoir, while in the CO_2ER chamber electrons are partitioned between CO_2-to-formate conversion via hydride transfer and competitive proton–hydride coupling leading to H_2 evolution.

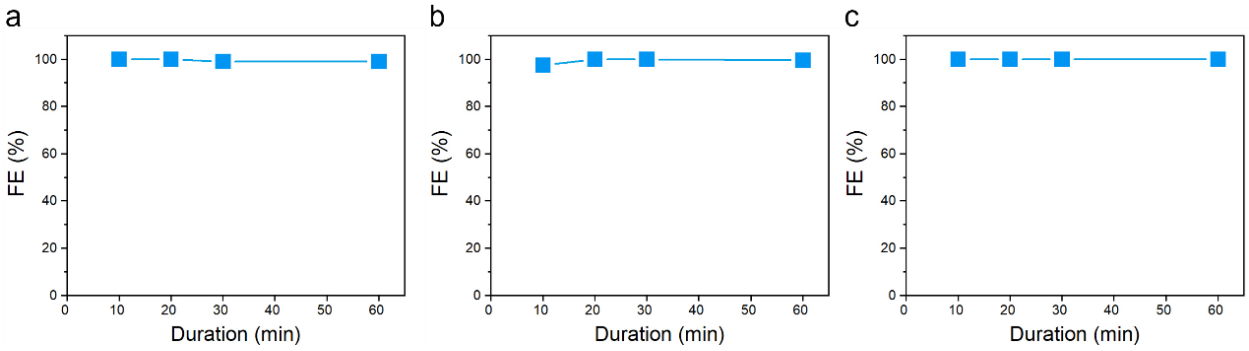

Supplementary Fig. 5. Hydrogen generation capability of an immersed Pd membrane (1 M KOH) as a function of time at different current densities, measured by H_2 collection via water displacement. (a) –10 mA cm^{-2}; (b) –25 mA cm^{-2}; (c) –50 mA cm^{-2}.

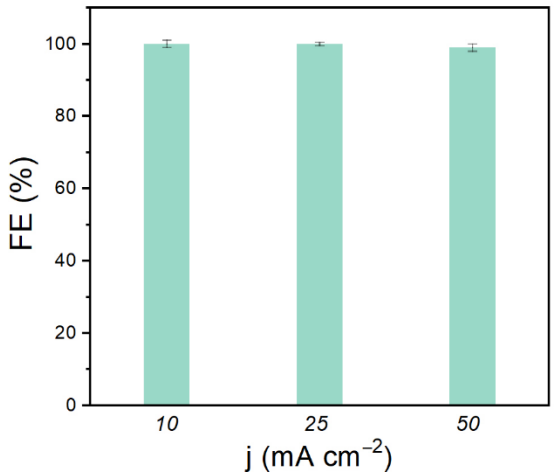

Supplementary Fig. 6. Pd membrane immersed in electrolyte (1 M KOH): hydrogen generation capability on the Pd membrane at different current densities, measured by H_2 collection via water displacement.

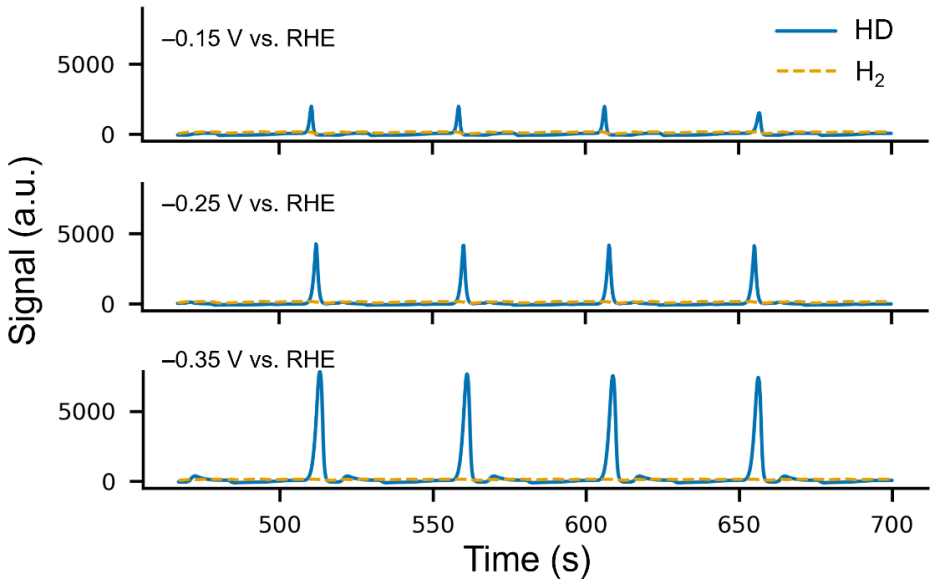

Fig. 4b. Isotope ratio mass spectrometry results recorded in the steady-state region of electrolysis at −0.15 V, −0.25 V and −0.35 V vs. RHE, illustrating highly reproducible HD signals (blue) and negligible H_2 response (orange) in the gas phase.

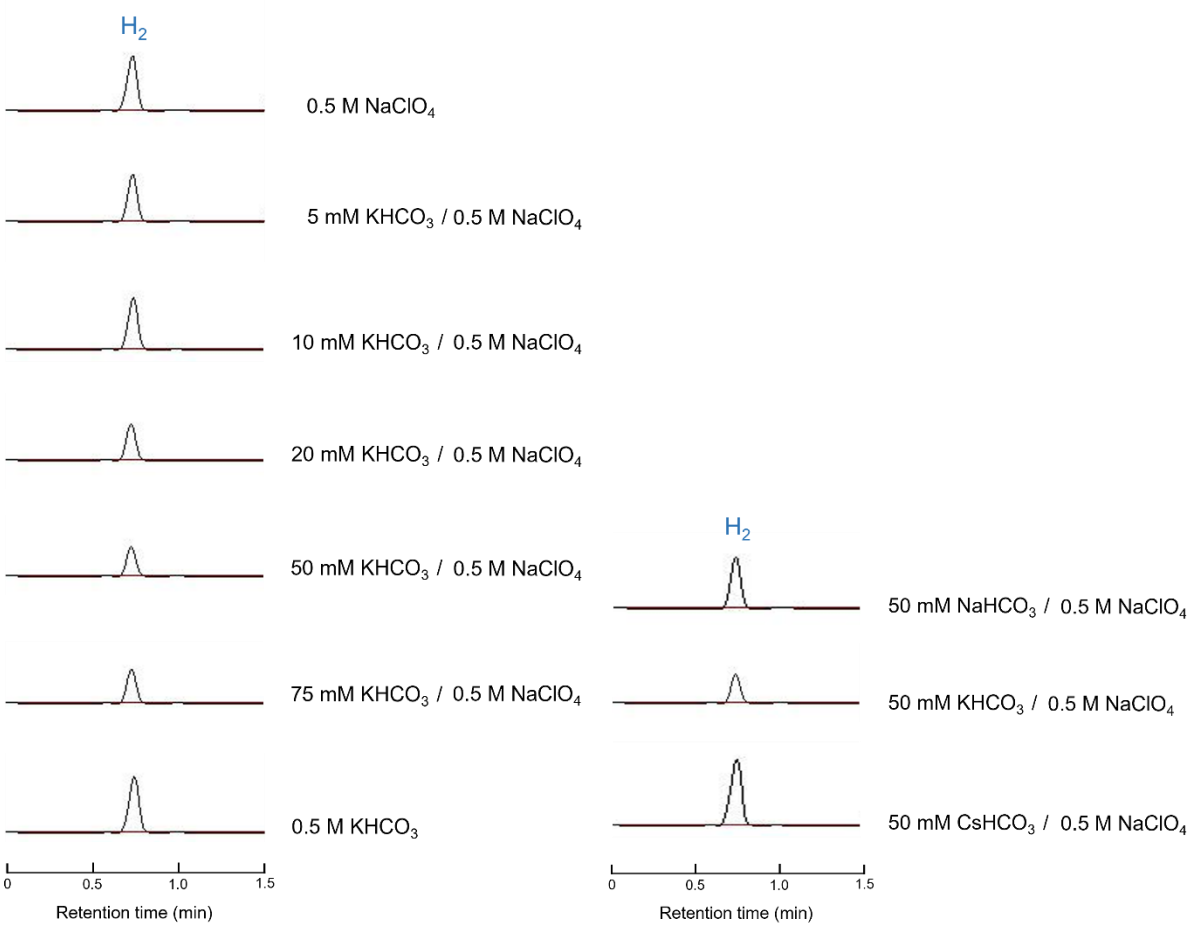

Supplementary Fig. 27. GC analysis after 3-h electrolysis at −0.25 V vs. RHE in the CO_2ER chamber using different electrolytes (j_{HER} = −10 mA cm^{-2}).

5. The Janus hydrogenation system features two independent circuits and their respective polarization effects on hydrogen species. However, whether a synergistic interaction exists between these two circuits remains unexplored. This study (Chem Catal. 2026, https://doi.org/10.1016/j.checat.2025.101602) aims to address this gap.

Response: We appreciate the reviewer for raising the point regarding the possible synergistic interaction between the two independently polarized circuits in the Janus hydrogenation system. We agree that the interplay between hydrogen generation, transmembrane hydrogen transport, and interfacial hydrogen utilization is fundamentally important in Pd-membrane-based hydrogenation systems. As highlighted in the recent Chem Catalysis study suggested by the reviewer (Chem Catal. 2026, https://doi.org/10.1016/j.checat.2025.101602), independently polarized interfaces can exhibit cooperative effects arising from the distinct kinetic roles of bulk hydrogen species and surface hydrogen species. In our J-Pd_m system, although the HER and CO_2ER chambers operate using electrically independent circuits, they are intrinsically coupled through Pd–H generation, hydrogen permeation, and hydride consumption across the Pd membrane. Specifically, the HER chamber continuously supplies hydrogen species to maintain sufficient Pd–H coverage on the CO_2-facing side of the membrane, whereas the CO_2ER chamber governs the subsequent utilization pathways of Pd–H species, including hydride transfer to CO_2 and competing proton–hydride coupling leading to H_2 evolution. This coupling behavior is reflected in the HER-current-

dependent experiments presented in this work (**Fig. 2d** and **Supplementary Figs. 45–47**). At low HER-side current densities, insufficient hydrogen supply limits Pd–H availability at the CO_2-facing interface. In contrast, increasing the HER-side current density beyond an optimal range does not further improve formate production, indicating that the hydrogen utilization process at the CO_2ER interface rather than hydrogen supply itself becomes the dominant limitation. While the primary focus of the present work is the hydride-transfer-mediated CO_2 reduction mechanism enabled by the Janus Pd membrane architecture, the reviewer's comment and the recent Chem Catalysis study provide important perspectives for understanding interfacial coupling and cooperative hydrogen regulation in dual-circuit Pd membrane systems.

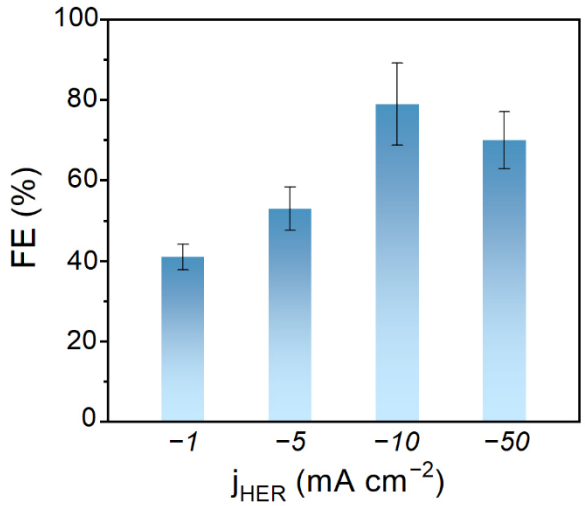

Fig. 2d. Faradaic efficiencies of formate production after 3-h electrolysis at –0.25 V vs. RHE in the CO_2ER chamber with varying j_{HER}. The HER chamber electrolyte was 1.0 M KOH in H_2O, and the CO_2ER chamber electrolyte was 50 mM $KHCO_3$ and 0.5 M $NaClO_4$ in H_2O.

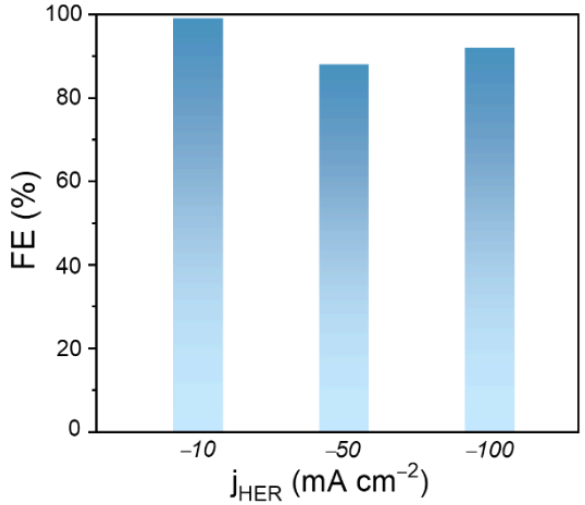

Supplementary Fig. 45. Faradaic efficiency of formate formation: effect of HER chamber current density (j_{HER}) on CO_2 reduction performance after a 3-h reaction at –0.25 V vs. RHE in the CO_2ER chamber (J-Pd_m system, 50 mM $KHCO_3$ + 0.5 M $NaClO_4$ (aq)), with Pd_{np}/Pd_m (2 cm^2).

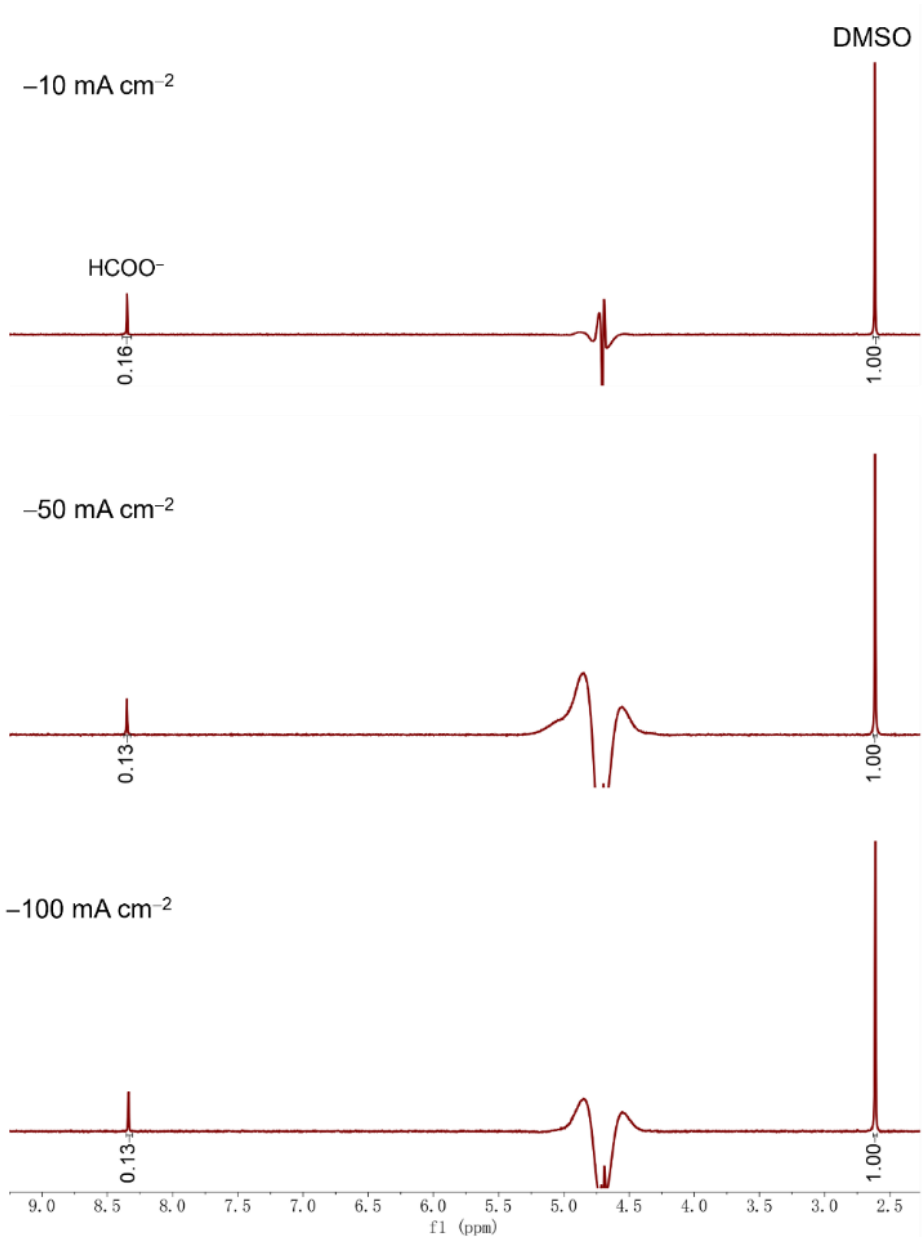

Supplementary Fig. 46. ^{1}H spectra: effect of HER chamber current density (j_{HER}) on CO_2 reduction performance after a 3-h reaction at –0.25 V vs. RHE in the CO_2ER chamber (J-Pd_m system, 50 mM $KHCO_3$ + 0.5 M $NaClO_4$ (aq)), with Pd_{np}/Pd_m (2 cm^2).

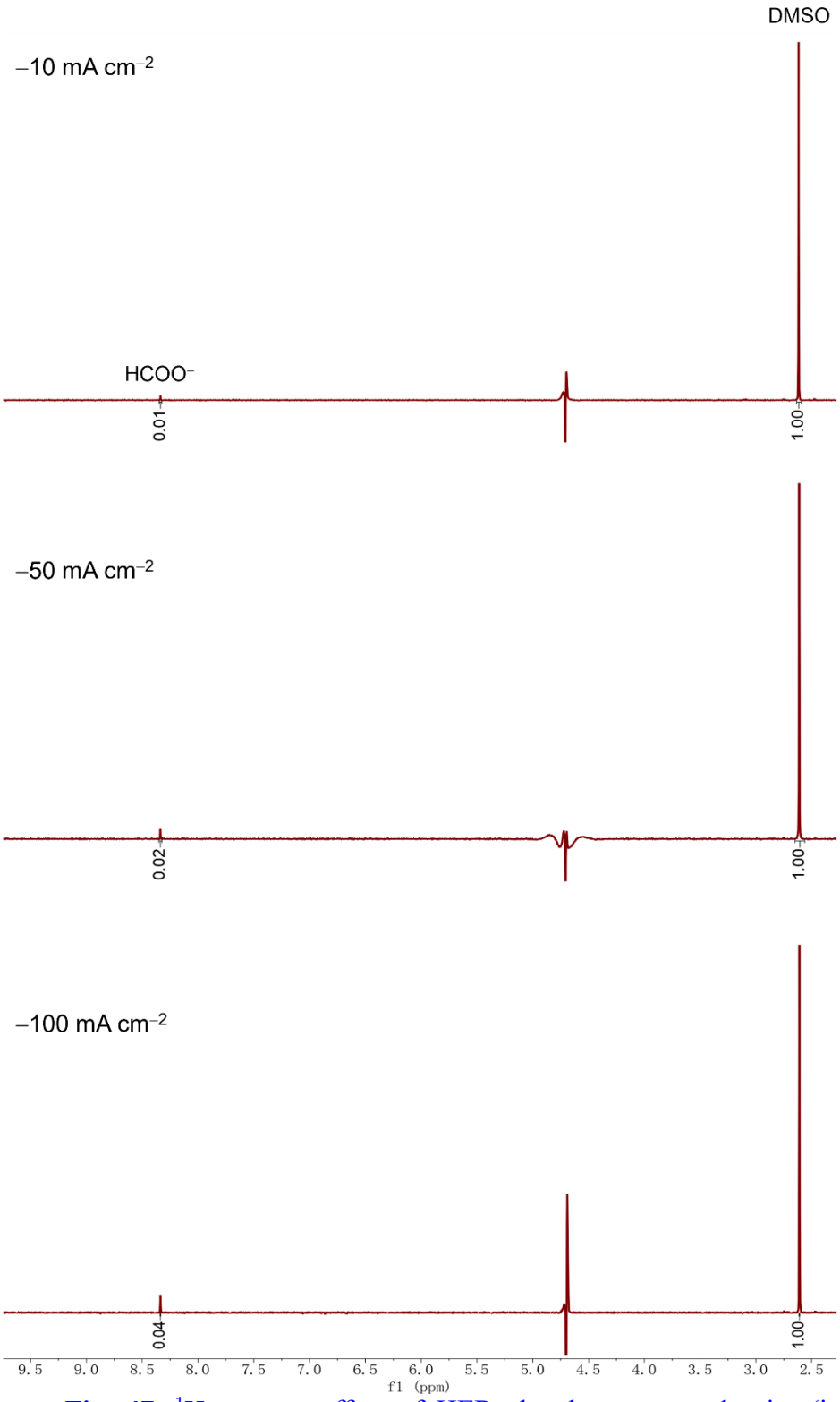

Supplementary Fig. 47. ^{1}H spectra: effect of HER chamber current density (j_{HER}) on CO_2 reduction performance after a 3-h reaction under conditions without potential applied to the CO_2ER chamber with 50 mM $KHCO_3$ and 0.5 M $NaClO_4$ in water (ePMR system, Pd_{np}/Pd_m: 2 cm^2).

6. In the Figure 1b, it is proposed that HCOOH production in aprotic solvents is forbidden in ePMR. The CO_2 hydrogenation experimental results without the CO_2ER polarization in aprotic solvents should be provided as a response.

Response: We appreciate the reviewer for pointing out the need for experimental verification of the proposed behavior shown in **Fig. 1b**. In response, we performed additional ePMR control experiments in CO_2-saturated acetonitrile without applying CO_2ER-side polarization. HER-side current densities of −10, −50, and −100 mA cm^{-2} were examined, and no detectable formate product was observed under all tested conditions (**Supplementary Fig. 62**). These results indicate that, although hydrogen permeation through the Pd membrane can still occur under aprotic conditions, CO_2 hydrogenation to formate was not observed in the absence of CO_2ER-side electrochemical polarization. The corresponding experimental results and related discussion have been incorporated into the revised manuscript and Supplementary Information.

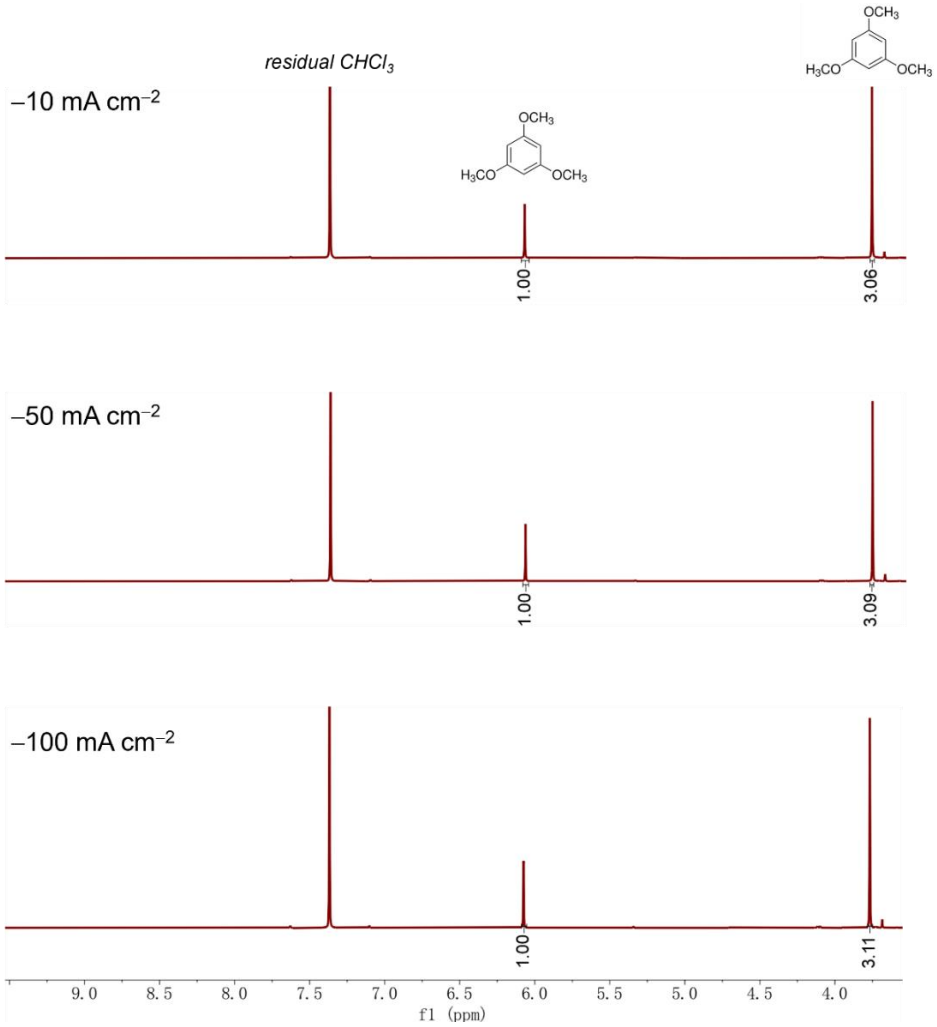

Supplementary Fig. 62. ^1H spectra: effect of HER chamber current density (j_{HER}) on CO_2 reduction performance after 6-h reaction under conditions without potential applied to the CO_2ER chamber with 0.1 M $TBABF_4$ inCH_3CN (ePMR system).

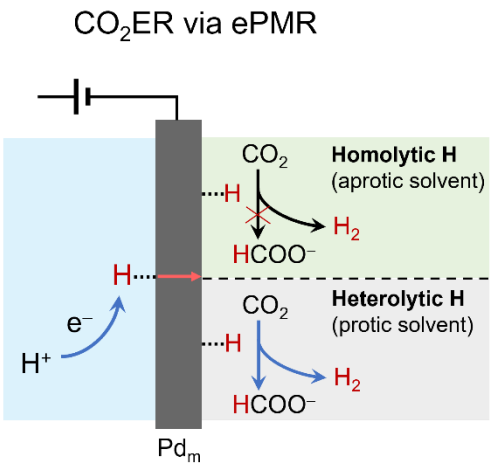

Fig. 1b. Electrocatalytic CO_2 reduction in a palladium membrane reactor.

7. I noticed that when applying a more negative potential at the chemical compartment, FE of formate reduced under different conditions (Fig. 2b, Fig. 3b, Fig. 5c). The reason for this observation under specific conditions requires further explanation, more than simply attribute it to the competition of HER. I assumed that delta G of Pd-H species should be larger at more negative potential, making it easier for CO_2RR. In addition, since the current density at electrochemical chamber is fixed, leading to a similar migrated H species amount and thus H species coverage at Pd surface in the chemical chamber, the recombination of H species to give H_2 may not be more competitive.

Response: We thank the reviewer for this insightful comment regarding the potential-dependent variation in formate Faradaic efficiency. We agree that applying more negative polarization at the CO_2-facing side can, in principle, increase the thermodynamic driving force associated with hydride transfer from Pd–H species. However, the observed decrease in formate Faradaic efficiency at more negative potentials indicates that the overall selectivity is not determined solely by hydride transfer thermodynamics, but by the balance between interfacial hydride-transfer kinetics and competing surface processes at the CO_2-facing electrode, which become increasingly significant under stronger polarization conditions.

In aqueous electrolytes, the primary competing pathway to CO_2 hydride transfer is proton–hydride recombination ($H^+ + H^- \rightarrow H_2$). This is directly supported by isotopic labeling experiments. When H_2O in the HER chamber is replaced by D_2O, the hydride species transported to the CO_2ER side is converted to D^-. In addition to the formation of $DCOO^-$ (**Fig. 3**), the only gaseous product detected is HD, with no H_2 observed (**Fig. 4b**), confirming that the dominant competing pathway is hydride–proton coupling rather than conventional D_2 (or H_2) evolution at the CO_2-facing interface. As reported in the literature (Acc. Chem. Res. 2024, 57, 3488–3499), in aqueous media proton–hydride recombination to form H_2 is thermodynamically more favorable than hydride transfer to CO_2 to form formate, with the corresponding hydricity thresholds required for Pd–H species estimated at 34.2 and 24.1 kcal mol^{-1}, respectively (**Fig. R1**). In our $KHCO_3$/$NaClO_4$ mixed electrolyte system, the CO_2/HCO_3^- equilibrium together with interfacial buffering capacity (J. Am. Chem. Soc. 2020, 142, 13384–13390) enhances CO_2 availability while maintaining favorable interfacial polarization conditions. This optimized interfacial environment shifts the reaction competition such that hydride transfer to CO_2 is favored over proton consumption to form

H_2. At more negative applied potentials, however, stronger driving forces induce local CO_2 mass-transport limitations and partial disruption of the buffering equilibrium. Under these conditions, the polarized Pd–H species increasingly undergo competing reactions with protons, leading to decreased formate Faradaic efficiency.

In aprotic acetonitrile, proton-mediated H_2 evolution is absent. However, Pd exhibits strong CO_2 adsorption and can catalyze direct electron-transfer pathways leading to CO formation and carbonate species (CO_3^{2-}) (ACS Catal. 2023, 13, 5780–5786), consistent with our LSV results in **Fig. 5b**. Even under conditions where no current is applied on the HER side, Pd alone can promote CO_2 reduction, and both CO and CO_3^{2-} are detected experimentally (**Fig. 5e, f**). At more negative potentials, this direct CO_2 reduction pathway is further enhanced. The generated CO strongly adsorbs on Pd, partially blocking active sites and thereby reducing the accessibility of interfacial Pd–H species. This site-blocking effect suppresses hydrogen permeation and limits exposure of Pd–H active sites, ultimately decreasing hydride transfer to CO_2 and reducing formate Faradaic efficiency.

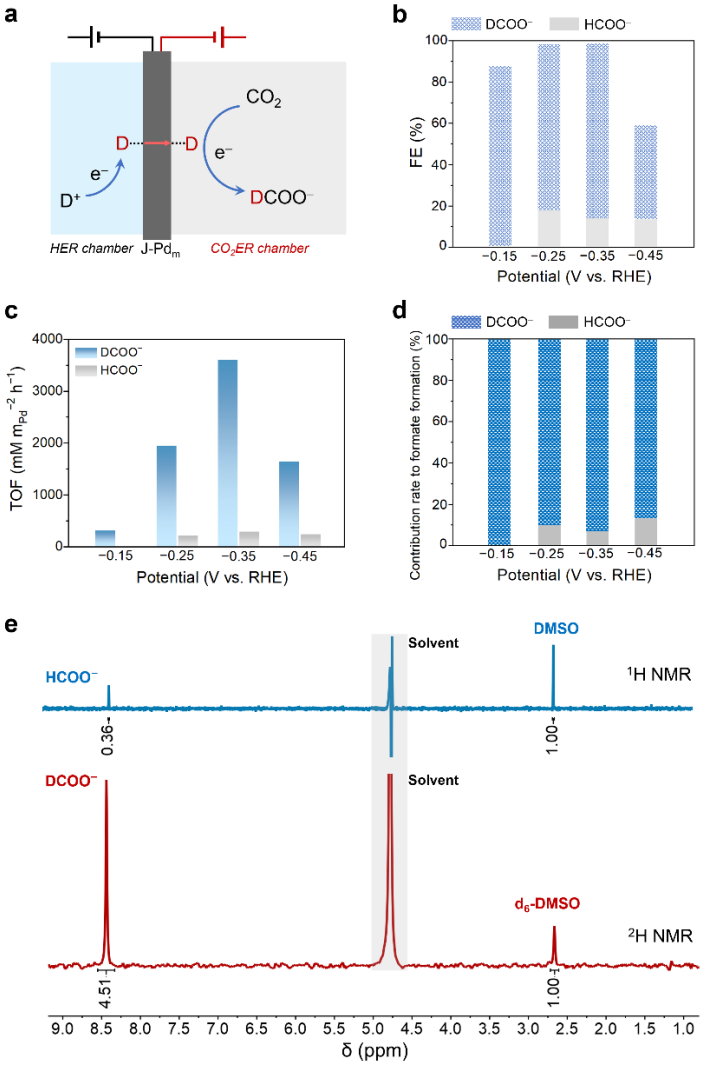

Fig. 3 | Electrolysis experiments to differentiate hydrogen source in CO_2ER via J-Pd$_m$. a, Schematic of J-Pd$_m$ with the HER chamber charged with a deuterated electrolyte. **b**, Faradaic

efficiencies for the formation of normal versus deuterated formate at varying potentials. **c**, Turnover frequencies to produce normal and deuterated formate at varying potentials. **d**, Relative contribution of normal versus deuterated formate production to the overall CO_2ER at varying potentials. **e**, ^1H and ^2H NMR spectra of the CO_2ER chamber electrolyte after electrolysis at –0.35 V vs. RHE. For **a**–**e**, the HER chamber electrolyte was 1.0 M $NaClO_4$ in D_2O and the CO_2ER chamber electrolyte was 50 mM $KHCO_3$ and 0.5 M $NaClO_4$ in H_2O. All the electrolysis experiments were carried out for three hours with j_{HER} = –10 mA cm^{-2}. For **e**, the concentrations of the internal standards, DMSO and d_6-DMSO, were both 1 mM.

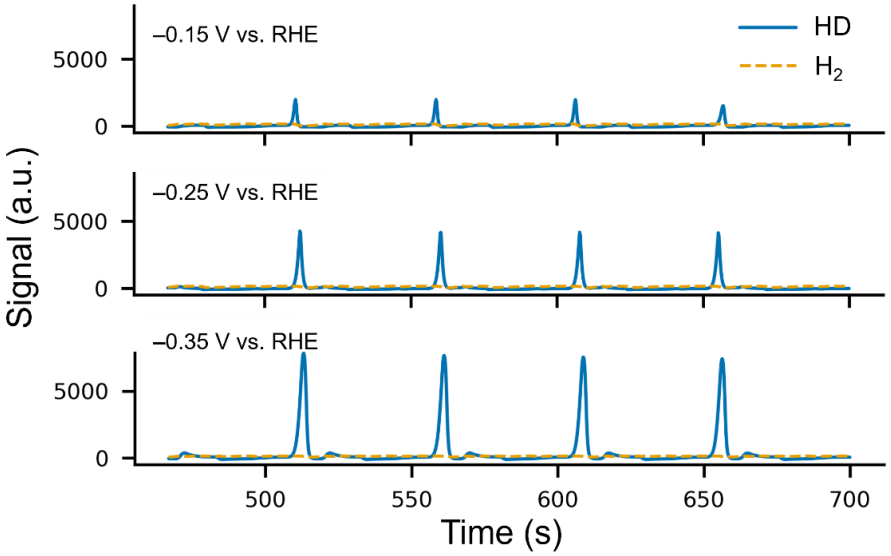

Fig. 4b. Isotope ratio mass spectrometry results recorded in the steady-state region of electrolysis at −0.15 V, −0.25 V and −0.35 V vs. RHE, illustrating highly reproducible HD signals (blue) and negligible H_2 response (orange) in the gas phase.

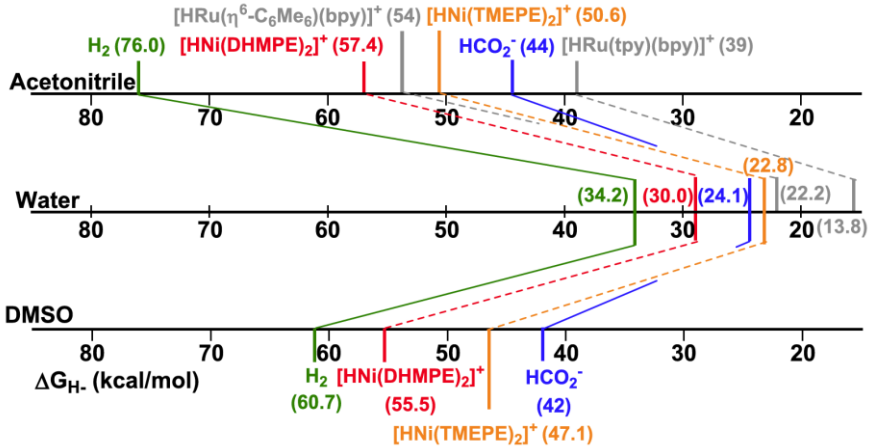

Fig. R1. Hydricity values of formate and H_2 in different solvents, reflecting the relative thermodynamic favorability of hydride transfer reactions involving CO_2 reduction and proton reduction. (Acc. Chem. Res. 2024, 57, 3488−3499.)

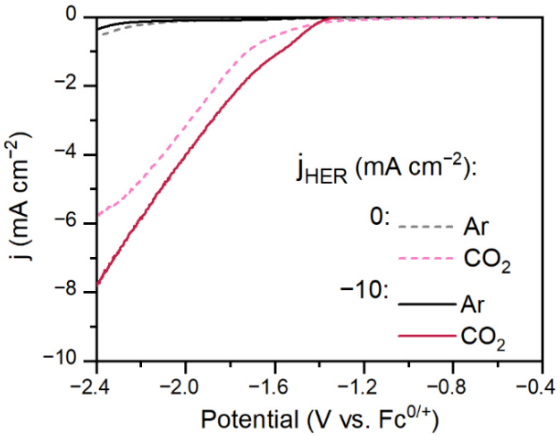

Fig. 5b. Linear sweep voltammograms collected on the CO_2ER side of J-Pd_m in an either Ar- or CO_2-saturated acetonitrile electrolyte, together with or without j_{HER} = –10 mA cm^{-2} applied on the HER side.

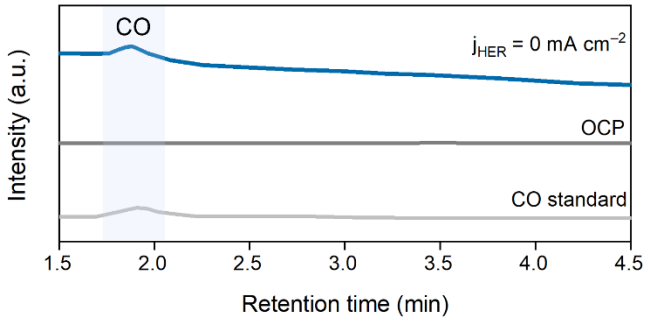

Fig. 5e. Gas chromatograms of headspace samples collected after 3-h electrolysis of CO_2ER in a CO_2-saturated acetonitrile electrolyte with j_{HER} = 0 mA cm^{-2}.

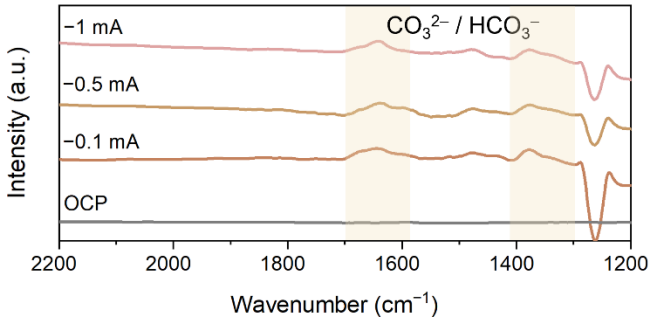

Fig. 5f. *In situ* ATR-SEIRAS spectra collected on a palladium electrode for CO_2ER without permeated hydrogen supplies under varying cathodic current.